Mangrove-Sediment Connectivity in the Presence of Structures Used to Aid Restoration

A Demak Case Study

Nirubha Raghavi Thillaigovindarasu

Delft University of Technology

TU Delft

Mangrove-Sediment Connectivity in the Presence of Structures Used to Aid Restoration

A Demak Case Study

by

Nirubha Raghavi Thillaigovindarasu

to obtain the degree of Master of Science
at the Delft University of Technology,
to be defended publicly on Thursday December 13, 2023 at 01:30 PM.

Student number:	5461103	
Project duration:	February 23, 2023 – December 13, 2023	
Thesis committee:	Prof. dr. ir. A. J. H. M. Reniers,	TU Delft, chair
	Dr. ir. A. Gijón Mancheño,	TU Delft, daily supervisor
	Dr. ir. S. G. Pearson,	TU Delft, daily supervisor
	Ir. I. Gerritsma,	Deltares, supervisor

Cover: Silhoutte of mangrove trees during sunset by Alexey Demidov

TU Delft

Acknowledgements

Kural 101

செய்யாமல் செய்த உதவிக்கு வையகமும்
வானகமும் ஆற்றல் அரிது

Assistance given by those who ne'er received our aid,
Is debt by gift of heaven and earth but poorly paid.

- Thiruvalluvar

To call the experience of working on this thesis for the past 11 months humbling, would be underselling it. The amount of professional, and more importantly, immense personal growth I have undergone the past year, is thanks to a few people. I feel an absurd amount of gratitude. Firstly, I truly believe I could not have, even in my dreams, orchestrated to bring a more incredible set of people together to help and mentor me as my committee. Ad, after every meeting with you, I always leave with a sense of awe of your knowledge and your ability to convey it in the least number of words possible, and more confident of my own abilities at the same time. To this day, I do not understand how those feelings go together. Thank you for always making time for my questions and for your quiet confidence in me. Stuart, it has been a year and a half now since I started working with you and I think it is safe to say that it is not just because of our shared love for cool sediment transport things. I feel incredibly lucky and consider it a privilege to have gotten to learn from you from close quarters, on more than one occasion. Thank you for being a constant cheerleader undeterred by my lack of confidence. It has meant more than I could find words for here. I hope I get to collaborate with you for many years to come. Alejandra, before I met you I did not think I would find a kinder person than Stuart in academia, and I truly cannot be more grateful to have been proven wrong. From our very first meeting, I knew I wanted to work on this topic. I had been under the impression that it was solely due to my passion for the subject. I have since come to realise that it was also because of your own passion for the world, and more importantly, the warmth you exuded then that has never waned. Your contribution to my scientific rigour and how I view myself as a person now has been monumental. Thank you for the continued inspiration. Isabel, your readiness to help at any given moment, no matter the effort required, has been instrumental in making the thesis what it is now. Thank you.

DD, in the eight years that I have known you, your number being the first I dial whenever I have happiness to share, existential questions I want answered, and aches I could burden no one else with has not changed, and I do not see that changing in the near and far future. Thank you for always having been and continuing to be my north star. Sujana, as we keep saying, we have seen the highest of highs and the lowest of lows together, and I am incredibly grateful we had each other through it all. Abishek, a constant through life, thank you for the almost decade-long companionship. You keep setting the bar higher everyday and inspire us all. Kanna, from the final year project shenanigans through to shared heart-numbing grief, you always make life easier and more fun. Thank you. Karthi and Mukil, thank you for providing a semblance of home here, thousands of miles away from the actual one. Although the both of you try almost everyday to make me a social being with a near-zero success rate, the least I can do is acknowledge your efforts here. Kanagaraj, Ramya and Abhishek, thank you for having made the year after lockdown tolerable and the years since a lot sweeter. I owe my sanity to the three of you.

Amma and Appa, for the innumerable sacrifices you have made to get me where I am today, thanking you will not suffice. But, thank you anyway. I hope I have made you proud.

Nirubha Raghavi Thillaigovindarasu
Delft, December 2023

Abstract

Mangrove forests are important wetland ecosystems that inhabit intertidal zones within tropical and sub-tropical latitudes. They offer a diverse array of ecosystem services, including coastal protection and carbon sequestration. Despite their significance, global mangrove cover has declined in recent decades, prompting various restoration initiatives, most of which often fail due to a lack of system understanding of the local mangrove habitat and associated physical and biological processes. A method gaining prominence involves the use of permeable dams to restore the sediment balance along eroding coastlines, thereby facilitating the restoration of mangroves in the area. These dams help dissipate the approaching waves and reduce current magnitudes, thus creating a low energy environment behind them, ideal for sediment deposition. However, a comprehensive understanding of the system-wide implications of utilisation of permeable dams remains largely unexplored.

The study is focused on examining the response of a coastal system to structural presence, based on currents, waves and sediment and propagule pathways, to optimise restoration strategies. The coastline of Demak in Indonesia is chosen as the system to be modelled due to the persistent erosion problem in the region and the ongoing use of permeable and impermeable structures to mitigate the problem. A nested model was set-up in Delft3D-4 to estimate the flow hydrodynamics resulting from river discharge, tide and wind forcing in the area. Wave propagation in the region was also modelled using Delft3D-4 with a standalone nested wave model. Output from the hydrodynamic models served as input for the Lagrangian particle tracking model, SedTRAILS, to compute the sediment and propagule pathways.

The hydrodynamic models demonstrate a decrease in both current magnitude and wave activity behind the structures, with a greater reduction observed in the case of impermeable structures. However, the radius of influence is constrained to less than a kilometre from the structures. The sediment pathways reveal reduced sediment movement behind the structures. However, the sediment imported due to the structures are sourced from within the intertidal basin which could trigger coastline retreat in the region. Additional tests uncover impermeable structures with larger length to opening size ratio, placed closer to the mangrove fringe to be able to retain sediment with comparatively higher efficiency. In case of propagules, the trapping behaviour of the structures is less apparent, with dependencies on the relative location of the structure to the sources and the direction of wind. In Demak, when structures are located relatively offshore to the propagule sources, they are able to trap the propagules, thereby creating a possibility for mangrove restoration. The study concludes that coastal structures enhance sediment and propagule retention, with varying efficacy depending on the type, location and length of the structure, suggesting their potential utility as a valuable tool for mangrove restoration.

Contents

Acknowledgements ii

Abstract iv

1 Introduction 1
- 1.1 Context . . . 1
- 1.2 Problem Statement . . . 2
- 1.3 Objectives . . . 3
- 1.4 Thesis Outline . . . 3

2 Literature 5
- 2.1 Mangrove Ecology . . . 5
  - 2.1.1 Mangroves and Mangrove Ecosystems . . . 5
  - 2.1.2 Propagules . . . 6
  - 2.1.3 Mangrove Establishment . . . 7
  - 2.1.4 Long-term Mangrove Survival . . . 8
- 2.2 Drivers of Mangrove Loss . . . 9
- 2.3 Mangrove Restoration on Muddy Coastlines . . . 11
  - 2.3.1 Requirements for Restoration . . . 11
  - 2.3.2 Rehabilitation Measures . . . 12
- 2.4 Morphodynamic Restoration Using Structures . . . 14
  - 2.4.1 Do Permeable Structures Work? . . . 14
  - 2.4.2 Restoration Project Examples . . . 16
  - 2.4.3 Knowledge Gap . . . 18
- 2.5 Summary . . . 19

3 Study Area 21
- 3.1 Location . . . 21
- 3.2 Site Characteristics . . . 22
  - 3.2.1 Meteorology . . . 22
  - 3.2.2 Hydrodynamics . . . 23
  - 3.2.3 Morphodynamics . . . 25
  - 3.2.4 Mangroves . . . 26
- 3.3 Shoreline Erosion . . . 27

4 Modelling 29
- 4.1 Model Selection . . . 29
- 4.2 Delft3D . . . 29
  - 4.2.1 Nested Flow Model Set-Up . . . 30
  - 4.2.2 Model Calibration and Validation . . . 36
  - 4.2.3 Wave Model Set-Up . . . 39
- 4.3 SedTRAILS . . . 40
  - 4.3.1 Domain . . . 40
  - 4.3.2 Structures . . . 41
  - 4.3.3 Sediment Module . . . 42
  - 4.3.4 Propagule Module . . . 44

5 Results 47
- 5.1 Hydrodynamics . . . 47
  - 5.1.1 Currents . . . 47
  - 5.1.2 Waves . . . 50
- 5.2 Sediment Pathways . . . 51

5.2.1 Large-scale Pathways . . . 51
5.2.2 Influence of Structures on Pathways . . . 54
5.2.3 Structure Characteristics . . . 55
5.3 Propagule Pathways . . . 60
5.3.1 Large-scale Pathways . . . 60
5.3.2 Influence of Structures on Pathways . . . 62

6 Discussion **65**
6.1 Methodological Limitations . . . 65
6.1.1 Delft3D Model Limitations . . . 65
6.1.2 SedTRAILS Model Limitations . . . 67
6.1.3 Other Assumptions . . . 68
6.2 Knowledge Contribution . . . 69
6.2.1 River Plume . . . 70
6.2.2 Structure Permeability . . . 70
6.2.3 Sediment Sources . . . 70
6.2.4 Propagule Dispersal . . . 70
6.2.5 Mangrove Restoration . . . 71
6.3 Application . . . 71

7 Conclusions and Recommendations **73**
7.1 Conclusions . . . 73
7.1.1 Primary Research Objective . . . 73
7.2 Recommendations . . . 75
7.2.1 Bathymetry . . . 75
7.2.2 Vegetation . . . 75
7.2.3 Transport Formulation . . . 75
7.2.4 Morphodynamic Approach . . . 75

References **77**

A Bathymetry of Nested Model **85**

B Porous Plates **89**

C Bed Shear Stress **93**

D Sediment Retention - Sensitivity Analysis **95**

1

Introduction

1.1. Context

Mangrove forests are important ecosystems offering a plethora of services that benefit communities around and away from them. Services offered by the ecosystems include but are not limited to, provisions like timber, fuel wood, habitats for various species, coastal and flood protection against storms and, in certain circumstances, tsunamis, among other flood hazards, the value of which is estimated at 2,000 to 9,000 USD per hectare per year (Barbier et al., 2011; Alongi, 2008; Kathiresan and Rajendran, 2005; Spalding, 2010).

These impressive ecosystems persist in the portion of the tidal zone from mean sea level (MSL) to highest spring tide. They are generally found in the tropical and subtropical regions and covered a total of 137,760 square kilometres globally in the year 2000 (Alongi, 2002; Giri et al., 2011). However, the mangrove cover has been in decline over the years at a rate of 0.16% to 0.39% per year globally since 2000 (Hamilton et al., 2016). While the rate of loss seems to have decreased when compared to previous decades, there still exist causes for concern especially in the region of Southeast Asia. In Indonesia, the annual mangrove deforestation rate ranges from 0.26% to 0.64%, which is approximately twice the global average (Hamilton et al., 2016). This decline in mangrove forest cover worldwide can be attributed mainly to anthropogenic activities such as urban development, transformation of forests into economic land use such as aquaculture and agriculture, and demand for wood (Winterwerp et al., 2020). It is however important to note here that, while economic growth was one of the key drivers of mangrove loss in the past (1996 to 2006 to be precise), during the recent years, net gain of mangrove cover was observed to correspond to regions of higher economic growth (Hagger et al., 2022). This suggests that increased wealth and education, and improved agricultural productivity could ultimately reduce development pressure, thus aiding restoration efforts (Ceddia, 2019).

Although restoration efforts have not been lacking, few appear to have succeeded, mainly due to uninformed selection of sites and species (Wodehouse and Rayment, 2019). Restoration has also often failed when planting is done within habitats that would not support their natural recruitment (Primavera and Esteban, 2008; Bayraktarov et al., 2016). It is therefore important to obtain knowledge on the physical and biological processes at site, to inform the design and implementation of rehabilitation strategies. One of the most efficient strategies in use is Ecological Mangrove Restoration (EMR) (Lewis, 2001). In this approach, it is attempted to restore habitat favourable for mangrove growth without any planting in general, as it is well known that mangrove forests can self-repair provided the habitat allows for it (Lewis III, 2005). Principles of EMR have been successfully implemented in various restoration efforts across the world.

The coastal area of Demak district in Central Java, Indonesia suffers from tremendous erosion, which has lead to significant loss of the mangrove cover there (Ecoshape, 2015). The erosion can be ascribed to excessive aquaculture and subsidence (Winterwerp et al., 2020). Subsidence is a major threat to mangrove forests in the Demak coastal system with rates exceeding 8 cm/year in Sayung district of Demak close to the coast which is an order of magnitude higher than eustatic sea level rise (Deltares, 2021a). While mangroves are capable of keeping up with relative sea level rise by enhancing sediment accretion (see Figure 1.1), it follows that sediment availability is a key factor in determining if the mangroves can maintain sufficient surface accretion (Lovelock et al., 2015). With rates of subsidence as high as observed in Indonesia, mangrove restoration projects planned for the area should also accrete enough sediment to facilitate growth of mangroves. A pilot rehabilitation project in Demak implemented EMR, and created the required habitat for mangrove expansion by use of temporary permeable structures made of brushwood and bamboo poles proposed by Winterwerp et al. (2013). The dams are used to dissipate waves and thereby trap sediment in the low energy environment behind them. Design of such structures has thus far been based on best-engineering practice and therefore do not always prove successful, which led to studies on developing physics-based models to optimise the design (Gijón Mancheño, 2022).

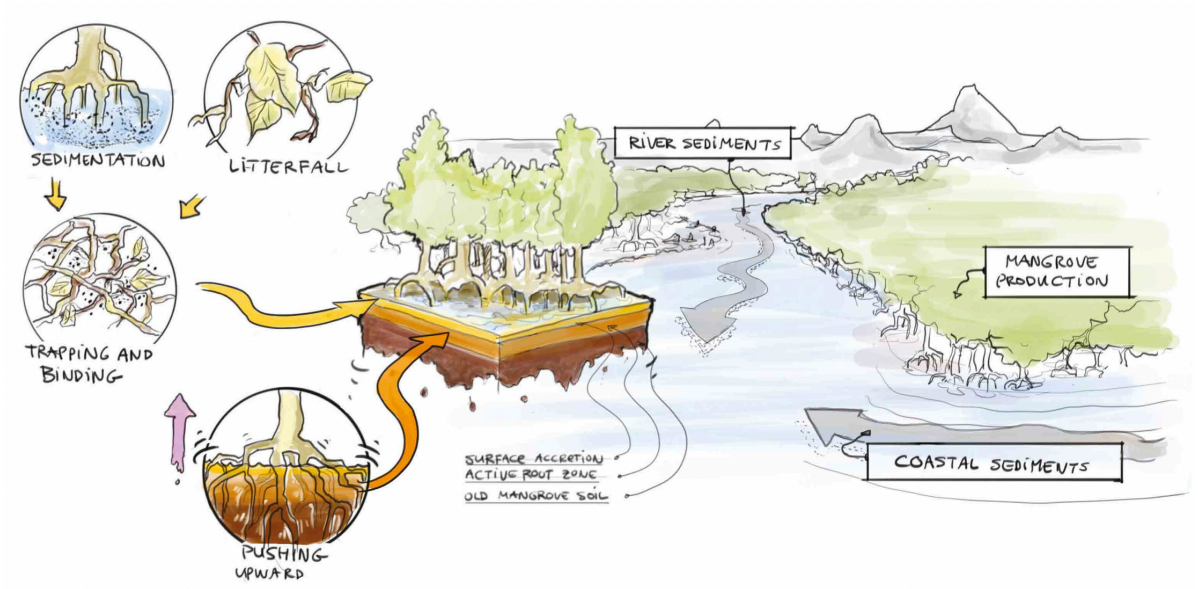

Figure 1.1: Potential damage limitation against sea level rise through sediment accretion by mangroves (From Spalding et al., 2014)

A systemic understanding of physical processes on site allows not only to optimise the design of structures used, but also the layout at the location, which helps devise the most effective rehabilitation strategies. While morphodynamic models and hence bed level changes in response to structures are available for the study area of Demak (see Smits, 2016), knowledge on sediment and mangrove propagule pathways would provide insights on the system connectivity for different structure characteristics and, thus optimise rehabilitation strategy so as to maximise the probability of success of the campaign.

1.2. Problem Statement

Mangrove coastlines globally are eroding due to a combination of various, mostly anthropogenous factors. To restore the eroding forests, temporary structures are being used to trap sediment and elevate bed to levels ideal for mangrove expansion. However, success of rehabilitation efforts depend on information about physical and ecological processes and, conditions like sediment availability at the target site. Insight into the system and its processes are thus required for successful restoration, but we lack models to understand sediment and propagule connectivity and hence, their availability and ability to reach the target locations in the system. While Bisschop (2023) took the first steps toward modelling

said pathways through an idealised model, the effect of structural interventions on the pathways is still unknown. Knowledge of the effects of structures in use and their characteristics on the pathways is thus required to better strategise restoration efforts.

1.3. Objectives

The objective of this research is to advance current knowledge on eroding coastal mangrove systems by modelling sediment and propagule pathways in such a system in the presence of structures. The resulting insights can be used to optimise rehabilitation strategies not only in the study area, but also in similar regions. The objective stated is reformulated as a research question.

How do coastal structures affect sediment and propagule pathways for mangrove restoration?

To answer the broad question posed, it is imperative to address it from the mechanisms and analyse the effect of individual drivers, which leads to the formation of the following sub-questions:

1. How are currents affected by the presence of structures used to trap sediment and thereby help rehabilitate mangrove systems?
2. What is the effect on wave transformation by the structures present in the region?
3. How do structures and their implementation in the model influence sediment pathways in the study area?
4. How do structures influence mangrove propagule pathways in the study area?
5. How do different characteristics of the structures affect the sediment pathways?
6. Do the pathways of sediment and propagules correlate to contribute to mangrove restoration?

1.4. Thesis Outline

The research questions posed will be answered by modelling the study area which requires a thorough literature study. Results from the model will then be fed to SedTRAILS to obtain the relevant sediment and mangrove propagule pathways.

A comprehensive literature study is done to understand the mangrove ecology and causes of mangrove loss globally. A general overview on the use of structures (permeable and hard) to rehabilitate mangroves is obtained from further study. This is expanded up on in Chapter 2.

Knowledge on the study area and the local hydro-, morpho- and sediment dynamics is acquired through study on the region of concern. The obtained knowledge is presented in Chapter 3.

The choice of model is done based on a variety of factors explained in Chapter 4. The study area of Demak coastal region is modelled using the chosen software for preliminary tests of the processes in the system and validated using results produced by Bisschop (2023). A more extensive morphostatic model with coastal structures is then built. The methodology for both hydrodynamic and Lagrangian pathway modelling is expounded up on in Chapter 4.

Results from the individual models is then used in SedTRAILS (Sediment TRAnsport vIsualization & Lagrangian Simulator) to obtain the pathways of sediment and mangrove propagules for the various cases discussed which is showcased along with results from the hydrodynamic models in Chapter 5. The obtained pathways are then used to reflect on their application and answer the research questions posed in Chapter 6 and Chapter 7 respectively.

2

Literature

This chapter presents a review of the literature on mangrove ecology and propagule characteristics, drivers of mangrove loss, and the use and effect of structures to rehabilitate mangroves at eroding coastlines.

2.1. Mangrove Ecology

This section provides an overview on the available literature on mangrove and mangrove propagule characteristics, requirements for mangrove establishment and long-term survival.

2.1.1. Mangroves and Mangrove Ecosystems

Mangrove ecosystems consist of trees and shrubs that grow at the interface between land and sea in tropical and sub-tropical latitudes (30°N to 37°S). These span considerable variations in tidal height (<1 m to >4 m), geomorphology (coastal to riverine systems), sedimentary environment (peat to alluvial), climate (warm temperate to both arid and wet tropics), and nutrient availability (oligotrophic to eutrophic) (Feller et al., 2010). Because of their environment, mangroves are necessarily tolerant of, and have therefore adapted to, high levels of salinity, anaerobic conditions and high temperatures (Kathiresan and Bingham, 2001).

Mangrove forests create unique ecological environments that host a rich variety of species. The loose sediments of the forests are home to a wide assortment of invertebrates (Kathiresan and Bingham, 2001). The complex root system of the trees also serves as a nursery habitat for crab, prawn and fish species providing an abundance of food and shelter (Nagelkerken et al., 2008). Above the water surface, mangrove trees and canopy provide habitat for a range of species including birds, mammals, amphibians and reptiles (Rajpar and Zakaria, 2014).

Apart from hosting a large variety of fauna, mangroves also support a wide range of ecosystem services. They protect coastlines, enhance water quality, yield commercial forest products, sequester carbon among other services (Mitra, 2020). Mangroves contribute to coastal protection by their ability to attenuate waves by exerting resistance on the approaching waves, as they propagate across the trunks and root systems of the trees (Mazda et al., 2006). Additionally, mangroves can promote accumulation and stabilisation of coastal sediments with their complex root systems (Furukawa et al., 1997). Mangroves effectively slow down and decelerate water flow, mainly as a function of the trees' three-dimensional structure and the complex topographical features of channels, creeks, etc. This enables efficient trapping of suspended and particulate matter, which can lead to land accretion, buffering against storms and sea level rise (Walters et al., 2008). Besides coastal protection, mangroves and

their biota also help remove excess nutrients from the water thereby aiding the purification of water to an extent (Spalding et al., 2014; Trégarot et al., 2021). Mangrove forests also provide a livelihood to local communities through fisheries and wood for fuel and construction (Glaser, 2003; Rönnbäck et al., 2007). Mangrove tourism is also estimated to attract tens to hundreds of millions of visitors annually and is a multi-billion dollar industry (Spalding and Parrett, 2019). With respect to carbon sequestration, mangrove ecosystems are among the most productive and biogeochemically active ecosystems (Eong, 1993). Mangrove forests are highly productive, with carbon production rates equivalent to tropical humid forests (Alongi, 2012). The carbon stock per unit area is also enormous as the top layers of mangrove sediments store large amounts of organic carbon, typically an order of magnitude higher than those of other tropical forests (Walters et al., 2008). Mangrove forests are thus hugely important ecosystems providing services to communities at both local and global scales.

2.1.2. Propagules

Mangroves reproduce through propagules, which are seeds that germinate while still attached to the parent tree. These propagules are then dispersed through water, during which period embryonic development continues (NHMI, 2000). To allow for sufficient development, the propagules must remain floating for an obligate dispersal period which is species-dependent (Rabinowitz, 1978). On reaching a favourable site, the propagules get stranded and establish themselves rapidly as seen in Figure 2.1 (Osborne and Berjak, 1997).

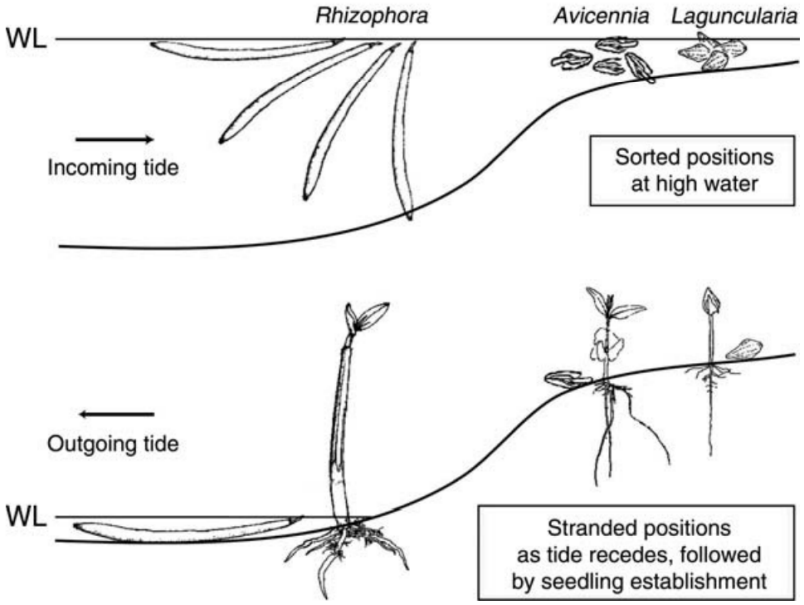

Figure 2.1: Different species of mangrove propagules stranded during receding tide and their establishment thereafter to seedlings (from Sousa et al., 2007)

The process of dispersal is crucial for the distribution and connectivity of mangrove populations, contributing to shifting distributions in response to environmental changes (van der Stocken, Carroll, et al., 2019; van der Stocken, Wee, et al., 2019). Dispersal of propagules is determined by a range of factors from propagule traits such as its density and buoyancy to vector properties such as wind and water currents as depicted in Figure 2.2 (van der Stocken, Wee, et al., 2019). The contribution of wind to dispersal of propagules is found to be significant (Di Nitto et al., 2013) and dependent on propagule characteristics such as buoyancy, density, morphology and floating orientation (van der Stocken et al., 2013; van der Stocken et al., 2015). Water temperature and salinity can affect the density of water and therefore the buoyancy of propagules. Salinity is a vital factor that affects the buoyancy of mangrove propagules, including their flotation period and viability (Wang et al., 2019). With the threat of climate change, in the future, a warmer and fresher ocean is likely to alter dispersal trajectories of man-

grove propagules and increase rates of sinking in unsuitable offshore locations, potentially reducing the resilience of mangrove forests (van der Stocken et al., 2022).

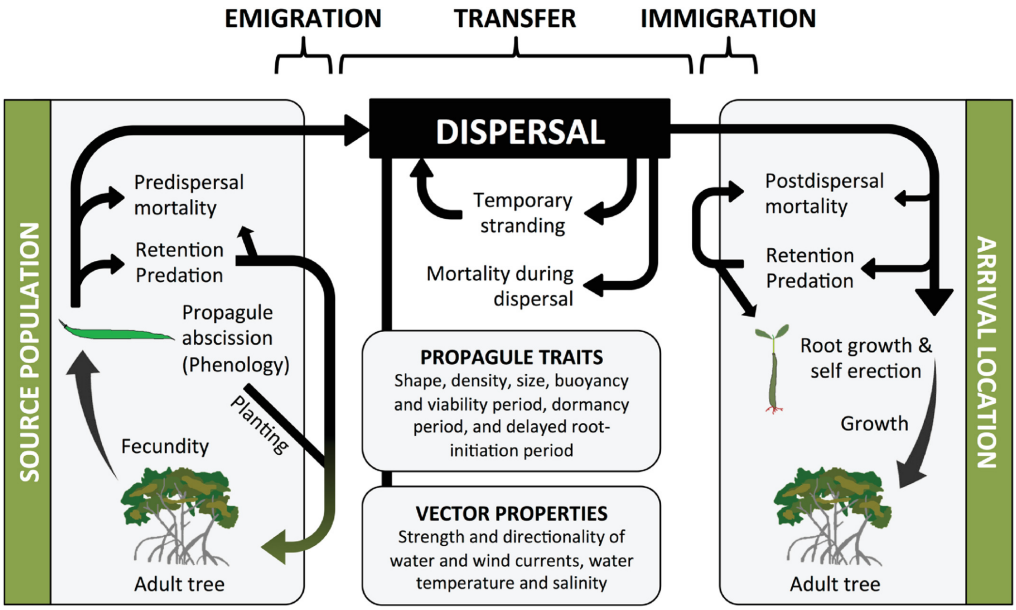

Figure 2.2: Mangrove dispersal is dependent on factors for propagule emigration, transfer and immigration. Fecundity, predation and local retention determine the amount of emigrant propagules from the area. While in transportation, propagule traits such as its density and viability period and, vector properties like salinity and water and wind current velocities determine dispersal trajectories and probability of reaching a favourable site. Once the propagule reaches a desired location, its establishment depends on factors such as retention (based on factors of shear stress, flooding, sediment conditions, etc.) and predation in the area. (From van der Stocken, Wee, et al., 2019)

Dispersal of propagules can occur within the same population (short-distance dispersal (SDD)), to nearby or distant populations (long-distance dispersal (LDD)), or between a mangrove stand and a new location that lacks established mangroves (van der Stocken, Wee, et al., 2019). LDD allows for the large-scale exchange of propagules between populations and the colonisation of unoccupied habitats (Nathan et al., 2008). Hence, LDD, rather than local dispersal, determines large-scale phenomena of greatest conservation concern, such as the spread of invasive plants, range shifts following climate change, etc., (Trakhtenbrot et al., 2005). However, local establishment, predation and local propagule retention ensure that a large amount of propagules will not leave the parental stand (van der Stocken, Wee, et al., 2019; Di Nitto et al., 2013). The focus of this thesis is on SDD to understand the pathways taken by propagules in the presence of local interventions.

2.1.3. Mangrove Establishment

On reaching a favourable location, propagules can establish as seedlings which grow into mangrove trees. For successful establishment, a number of criteria need to be fulfilled. Balke et al. (2011) found that the stranded propagules must overcome three main thresholds seen in Figure 2.3 for establishment to seedlings:

1. Stranded propagules need an inundation-free period to rapidly develop roots that are long enough to withstand displacement by flooding
2. Roots need to become long enough to withstand seedling dislodgement by hydrodynamic forces from waves and currents, with the required root length being proportional to the force that needs to be resisted
3. Even longer roots are needed to survive high energy events that can cause sheet erosion and thereby induce seedling dislodgement

These thresholds can also be overcome with the help of interventions such as permeable dams (van Bijsterveldt et al., 2022). With a thorough understanding of the system, installation of such dams can increase the bed level through sediment trapping (helping overcome the first threshold) and mitigate the wave stress (helping with the second and third thresholds), allowing an increase in the natural seedling recruitment (Van Cuong et al., 2015).

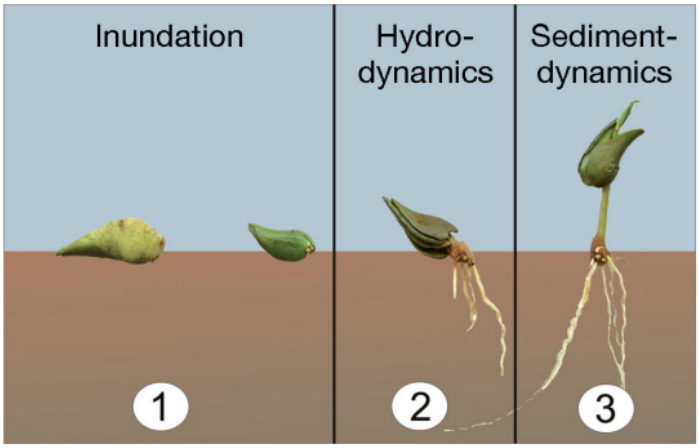

Figure 2.3: Thresholds stranded propagules need to overcome for successful establishment to seedlings (alternatively known as windows of opportunity) (from Balke et al., 2011)

For the purpose of mangrove restoration, van Bijsterveldt et al. (2022) extended the list of thresholds to include propagule availability (phase 0) and growth limitations (phase 4). When aiming for rehabilitation without planting, propagule availability is of tremendous importance. Lewis III (2005) effectively showcased this by re-establishing aquatic connectivity at a site deprived of propagules, consequently triggering the initiation of mangrove regeneration. Once established, the seedlings need to overcome growth limitations such as predation, disease or other stressors to grow into reproductive trees (van Bijsterveldt et al., 2022). The thresholds vary for different species of mangroves, knowledge of which helps with the success of restoration efforts.

2.1.4. Long-term Mangrove Survival

Mangroves have evolved several strategies to ensure survival in the harsh environments they inhabit. Genetic diversity is one such strategy born as a result of numerous evolutionary processes and, is crucial for adaptability and environmental resilience (Duke, 1995). A diverse genetic makeup also reduces the vulnerability to diseases and pests by increasing the probability of having individuals with natural resistance mechanisms (Pautasso et al., 2005). In the face of natural disasters that could cause potential flooding, genetically diverse mangrove populations have a higher chance of survival (Guo et al., 2018). Some individuals may have traits that confer resistance to damage caused by extreme events, ensuring the population's recovery (Alongi, 2008).

Within a genetically diverse mangrove system, zonation is characterised by distinct zones of mangrove species at different elevations or at different distances from the shoreline (see Figure 2.4). The phenomenon is attributed to the responses of individual species to variation in degree of tidal inundation, salinity and other factors varying across the intertidal regime (Smith III, 1992). Such structure of the forests are the result of a complex interplay of physiological tolerances and competitive interactions ensuring survival of the population (Alongi, 2008).

As climate change continues to exert a growing influence globally, certain associated stressors like carbon dioxide enrichment are projected to benefit mangrove populations, leading to heightened growth and productivity (McKee et al., 2012). However, the net impact of climate change on mangroves is anticipated to be significantly adverse with relative sea-level rise playing a pivotal role in determining

their long-term survival (Friess et al., 2022). Mangroves can potentially keep pace with and adapt to moderate rates of sea-level rise through a number of physical and biological mechanisms, including the trapping of sediment from fluvial or surrounding coastal sources, below-ground root production, leaf litter additions, microbial and algal mat production, etc., (Krauss et al., 2014). Consequently, the current and future mangrove surface elevation dynamics are strongly influenced by the broader coastal sediment budget (Lovelock et al., 2015). Studies from across the world show that mangrove forests in the past have been able to keep pace with sea-level rise when the latter is limited to rates of less than 7 mm per year (Saintilan et al., 2020). However, in addition, possible landward migration of the forest in response to sea-level rise is limited by urbanisation (Enwright et al., 2016). Climate change is also predicted to result in higher intensities of storms, which could lead to increased damage and/or mortality of mangroves (Walsh et al., 2016; Gilman et al., 2008). Storm impacts on mangrove forests can persist for years as legacies of past disturbance (Krauss and Osland, 2020). These ecosystems can recover over time but their resilience depends on the size of the forest. Mangrove forests that cover larger spatial areas might exhibit greater resilience compared to smaller stands, as the damage aligns with the trajectory of cyclones, causing partial harm, with surviving regions serving as propagule sources for affected areas (Krauss and Osland, 2020).

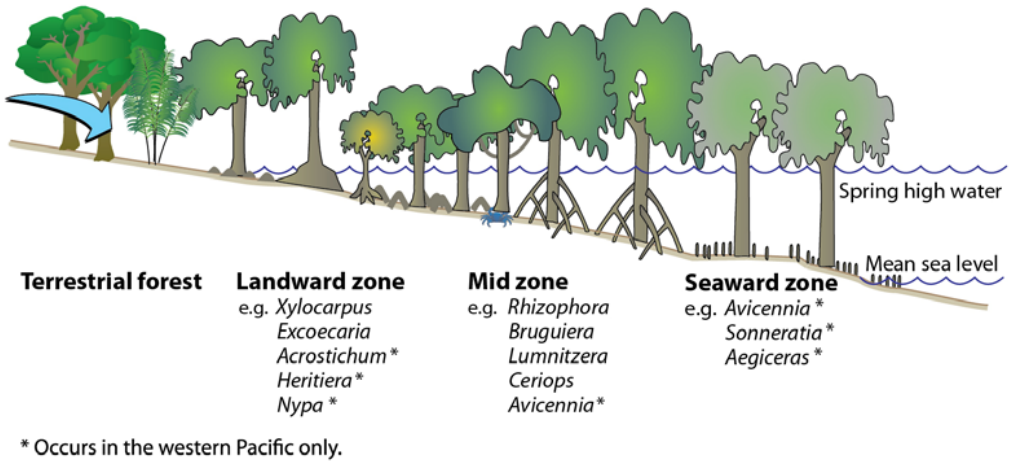

Figure 2.4: An example of mangrove zonation that occurs in the tropical Pacific listing the prominent species of each zone

2.2. Drivers of Mangrove Loss

Globally, a net 3.4% of mangrove extent has been lost between 1996 and 2020 (Bunting et al., 2022). This loss can be attributed to a variety of reasons both natural and anthropogenic. Erosion in high-energy environments during storms is an example of natural loss, while direct removal due to deforestation can be attributed to humans. Goldberg et al. (2020) identifies five main categories of drivers comprising of anthropogenic causes such as commodities, non-productive conversion, reclaimed land for human settlement and, natural causes of shoreline erosion and extreme weather events. From 2000 to 2016, agriculture and aquaculture, including rice, shrimp, and oil palm cultivation, served as the primary global driver of mangrove loss, constituting 47% of global losses (Goldberg et al., 2020). Shoreline erosion, a natural driver, represented the second highest percentage of global losses at 27% (Goldberg et al., 2020). The share of all five drivers in global mangrove loss can be seen in Figure 2.5.

Within Southeast Asia, a substantial 82% of mangrove loss was found to be human driven, compared to 33% in the rest of the world (Goldberg et al., 2020). The primary driver of anthropogenic mangrove loss was found to be the conversion of mangroves to aquaculture and agriculture during the period 1996-2010 with historical evidence prior to 1996 (Thomas et al., 2017). In Indonesia, documented instances of exploitation of the mangrove forests for timber and conversion to fish ponds have emerged as the predominant drivers of loss in the region (Ilman et al., 2016).

Throughout the world however, natural losses of mangrove forests through erosion and extreme weather events remain pervasive. Erosion is most commonly observed in high-energy environments, such as along exposed coastlines and at the confluence of rivers and at river mouths (Thomas et al., 2017). Shoreline erosion in mangrove ecosystems is the result of variability in sea-level rise, rainfall, temperature, and wave activity (Friess et al., 2022). In addition, a potential bottleneck in the form of sediment supply to the coast, when critically lowered, will exacerbate shoreline retreat. In the delta of the Chao Phraya River in Thailand, a substantial reduction of approximately 80% in sediment supply, along with surface subsidence resulting from groundwater extraction, led to the extensive retreat of mangrove shorelines for several kilometers (Lovelock et al., 2015). Activities such as upstream urbanisation, mining and deforestation directly impact sediment influx into mangrove forests and would need to be monitored (Thomas et al., 2017).

Anticipated future land-use scenarios highlight coastal development as a significant factor contributing to substantial mangrove ecosystem loss within the Indonesian archipelago (Ilman et al., 2016). An example is the city of Semarang in Indonesia, grappling with ongoing subsidence primarily caused by urban development (Abidin et al., 2013). This situation has resulted in recurrent coastal flooding, eventually leading to the loss of mangroves in the vicinity of the city and neighbouring areas, owing to shoreline erosion (Ilman et al., 2016). Recent research by van Bijsterveldt, Herman, et al. (2023) in the area has been able to successfully quantify the relative sea-level rise (RSLR) experienced by the rural areas near the coastline and associated mangroves in the Demak region. The findings indicated that although individual trees were resilient to RSLR with high sediment deposition due to numerous root adaptations, a sediment deficit with respect to RSLR ultimately led to erosion of the shoreline and lateral retreat of the mangroves.

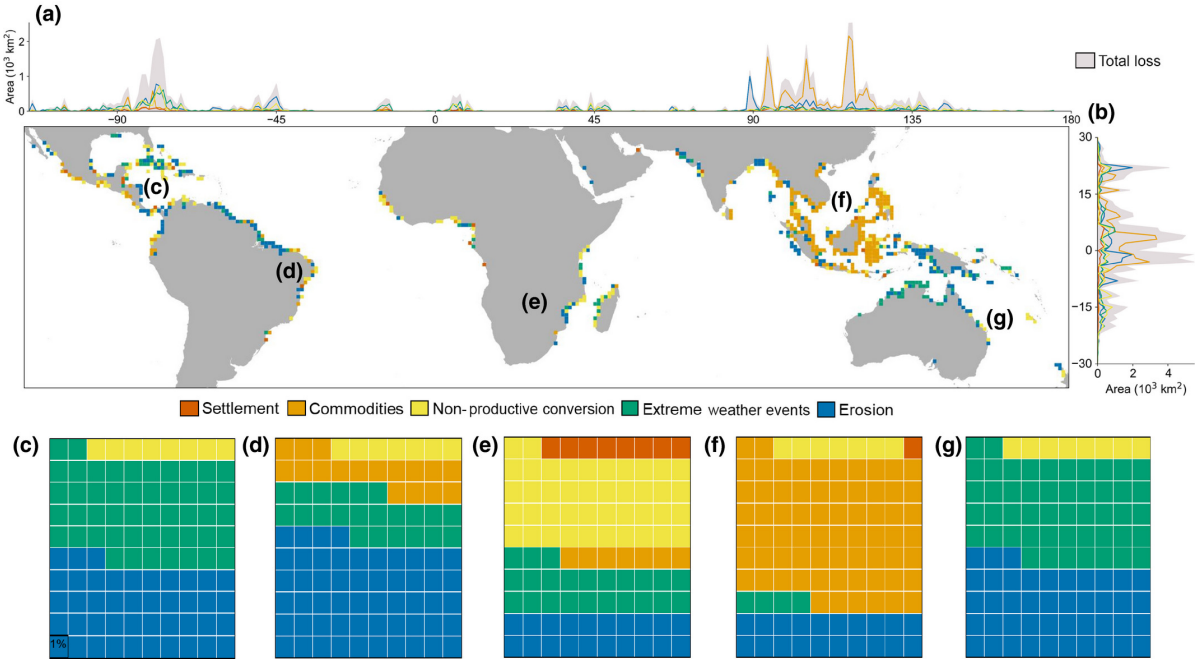

Figure 2.5: Drivers of global mangrove loss showcasing (a) longitudinal, (b) latitudinal distribution of total mangrove loss and the relative contribution of its primary drivers and, (c-g) global distribution of mangrove loss and associated drivers from 2000 to 2016 at 1°×1° resolution (top), with the relative contribution of primary drivers per continent (bottom): (c) North America, (d) South America, (e) Africa, (f) Asia, (g) Oceania. While natural causes seem to be the primary drivers of loss in the Americas and Oceania, human driven causes seem to have had a much greater impact in Asia and Africa. (from Goldberg et al., 2020)

A field study by van Bijsterveldt et al. (2020) in Indonesia of a stretch of mangrove-mud coastline found that seaward retreat of mangroves was observed in the regions with steep foreshores. Deep foreshores exert less bottom friction on waves and therefore allow more wave energy to reach the shoreline. In addition, with a steep elevation change from foreshore to shoreline (i.e., a concave profile), deeper foreshores cause waves to come closer to the shoreline, which can further excavate the foreshore

bed, creating a positive erosional feedback loop (Winterwerp et al., 2013). This disturbance in the sediment balance has often been a major driver of furthering mangrove loss across the world (Anthony and Gratiot, 2012; Besset et al., 2019; van Bijsterveldt, Herman, et al., 2023).

Apart from the various anthropogenic and biophysical drivers, socioeconomic variables are also found to play an influential role in the potential loss of mangroves (Hagger et al., 2022). Both gross and net loss of mangroves at a global scale from 1996 to 2016 were found to be negatively correlated to travel time to the nearest city which served as a measure of market accessibility (Hagger et al., 2022). This indicates access to markets to be a strong driver of mangrove loss. Hagger et al. (2022) observed that the adverse impacts on mangroves resulting from increased market accessibility were somewhat mitigated in countries with high levels of economic complexity and democracy, although the reduction was not deemed statistically significant.

2.3. Mangrove Restoration on Muddy Coastlines

This section expounds on the factors required for successful restoration efforts and possible measures that can be taken for rehabilitation.

2.3.1. Requirements for Restoration

Restoration by definition is the act of returning something to its former position or condition. For mangroves to be restored where lost, it then follows that first and foremost, the driver(s) of loss at the site needs to be studied and prevented from recurring. This requires a good understanding of the conditions of the site being restored, which includes prior knowledge of both ecology and hydrology (Worthington and Spalding, 2018). Of the numerous restoration efforts initiated in the past, few have been successful, primarily because the local site conditions and the causes of loss there were poorly understood which led to implementation of ill-suited measures (Lewis III, 2005; Wodehouse and Rayment, 2019).

Worthington and Spalding (2018) mention that as a starting point for mangrove restoration, it is prudent to consider locations where mangroves have recently been lost. These areas are highly likely to possess local soil conditions, tidal patterns, and elevation levels suitable for successful restoration. Additionally, such locations are expected to facilitate sufficient free exchange of seawater with the adjacent ocean or estuary and situated at an optimal distance from the source of freshwater supply. This consideration is crucial, as a decrease in freshwater availability can elevate salinity levels, potentially harming mangroves at the restoration sites (McKee and Faulkner, 2000). Moreover, their proximity to existing mangroves significantly aids in fostering natural regeneration processes.

When taking climate change and the associated variables into account, relative sea-level rise becomes an important parameter that determines the success of restoration efforts. After initial efforts to elevate bed levels and/or plant seedlings, the sedimentation rates thereafter must be large enough to facilitate long-term growth under rising sea levels (van Bijsterveldt et al., 2022).

One of the main factors determining the success of restoration efforts worldwide is the involvement and collaboration of local communities and stakeholders (Holl et al., 2020; Randy et al., 2015). The knowledge, support, and active participation of the communities contribute to the long-term success and sustainability of restoration initiatives. Involvement of the community is expected to increase the credibility of the restoration project and increase the likelihood of sustainable use in the future, as well as compliance with regulatory measures to protect the developing stands of restored mangroves (Rönnbäck et al., 2007).

To enhance the probability of a successful restoration, it is crucial to integrate long-term monitoring and site management into the procedural framework of projects (Biswas et al., 2009; Randy et al., 2015). Establishing a comprehensive, long-term monitoring program is essential to assess whether the project is making measurable progress, enabling identification of mid-course adjustments and informed modifications for future rehabilitation efforts based on the gathered and reported data (Lewis III et

al., 2019). The plan should entail monitoring the growth and survival of mangrove species, as well as carrying out ongoing or additional hydrological modifications, supplementary planting or weed/pest removal (Worthington and Spalding, 2018). Monitoring, along with potential plan adjustments stemming from it, should be recognised as a fundamental component of successful mangrove rehabilitation.

2.3.2. Rehabilitation Measures

Numerous mangrove restoration projects have been implemented worldwide, employing a variety of methods. Of such methods, reforestation through planting and ecological restoration have emerged as the most prevalent approaches. An illustrative instance of large-scale restoration is the extensive replanting undertaken at the Mekong Delta in Vietnam between 1978 and 1998 (Van et al., 2015). In Florida, over a period of approximately seven years, mangroves were restored across a 500 ha site through hydrologic restoration without additional planting (Lewis III, 1990). Over time, these methods have undergone significant refinement and, when applied properly, have shown a high success rate (Worthington and Spalding, 2018).

When rehabilitation through planting is considered, possessing a sound ecological understanding is pivotal. Often, unsuccessful outcomes in a project are attributed to the planting of species ill-suited to the particular site (Bayraktarov et al., 2016). Individual species exhibit varied tolerances to distinct biogeochemical factors and gradients across the intertidal area, showcasing different preferences for elevation and location (see section 2.1.4). Hence, it is imperative to ensure the accurate species selection and their planting at suitable locations within different segments of a system and, at varying elevations to guarantee their survival. Moreover, barnacles, filamentous algae, and sedimentation commonly inflicted damage upon the planted mangroves, underscoring the significance of appropriate site selection and mitigation of stressors (Bayraktarov et al., 2016).

In many cases, restoration can largely be achieved through the restoration of physical hydrological process, obviating the need for supplementary planting (Wodehouse and Rayment, 2019) (see Figure 2.6). Restoring water flow and land elevation facilitates the natural transportation of mangrove propagules, and over time mangrove regeneration can occur with no planting (Worthington and Spalding, 2018). However, planting can help both to accelerate recovery rates and restore mangroves in places where natural recruitment may be reduced (van Bijsterveldt et al., 2022).

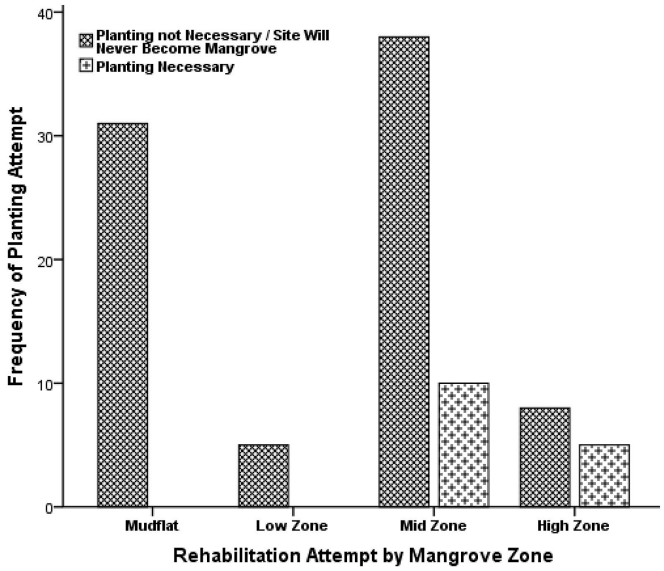

Figure 2.6: Necessity for planting observed from restoration sites in Thailand and Philippines demarcated by zones. Only 16% of the planting efforts were deemed necessary in total, exclusively within the mid and high intertidal zones (from Wodehouse and Rayment, 2019).

Ecological restoration of a site can often be achieved by simply removing the stressor that caused the loss of mangroves in the location, which then allows for natural regeneration (delos Santos et al., 2022). At eroding muddy coastlines, seaward expansion of mangrove stands requires an equilibrious or accreting, convex shaped foreshore whereas, landward expansion is associated with optimal bed level elevations and drainage (van Bijsterveldt et al., 2020). Consequently, rehabilitation measures should aim to allow for sedimentation such that elevations of levels required for seedling establishment are achieved. Landward expansion can be further induced by improving drainage of abandoned aquaculture ponds, if any.

Across the world, the sedimentation required for restoration has been achieved primarily through the usage of coastal structures such as breakwaters or sea walls and, temporary structures known as permeable dams (Kamali and Hashim, 2011; Winterwerp et al., 2020). The structures block or dissipate waves, thereby reducing the bed shear stress behind them and hence the erosive capability of waves. The reduction in shear stress in turn allows for the incoming sediment to settle without the resuspension by the waves (Winterwerp et al., 2020; Bosboom and Stive, 2021). However, when hard structures are in use, the reflection of incoming waves erode the soil at the foot of the structures, scouring sediment locally (Winterwerp et al., 2013). This could prove especially counterproductive along muddy coastlines where the large water content of the fine sediment increases the risk of liquefaction due to the reflected waves which, when combined with cohesive property of mud can enhance erosion through formation of fluid mud and thereby, cause collapse of the structure. Once erosion is underway, a positive feedback loop is generated inducing the erosive concave-up profile (Winterwerp et al., 2013).

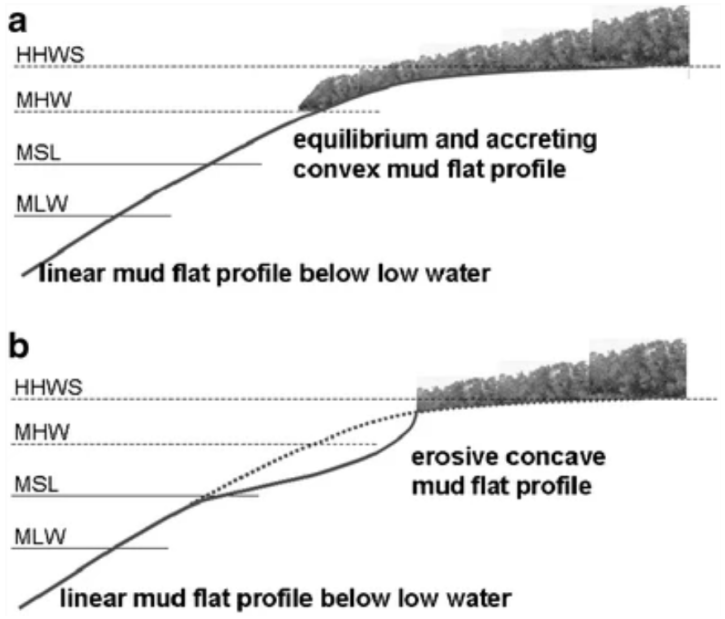

Figure 2.7: The two different profiles of muddy foreshores with the convex profile concurrent to states of accretion or equilibrium and the concave profile causing further erosion by allowing larger waves near the mangroves (from Winterwerp et al., 2013)

2.4. Morphodynamic Restoration Using Structures

This section expands upon the principle behind using temporary structures for rehabilitation of mangroves, examples of restoration projects using such structures and what we still need to understand about using permeable dams for restoration.

2.4.1. Do Permeable Structures Work?

The concept of employing permeable dams for mangrove rehabilitation draws from the Schleswig-Holstein method for salt marsh creation. In this method, interconnected sedimentation basins were created in front of the higher intertidal flats using permeable dams made of locally sourced natural materials (Winterwerp et al., 2020). The skeleton of such dams are formed by two rows of vertical poles of local wood between which brushwood bundles are used as the fill material (Winterwerp et al., 2020). The brushwood was found to be susceptible to damage from wave action and shipworm, and if not replaced early enough, affected the efficacy of the structures to induce sedimentation (Gijón Mancheño, 2022). These structures are installed in the field with gaps between them typically an order of magnitude smaller than their lengths, to allow for the influx of sediment-laden flow by the tide (Gijón Mancheño, 2022). The dams are designed to emulate the lost vegetation and are thus believed to play a role in reducing current velocities and dissipating waves, thereby enhancing the deposition of fine sediment.

Figure 2.8: Permeable dam in use in the Indonesian coastal region. The vertical poles act as the framework supporting the brushwood bundles (picture courtesy of A. Gijón Mancheño)

When currents come into contact with a structure, the ensuing flow separation produces drag forces on the framework of the structure, leading to energy dissipation and thus, lower velocities behind the structure. To estimate the drag forces on the structure, there are two key factors to consider, namely, blockage and sheltering. The presence of poles decreases the available cross-sectional area for the flow, consequently elevating the velocities between the elements due to mass conservation. This effect is referred to as blockage (Etminan et al., 2017). On the contrary, the poles also diminish the velocities acting on the downstream elements due to the creation of wakes behind the elements upstream. This phenomenon is termed sheltering (Etminan et al., 2017). The relative importance of the two processes is contingent upon the flow conditions, as well as the size and spacing of the poles (Gijón Mancheño, Jansen, Winterwerp, et al., 2021). From Figure 2.9, it can be seen that for a constant porosity of the structural arrangement of poles, higher resistance of the flow per element can be achieved for smaller spanwise spacing, which enhances blockage and, larger streamwise spacing, so that elements downstream experience less velocity reduction.

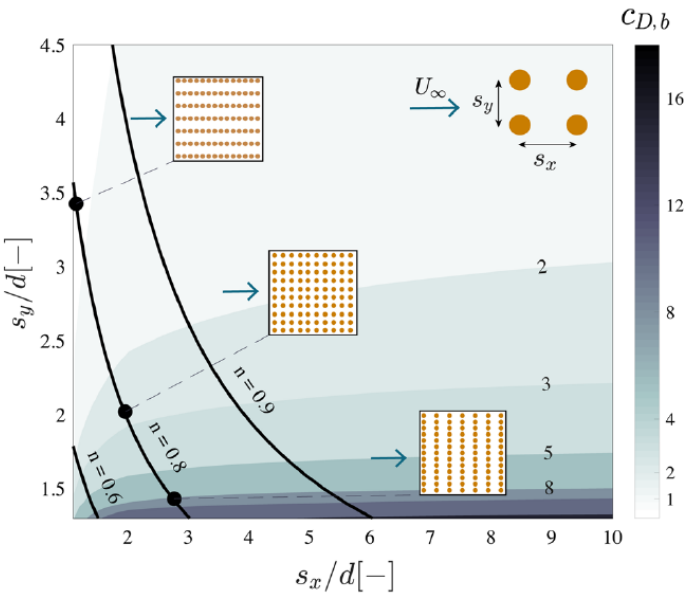

Figure 2.9: Predicted bulk drag coefficient $C_{D,b}$ as a function of the streamwise spacing s_x and spanwise spacing s_y of the poles compared to the pole diameter, d. The lines of constant volumetric porosity n are shown in black (from Gijón Mancheño, Jansen, Winterwerp, et al., 2021).

When a wave propagates through a permeable dam, part of its energy is reflected seawards, part is dissipated within the confines of the structure and, the rest is transmitted. The energy balance thus reads,

$$K_R^2 + K_D^2 + K_T^2 = 1 \tag{2.1}$$

where K_R, K_D and K_T are the reflection, dissipation and transmission coefficients respectively. The wave energy remaining after reflection traverses through the structure, exerting hydrodynamic forces, primarily in the form of drag and intertidal forces on the poles (Gijón Mancheño, Jansen, Uijttewaal, et al., 2021). This energy dissipation contributes to a reduction in the wave height transmitted through the dam. It is essential to aim for significant dissipation of the incoming wave energy, as excessive reflection can intensify local scour in front of the structure, and transmitted waves may trigger the re-suspension of fine sediment. In the case of long waves, the drag coefficient converges to that of steady flow (Gijón Mancheño, Jansen, Uijttewaal, et al., 2021). However, excessively narrow spanwise spacings, chosen to optimise resistance, can increase wave reflection and thus, the associated scour (Winterwerp et al., 2013). The dissipation by horizontal elements of the dam is more substantial due to form drag experienced in both horizontal and vertical directions, owing to the elliptical motion of water induced by waves (Suzuki et al., 2019). However, in shallow water, characterised by negligible vertical velocity components, orientation of the element becomes inconsequential (Winterwerp et al., 2020). Thus, the location of the structure and characteristics of the incoming wave can contribute significantly to the efficacy of the structure.

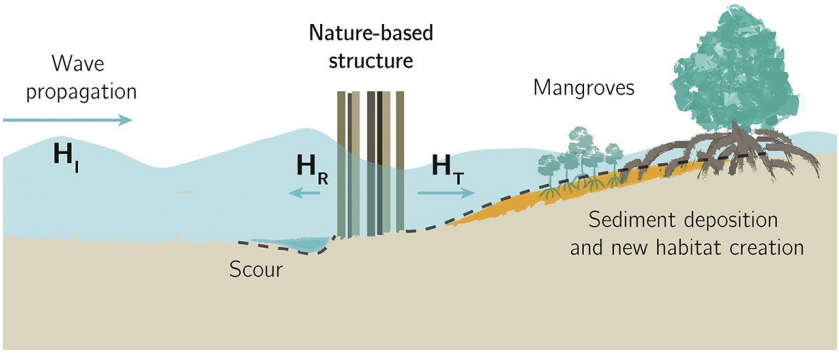

Figure 2.10: Wave transformation from its approach and travel through the permeable dam. The smaller wave height transmitted through the dam enables sediment deposition and potential mangrove colonisation (from Gijón Mancheño, Jansen, Uijttewaal, et al., 2021).

Permeable dams elevate bed levels behind them by attenuating both waves and currents. Research by Gijón Mancheño (2022) revealed that the depth at which the structure is situated significantly impacts its ability to trap sediment. While structures at deeper water have negligible influence on the coastline position, those above MSL are submerged for only a relatively small portion of the tidal cycle and hence do not cause substantial accretion behind them. However, considering longer time scales where land subsidence could be significant, structures in deeper waters were found to be more efficient (Gijón Mancheño, 2022). Consequently, when aiming for mangrove rehabilitation, the location of the dam plays a pivotal role in the success of the project. Furthermore, van Bijsterveldt et al. (2022) found that though the permeable dams utilised in the coastal region of Demak in Indonesia effectively trapped sediment, the established propagules were unable to thrive due to the extreme levels of subsidence in the area.

The salient features of permeable dams thus facilitate natural mangrove regeneration through the successful establishment of locally available propagules by creating the three distinct windows of opportunity as discussed in section 2.1.3. Firstly, by accumulating sediment and raising bed levels, the dams create an inundation-free period behind them. Subsequently, by dampening waves and currents and thus reducing the hydrodynamic forces on the propagules, they enable the development of roots to lengths necessary for surviving high energy events. In the absence or successful mitigation of stressors such as disease, predation, and similar factors, the established propagules can proceed to develop into robust trees within the ecosystem.

2.4.2. Restoration Project Examples

Knowledge of mangrove restoration projects at different locations across the world can provide useful insights into the spatial design and criteria for success and are therefore elaborated upon in this section.

Thailand

Coastal erosion has remained a persistent issue in the country, particularly noticeable in the Gulf of Thailand where erosion rates can reach up to 30 m/yr in certain areas (Winterwerp et al., 2005). This coastline is mostly muddy, with large areas of mangrove forests converted to aquaculture ponds. To combat erosion, various measures were implemented including low-crested revetments, sediment-filled geotextiles and bamboo fences with densely spaced single rows of poles (Winterwerp et al., 2020). Notably, the bamboo fencing was effective in enhancing sediment deposition at rates of 20-25 cm/yr (Saengsupavanich, 2013). However, during storms, the planted mangrove seedlings were often uprooted by high waves, resulting in their inability to survive (Saengsupavanich, 2013).

Vietnam

The Mekong Delta in Vietnam faces a number of challenges from urban development, unsustainable use of natural resources to sea-level rise and increased intensity of storms. Combination of such factors have led to erosion of the muddy coastline (Schmitt and Albers, 2014). To counteract the problem, T-shaped permeable dams were constructed at numerous locations (Winterwerp et al., 2020). The function of the long-shore dam component was to dampen the incoming wave energy, while that of the cross-shore component was to diminish the alongshore currents. Openings of about 20 m were made in the long-shore dams to allow for the influx of sediment and induce drainage (Winterwerp et al., 2020). Additionally, two types of brushwood bundles, stiff and flexible, were tested. Flexible bundles were found to be more efficient than their stiff counterpart in damping waves, with the former capable of inducing up to 80% reduction of the incoming wave height (Schmitt et al., 2013). It was found that the reduction in wave heights behind the dams also helped with the consolidation of the deposited mud, thereby increasing its stability against erosion (Winterwerp et al., 2020). Natural regeneration of mangroves was observed a few years after the erection of the dams.

Figure 2.11: Wave damping observed behind the T-shaped dams in Vietnam (picture courtesy of R. Sorgenfrei).

Indonesia

Indonesia has long-suffered from shoreline erosion and deforestation of mangroves due to urbanisation, conversion to aquaculture and subsidence (Ilman et al., 2016). Addressing this issue, a seawall constructed using concrete cylinders was implemented in Timbulsloko. Within approximately two years of its installation, sedimentation up to MSL occurred behind the seawall, and mangrove seedlings were observed one year thereafter (Winterwerp et al., 2020). Presently, a mature mangrove canopy has flourished behind the structure (see Figure 2.12). However, as a fully reflective hard structure, the seawall has contributed to the development of significant scour in front of it, inhibiting seaward expansion of the forest (Winterwerp et al., 2020).

At a nearby location, permeable dams were later erected to aid mangrove rehabilitation in the area (Ecoshape, 2015). In the extensive monitoring campaign for the project, it was noted that bed levels behind the dams rose considerably during the first twelve weeks, after which the trend plateaued (Deltares, 2021b). Winterwerp et al. (2020) notes that after the initial period of deposition, when the area behind the dams became intertidal, T-shaped dams would have served better to enhance sediment influx. Another important discovery emphasised the acute necessity of regular maintenance, without which, the degraded structures lost all the accumulated sediment. Mangroves were found to persist in only a few highly protected areas and diminished elsewhere after a year or two, largely due to subsidence (Deltares, 2021b; van Bijsterveldt et al., 2022).

Figure 2.12: Seawall of concrete cylinders in Timbulsloko with the growth of dense mangrove forest behind the structure (picture courtesy of COREM-UNDIP)

2.4.3. Knowledge Gap

Permeable dams, typically constructed from brushwood and locally-sourced wood, have been deployed in several locations, some of which are highlighted in section 2.4.2, to mitigate erosion and restore eroding mangrove coastlines. To effectively utilise such structures, the development of design guidelines is imperative, drawing from empirical knowledge, physical and numerical system modelling, and field measurements. Previous experiences with these temporary structures have yielded valuable empirical knowledge, leading to the establishment of qualitative design guidelines and success criteria (Winterwerp et al., 2020). Furthermore, investigations into quantifying the impact of these dams on waves, currents, and morphodynamics through physical modelling and select field measurements have contributed to defining criteria for the optimal arrangement and usage of structural components (Gijón Mancheño, 2022).

Nonetheless, despite these advancements, a comprehensive understanding of the systemic implications of using permeable dams remains a largely uncharted territory. Previous attempts to gain such insights, particularly within the pilot study area of Demak in Indonesia, implemented permeable dams as thin, hard, fully reflective structures in their numerical models which are not truly representative of the dams (Smits, 2016). Furthermore, the influence of design parameters, such as the permeability of the structure and spatial configuration, including aspects like structure length and size of openings, has not been explored in prior research, necessitating a comprehensive large-scale investigation. Therefore, the present study is focused on assessing the influence of various structures, encompassing both temporary and hard variants, on sediment and propagule pathways within the Demak coastal system. Beyond uncovering how these structures impact sediment and propagule transport in their vicinity, an examination of potential large-scale alterations in transport patterns within the entire system, spanning from source to sink, due to these interventions could provide invaluable context for the development of tailored design guidelines for these structures, specifically attuned to the system under consideration.

2.5. Summary

Mangrove ecosystems consist of trees and shrubs that grow at the interface between land and sea in tropical and sub-tropical latitudes, and provide a multitude of ecosystem services. Mangroves reproduce through propagules, which are seeds that germinate while still attached to the parent tree. The process of dispersal is crucial for the distribution and connectivity of mangrove populations, and depends on factors ranging from propagule characteristics such as their density and buoyancy to wind and water currents. The dispersed propagules on reaching a favourable location can establish as seedlings which grow into mangrove trees. For successful establishment, an inundation-free period and growth of roots to adequate lengths such that the seedlings can withstand hydrodynamic forces are required. For long-term survival, genetic diversity of mangrove systems and ample sediment supply are crucial.

Loss of mangroves across the world can be attributed to mainly anthropogenic causes such as deforestation for commodities and land-use change, and natural erosion of shoreline. Furthermore, when rates of relative sea-level rise are such that sediment supply cannot keep up, erosion of the shoreline and thereby, the lateral retreat of mangroves is inevitable. In muddy coastlines, seaward retreat of mangroves is amplified with steep foreshores which creates an erosional feedback loop and disturbance in the sediment balance.

For mangroves to be restored where lost, the drivers of loss at the site should at first be prevented from recurring. At sites with limited propagule availability, planting of mangrove seedlings can be considered. It is imperative to ensure the accurate species selection and their planting at suitable locations within the system. Natural regeneration of mangroves has been achieved predominantly through the use of structures. Hard structures however can do more harm than good in muddy environments, where reflection of the incoming wave can erode the fine sediment and possibly induce liquefaction and thereby, the collapse of the structure.

When temporary structures are used, they can help rehabilitate mangroves by emulating the lost vegetation and damping both waves and currents such that the sediment influx can deposit and elevate bed levels behind the structures. The depth at which the structure is situated was found to significantly impact its ability to trap sediment. Permeable dams must be able to raise and maintain bed levels to the extent that the established seedlings are not uprooted during high-energy events. From previous experience in Indonesia and Vietnam, it was found that T-shaped permeable dams would serve better at the intertidal areas, with the cross-shore component reducing the alongshore current magnitudes and enhancing sediment deposition.

Presently, an ample empirical knowledge from past experiences with using permeable dams to restore mangrove coastlines and, quantification of the impact of such dams on waves and currents have contributed to the development of design criteria for the structures. However, a systemic understanding of the implications of using permeable dams, and their various design parameters and spatial configurations on the sediment and propagule pathways, is still unknown.

3

Study Area

This chapter describes the characteristics of the study area of the Demak coastal system in Indonesia, which extends from Semarang to the Wulan river delta.

3.1. Location

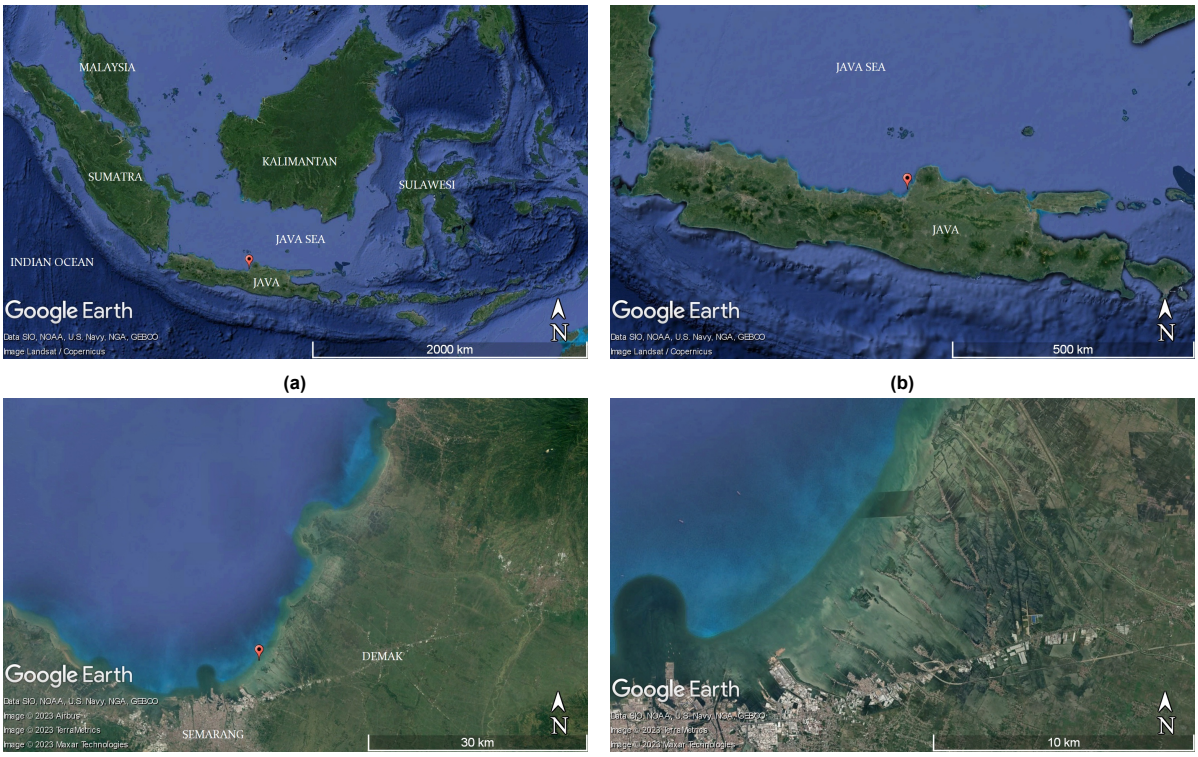

Figure 3.1: Overview of the study site at different spatial scales: a) The Indonesian archipelago b) The island of Java c) The coastal system of Demak and d) The intertidal basins of Timbulsoko

The study area for this thesis is the Demak coastal system, seen in Figure 3.1 at different scales. This location was chosen for the study since pilot projects on the use of temporary structures to rehabilitate

mangroves and subsequent studies on various phenomena have been carried out at the site (see Ecoshape, 2015; Gijón Mancheño, 2022; Tas, 2022; van Bijsterveldt et al., 2020).

Demak is a regency in Central Java, Indonesia, bordering the Java Sea in the northwest, the city of Semarang in the southwest and the Wulan river in the northeast. The coastal system of Demak is a part of the Java Sea, partially enclosed by Kalimantan to the North and Sumatra to the West, thus creating a shallow, sheltered basin. Situated near the equator, the area is home to a tropical monsoon climate (Tas et al., 2020). The location also has a persistent land subsidence problem with observed subsidence rates up to about 19 cm/year in Semarang (Abidin et al., 2016).

3.2. Site Characteristics

This section expounds upon the meteorological, hydrodynamic and morphodynamic characteristics of the Demak coastal region.

3.2.1. Meteorology

The study site, located in the tropical zone, is characterised by a seasonally reversing monsoon climate. The yearly climate is characterised by two predominant seasons, with the northwest monsoon (NW) running from December to March, and the southeast monsoon (SE) from April to October (Tas, 2022).

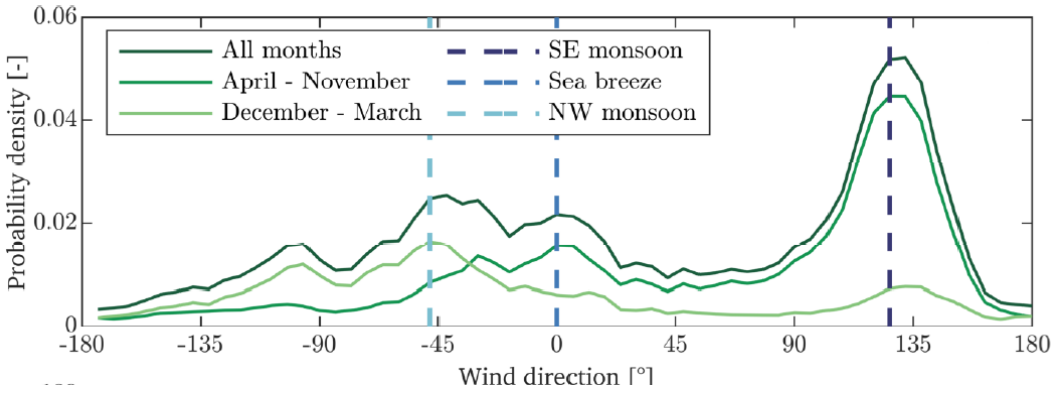

Figure 3.2: Probability density function of the wind direction over one year and during the NW and SE monsoon seasons with the peak wind directions of sea breeze and the two seasons indicated using dashed lines (from Tas, 2022). The general shoreline is oriented at about 31° from N (not indicated in the figure).

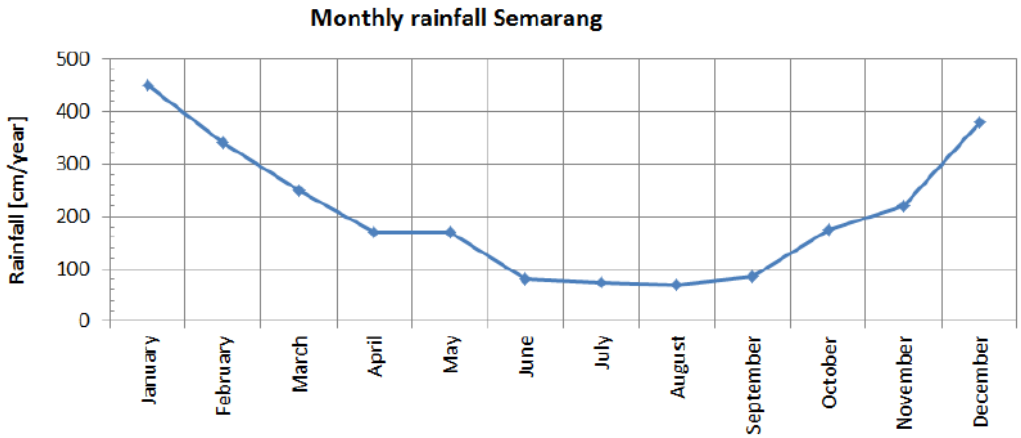

Figure 3.3: Monthly distribution of rainfall in Semarang (from Bayong Tjasyono et al., 2008).

The prevailing wind directions of NW during the NW monsoon and SE during the SE monsoon are shown in Figure 3.2. In addition to the principal monsoonal winds, a sea breeze primarily from the North, arising from differences in temperatures of land and sea, is also prevalent (Tas, 2022; Bosboom and Stive, 2021). The rainfall distribution in a year also varies depending on the monsoons (see Figure 3.3). The wettest months of the year occur during NW monsoon from December to February, with a mean rainfall of about 4 to 5 m/yr, whereas the driest months of June to August with average rainfall of approximately 1 m/year are during the SE monsoon season (Bayong Tjasyono et al., 2008). Consequently, the NW monsoon is commonly denoted as the wet season, while the SE monsoon is known as the dry season.

3.2.2. Hydrodynamics

River Discharge

Freshwater discharge in the study area is primarily from the Wulan River. The seasonal variation in rainfall in the region is a good indicator for the distribution of discharge from the Wulan river as seen from Figure 3.4. According to the records of Klambu Station, 48.63 km south of the river mouth, freshwater of as much as 350 m^3/s is discharged into the Wulan River (Fadlillah et al., 2019). The river bifurcates into two main channels called New Wulan River (NWR) and Old Wulan River (OWR). Owing to the intense sedimentation and decrease of water depth in the OWR, the NWR was intentionally developed to avoid flooding (Fadlillah et al., 2019). The average discharge from Klambu Station during the wet season (October to May) is 138.18 m^3/s, whereas the discharge amount during the dry season is 31.6 m^3/s (Fadlillah et al., 2019). Since the Klambu station is far from the mouth of the river, it does not present an accurate distribution of the discharge near the coast. At a measurement station near the coast before the river bifurcates, the average discharge of 2016 was measured to be 132.95 m^3/s in the wet season and, 63.14 m^3/s in the dry season. Additionally, the sediment load of the Wulan River discharge is a main source of local sediment supply to the coastline (Bisschop, 2023). However, based on the information obtained from local communities, sediment supply from the river is decreasing due to agricultural and urban development upstream.

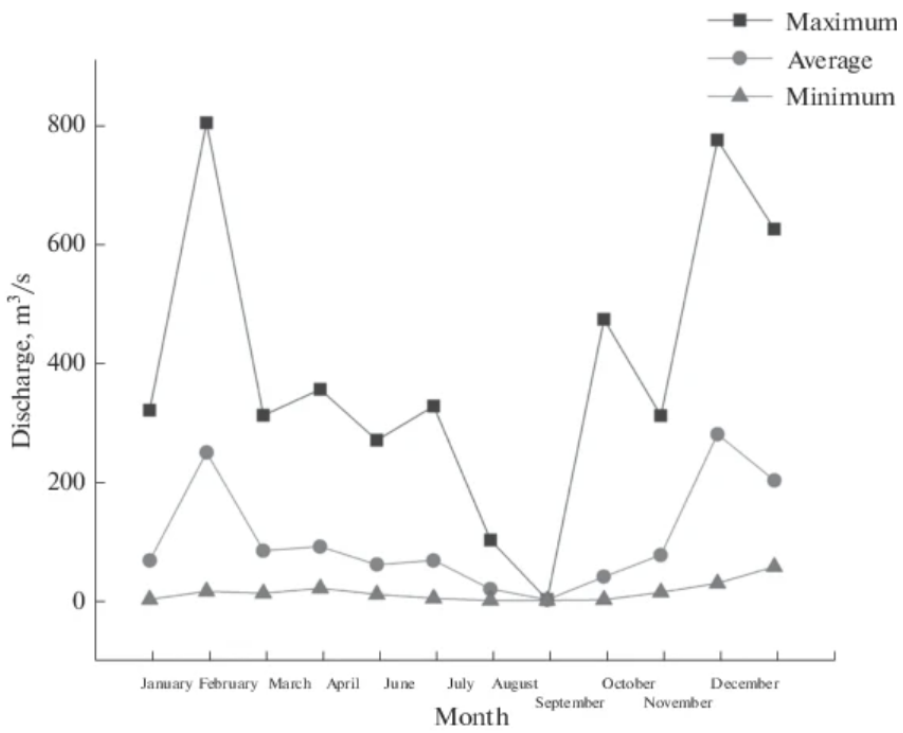

Figure 3.4: Monthly distribution of maximum, average and minimum discharge from the Wulan river measured at Klambu station (from Fadlillah et al., 2019).

Waves

The wave climate off the coastline of Demak also exhibits seasonal variations dependent on the monsoons. During the SE monsoon season, the general offshore wind direction contributes to mild wave conditions. Conversely, during the NW monsoon season, which is characterised by winds from the NW, larger waves, often reaching up to 2.5 meters in height with a period of about 5.5 s are generated (Smits, 2016; Deltares, 2020). The wave pattern during the SE monsoon season primarily features waves originating from the SE throughout most of the day, with a notable shift in the afternoon when waves start coming from the N due to the influence of the sea breeze (Tas, 2022). Mean wave heights of 0.5 m have been measured near the Demak coastline (Deltares, 2020).

Tide

In the coastal region of Demak, the tidal characteristics are primarily diurnal, with smaller semi-diurnal components, classifying it as a mixed tide (Tas, 2022). The tidal constituents determined by Tas (2022) through tidal harmonic analysis on water level data from 2016 to 2018 collected at the port of Semarang, are provided in Table 3.1.

Constituent	Name	Period [hr]	Amplitude [m]	Phase [deg]
K1	Lunar-solar declinational (diurnal)	23.93	0.226	245
M2	Principal lunar (semidiurnal)	12.42	0.103	55
S2	Principal solar (semidiurnal)	12.00	0.083	308
O1	Principal lunar (diurnal)	25.82	0.079	132
P1	Principal solar (diurnal)	24.07	0.071	247
SSA	Solar (semiannual)	4383	0.047	156
N2	Lunar elliptical (semidiurnal)	12.66	0.042	18
K2	Lunar-solar declinational (semidiurnal)	11.97	0.035	347
S1	Solar (diurnal)	24.00	0.022	64

Table 3.1: Primary tidal constituents in Semarang (from Tas, 2022)

The form factor, determined from the tidal constituents as:

$$F = \frac{K1 + O1}{M2 + S2} \tag{3.1}$$

was found to be 1.72, indicating the mixed diurnal nature of the tide (Tas, 2022). This mixed tide exhibits daily inequalities and variations in the spring-neap cycle, leading to an irregular periodicity (Smits, 2016). The spring tidal range is usually around 1 m, thereby falling into the micro-tidal regime (Tas, 2022; Bosboom and Stive, 2021).

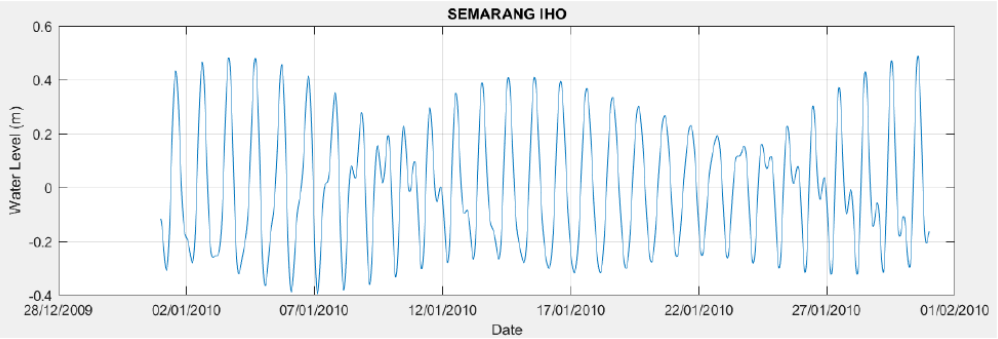

Figure 3.5: Water levels measured in Semarang IHO station downloaded from Delft DashBoard (from Bisschop, 2023).

Despite the general rule that tides propagate counterclockwise in the northern hemisphere and clockwise in the southern hemisphere, the tidal propagation in the Java Sea is complex due to its geographical location, bathymetry and surrounding land masses (Smits, 2016). The M2 tidal wave arrives from the Indian Ocean through the Flores Sea, while the K1 tidal wave comes through the Makassar strait from the Pacific Ocean. These two main constituents propagate westward in the Java Sea, creating a counterclockwise phase propagation, even though the region is in the southern hemisphere (Hatayama et al., 1996; Yusuf and Yanagi, 2013).

Currents

The broader oceanic circulation in the region is a consequence of the large-scale wind-driven circulation (Smits, 2016). Owing to the marked regularity and seasonal consistency of the monsoon, the residual ocean currents along the coast exhibit similar cyclic patterns, reversing their course twice annually. Specifically, during the period from May to September, the southeast monsoon propels the residual currents westward (Wyrtki, 1961). Conversely, in the presence of the northwest monsoon and during the transitional months spanning from October to April, the residual currents shift eastward (Wyrtki, 1961). Near the coastline, these currents primarily flow from the northeast to the southwest. These nearshore currents are characterised by their limited strength, resulting in minimal impact on sediment transport processes (Smits, 2016). Wave-induced currents are considered negligible, due to the low wave energy on mild foreshore slopes (Smits, 2016).

3.2.3. Morphodynamics

Bathymetry

The Demak coastal zone is very shallow, with slopes of about 1:1000 or even 1:1500 in stable and/or accreting areas, which are typical for mud-mangrove coasts (Deltares, 2020; Winterwerp et al., 2020). At eroding locations, comparatively steeper concave-shaped foreshores with slopes of about 1:600 have been observed (Deltares, 2020). Sediment deposited at the Wulan River mouth can form cheniers, which are narrow lenses of sand, under wave forcing (Tas, 2022). These cheniers can cause waves to break, thereby possibly inducing sedimentation behind them and stabilising eroding coastlines (Tas et al., 2020).

Sediment Characteristics

The substrate in the region consists primarily of muddy (80%) and sandy (20%) sediments that are spatially heterogeneous (van Domburg, 2018). van Domburg (2018) provided an analysis of sediment grain sizes along two distinct transects within the Demak area, one displaying accretion and the other undergoing erosion shown in Figure 3.6. The accreting transect is defined by the presence of a chenier and a vegetated area situated between the chenier and the coastline. Table 3.2 presents the grain size data for both transects. Upon examining the grain sizes, it is evident that the eroding transect contains coarser sediment (with a D_{50} of 24 µm) in contrast to the accreting transect, which features finer sediment (with a D_{50} of 12 µm), excluding location A3 at the chenier. In both transects, smaller grain sizes are observed closer to the shoreline, where the substrate transitions to a muddier composition. Furthermore, the chenier within the accreting transect is characterised by a predominantly sandy sediment composition (with a D_{50} of 145 µm), while Tas (2022) posited that the bed is primarily composed of mud with a minor sand fraction, featuring a D_{50} of 235 µm at the cheniers.

Furthermore, permeable dams used to trap sediment and rehabilitate mangroves at the eroding transects, are mostly implemented at a distance of about 100 to 200 m from the mangrove fringe in the region where sediment of size D_{50} = 57.61 µm are found.

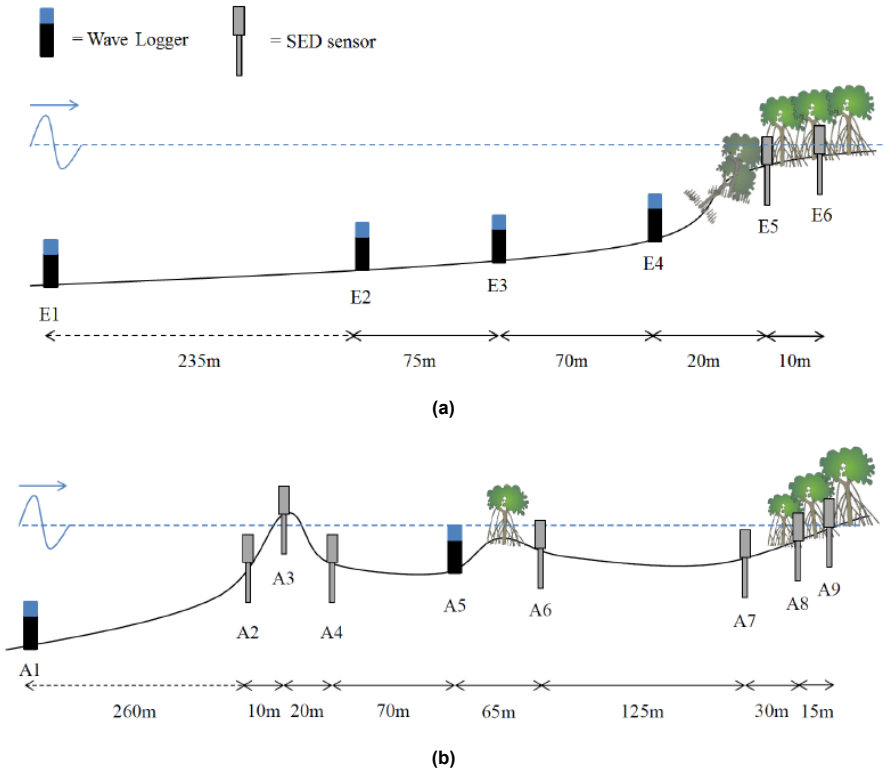

Figure 3.6: Schematisations of the experimental set-up at a) eroding transects and b) accreting transects

Location	D_{50} [µm]	Location	D_{50} [µm]
A1	13.94	E1	24.54
A2	12.47	E2	32.95
A3	145.22	E3	57.61
A5	10.68	E4	9.95
A6	27.05	E5	7.00
A7	7.35	E6	9.59
A8	7.28		
A9	6.42		

Table 3.2: Sediment grainsize per location

3.2.4. Mangroves

Avicennia marina (grey or white mangroves) and *Rhizophora mucronata* (red mangroves) are the most dominant species in Demak with an ample amount of propagules available in the region (Ecoshape, 2015). *Avicennia marina* is a pioneer species in Demak, which colonises intertidal regions above MSL (see also section 2.1.4), while *Rhizophora mucronata* is present chiefly along the river banks (Verschure, 2013). Considering the limitations for seedling establishment and growth, van Bijsterveldt et al. (2022) found that *Rhizophora mucronata* had a higher survival (67%) but lower growth rate, whereas *Avicennia marina* had lower survival rates (21%) but significantly higher growth rates.

3.3. Shoreline Erosion

Shoreline erosion in Demak is a complex issue driven by various factors. Prasetyo et al. (2019) conducted a study that found the absolute sea level rise to be increasing, with the coastline of Demak retreating significantly in recent years. However, erosion of the coastline is primarily caused by local land subsidence due to the excessive withdrawal of groundwater, natural consolidation, and the added load of construction in the area (Marfai and King, 2007). Rates of land subsidence vary across the region, with higher subsidence near urban areas such as Semarang, which are typically an order of magnitude higher than eustatic sea level rise in the region (Deltares, 2021a; van Bijsterveldt, Herman, et al., 2023).

Furthermore, the historical development of human interferences has significantly impacted the sediment budget, especially in Demak and Semarang (Marfai, 2011). The removal of mangrove forests in favour of shrimp ponds has led to the loss of historic deposits, contributing to coastal erosion (Ecoshape, 2015). This loss of mangrove habitat has reduced the resilience of the coast resilience and initiated a self-accelerating erosion process (Winterwerp et al., 2013).

The combination of land subsidence and sea level rise makes the Demak coastal system highly vulnerable to episodic events, which can lead to significant coastal erosion in short periods of time.

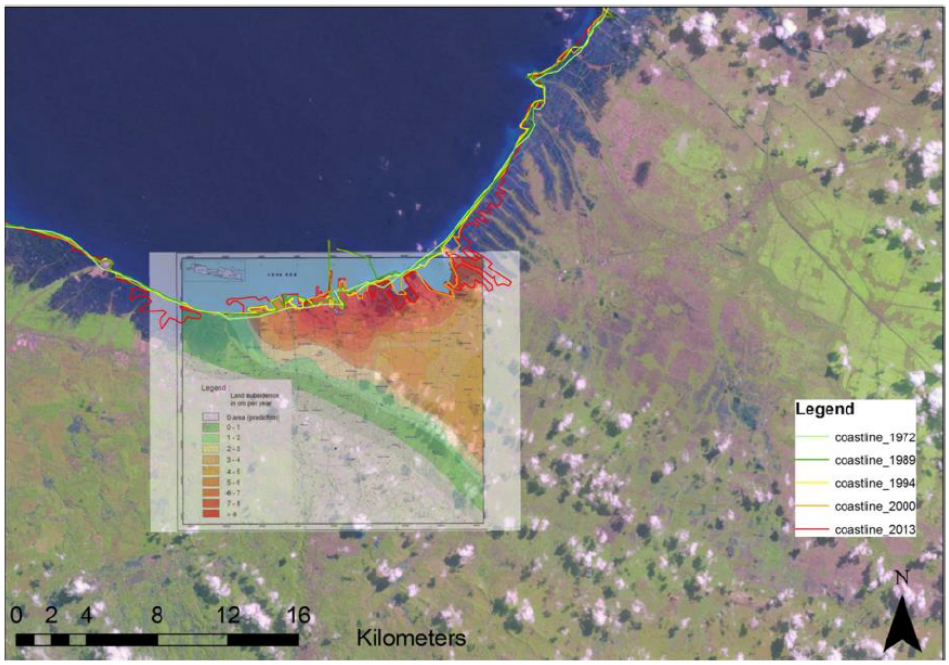

Figure 3.7: Overlay of subsidence in and around Semarang (the redder the colours the larger the subsidence) on the coastline retreat in the area since 1972 (from Ecoshape, 2015).

4

Modelling

This chapter expands upon the selection of the modelling software used, model set-up in Delft3D and provides an overview of SedTRAILS as a particle tracking tool and describes its implementation.

4.1. Model Selection

To model the relevant processes in the Demak coastal region, a hydrodynamic numerical model is required. A Lagrangian model is then needed to model the pathways of sediment and propagules based on the hydrodynamic output from the process-based model. Two alternatives of Delft3D and Delft3D-FM were considered to model flow in the study area. This section elaborates on the considerations that led to the choice of software.

Delft3D uses a structured grid for numerical modelling of the processes in the system. A grid is said to be structured when grid cells are well-ordered and array-like indices in three dimensions can be used to label and identify the different elements. With an unstructured grid, grid cells can be joined in any manner (FLOW-3D, 2022). The Delft3D-FM suite uses an unstructured grid which can be used to couple large regions with quadrangles using cells of other types such as triangles with relative ease. Grid refinement where necessary is then easily done with an unstructured grid whereas, with a structured grid, curvilinear grids are used for this purpose, which is not as computationally effective as the former. Delft3D-FM can therefore be preferable and computationally less expensive to model coastal processes when compared to Delft3D. However, nesting a smaller grid with a higher resolution in the area of interest within the larger domain of the overall grid is possible in Delft3D, and is a viable alternative.

For the present study, an important consideration when choosing the modelling software was the possibility of implementation of permeable structures. In Delft3D, structures of varying permeability can be implemented, which can be calibrated to well-represent the temporary structures used to rehabilitate mangroves in the study area. Delft3D-FM can currently only model structures as impermeable. Since the main aim of the thesis is to understand the impact of structures permeable and impermeable on the sediment and propagule pathways in the system, Delft3D was chosen to model the domain of interest.

4.2. Delft3D

Delft3D-4 can carry out numerical modelling of flows, sediment transport, waves, water quality, morphological developments and ecology (Deltares, 2018a). The Delft3D framework is composed of several modules, grouped around a mutual interface, while being capable to interact with one another. Most

notable of them are the Delft3D-FLOW and -WAVE modules which are used to model flow and, wave generation and propagation, respectively.

The WAVE module utilizes the SWAN (Simulating WAves Nearshore) model to simulate the evolution of random, short-crested wind-generated waves (Deltares, 2018c). Delft3D-FLOW on the other hand is a multi-dimensional (2D or 3D) hydrodynamic and transport simulation program which calculates non-steady flow and transport phenomena that result from tidal and meteorological forcing on a rectilinear or a curvilinear, boundary fitted grid (Deltares, 2018b). The module can also model density driven flows in terms of differences in salinity with time varying sources and sinks like river discharges and, temperature with heat flux models. Sediment transport and the associated change in morphology can also be computed using the FLOW module, but within this project changes in morphology are neglected to keep the model morphostatic by way of which the computational time remains reasonable. For 3D simulations, the model is resolved vertically into a user-specified number of layers in either the σ-grid with fixed number of layers or the Z-grid with fixed layer thickness.

4.2.1. Nested Flow Model Set-Up

Domain

A nested model was implemented in Delft3D with two grids, one covering a larger domain across the Demak coastal system with a lower resolution and, another smaller grid with a higher resolution nested within the larger model close to the coast where permeable structures are used to restore mangroves. The domain of the overall model is representative of the Demak coastal system and obtained from Bisschop (2023). It extends from the Wulan river delta to the North, to the city of Semarang at the southern end of the model domain (50 x 23 km) at a latitude of about -6.9 degrees. Grid size of 333 m by 333 m is enforced for the overall model. In the vertical direction, the σ-grid is used with 14 layers of increasing thickness from 2% from both the bottom and the surface layers, producing a grid with layers of thickness [2, 3, 4, 6, 8, 11, 16, 16, 11, 8, 6, 4, 3, 2]%. The gradually varying layer thickness allows for resolving the logarithmic profile of the horizontal velocity components and to account for wind as a main driving force of flow.

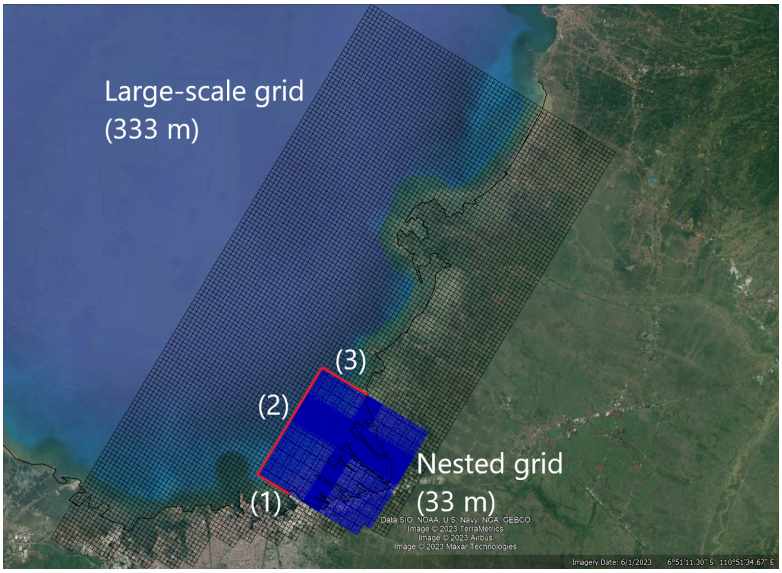

Figure 4.1: Grids used for computation in Delft3D (overall large-scale grid in black and nested grid in blue) with the land boundary (black line). The three open boundaries are annotated as (1) South boundary, (2) Offshore boundary and (3) North boundary

The domain of the nested model extends 10 km by 10 km in the intertidal area near Timbulsloko. A grid of varying grid size from 100 m by 100 m near the edges, with further refinement to a size of 33 m

at the area of interest to better resolve processes there, was used. The nested model is also enforced with a vertical σ-grid of 14 layers.

Bathymetry

The bathymetry for the overall model was adapted from Bisschop (2023), originally built from the General Bathymetric Chart of the Oceans (GEBCO'08) dataset from Delft dashboard and corrected where needed using the QUICKIN tool in Delft3D (van Ormondt et al., 2020). The dataset was also extended in a few regions with additional control contours and sounding point data. It is a continuous digital terrain model for ocean and land, with land elevations derived from the Global Land One-km Base Elevation (GLOBE) database.

Bathymetry of the nested model is a combination of the GEBCO dataset offshore and field measurements used in Deltares (2020) at the intertidal region. The combined bathymetry of the model was modified at the intersection of the two datasets using QUICKIN to smooth out any sharp gradients created due to combining the two different datasets (see Appendix A).

Bathymetry at the intertidal area of the overall model was also modified based on the field measurements from Deltares (2020). The final bathymetry used in the two models can be seen in Figure 4.2.

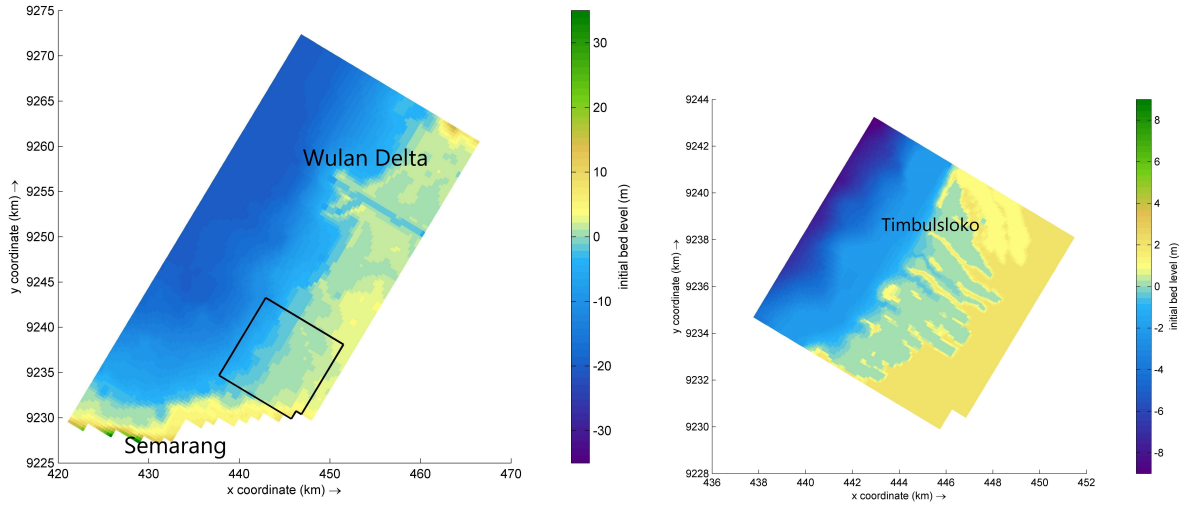

Figure 4.2: Bathymetry of a) the overall model with the outline of the nested model domain (black line) and b) the nested model

Time Frame

The coastal system of Demak is characterised by a NW monsoon (wet season) that runs from December to March and a SE monsoon (dry season) from April to October (Tas, 2022). Owing to the orientation of the coastline, the NW monsoon season has winds directed onshore and hence higher waves. Conversely, the dry season is characterised by calm conditions due to offshore directed wind. Hence, sediment transport is found to be negligible during the dry season and is not considered for the study (Bisschop, 2023). The simulation period for both models is chosen to be the full month of January in the wet season. A timestep of 1.5 minutes is chosen for the overall model and 0.5 minutes for the finer nested model owing to the Courant limitation.

Tide

Tide in the study region is classified as mixed and mainly diurnal, with the spring-neap variation dominated by a smaller semi-diurnal component (Tas, 2022). Tidal signal for a simulation period of the month of January is forced as the open boundary condition in the overall model with astronomic components. The required components are obtained from the global tidal model in Delft DashBoard (van Ormondt et al., 2020) for boundaries divided into smaller sections to account for tidal phase lag (Bisschop, 2023).

In the nested model, tide is forced as the boundary condition as a time-series of water level obtained from the results from the overall model run. Here the boundaries are sectioned based on the gradient of the bathymetry to allow for a more accurate interpolation.

A reflection parameter of 1000 s^2 and 300 s^2 is implemented in the overall and nested models respectively. Since the reflection coefficient is directly related to the time taken for a free surface wave to travel from the boundary on one end to the other of the domain, a smaller value of the coefficient is computed for the nested model and implemented as such (Deltares, 2018b).

River Discharge

Discharge from the Wulan river varies throughout the year with large fluctuations between the wet (November to March) and dry (May to September) seasons. The mean discharge during the wet season in 2016 recorded at a station near the mouth was 132.96 m^3/s (Bisschop, 2023). As the month of January during the wet season is chosen as the simulation period, the average discharge during the wet season is used as a boundary condition across the river.

Currents

Currents from each of the 14 vertical layers of the overall model are used as a boundary condition in the nested model. This allows for more control over the magnitude and direction of currents near the boundaries where necessary.

Wind

Wind in the Demak region is characterised by different directions and average magnitudes for the two predominant seasons prevailing there. Wind is offshore-directed from WNW during the NW monsoon season and onshore-directed from ESE during the SE monsoon season. For simplicity, a constant wind speed of 4.4 m/s from 292.5° is used in the model, corresponding to the wet season (Smits, 2016).

Physical Parameters

A uniform bottom roughness coefficient computed with the Manning formula is implemented in both overall and nested models at a value of 0.012 s/$m^{1/3}$.

The horizontal eddy viscosity and diffusivity values were an order larger near the open boundaries offshore for the overall model with values of 10 and 7 m^2/s respectively compared to the rest of the domain. This is done so as to eliminate any unwarranted circulatory currents near the boundaries. The eddy viscosity values provided as input to the model is depicted in Figure 4.3. Concurrently, domain of the nested model has an initial viscosity of 1 m^2/s in the overall model and hence is implemented as such in the nested model. Sub-grid Horizontal Large Eddy Simulation (HLES) is activated in both models with dimensional number 3 and a Prandtl-Schmidt number of 0.7.

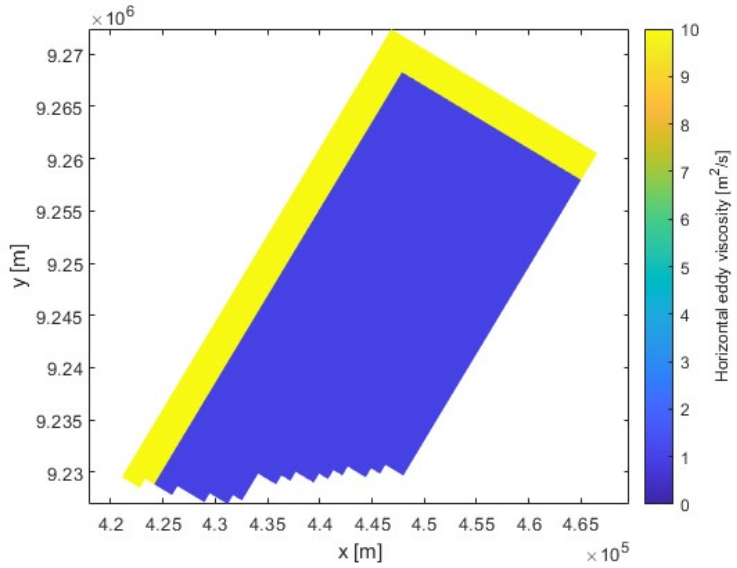

Figure 4.3: Horizontal eddy viscosity input to the overall model with higher values of viscosity offshore

Structures

The steady-state sub-critical flow rate, Q through a hydraulic structure is related to the difference between the upstream and downstream water levels:

$$Q = \mu A \sqrt{2g|\zeta_u - \zeta_d|} \tag{4.1}$$

where μ is the contraction coefficient that can range from 0 to 1, A is the wet flow-through area and ζ_u and ζ_d are the upstream and downstream water levels respectively. The contraction coefficient in Equation 4.1 is dependent on the type of hydraulic structure modelled (Deltares, 2018b). An assumption of local equilibrium between the force on the flow due to the obstruction and the local water level gradient is made. For a Q-H relation at a U-velocity point,

$$g\frac{\zeta_u - \zeta_d}{\Delta x} = \frac{Q^2}{2\mu^2 A^2 \Delta x} = c_{loss-U}\frac{U_{m,n}|\vec{U}_{m,n}|}{\Delta x} \tag{4.2}$$

the resistance coefficient c_{loss-U} acts as an input parameter for the structure (Deltares, 2018b).

The permeable dams used in the field are represented in the model using the additional parameter of porous plate in Delft3D. A porous plate is a semi-permeable structure that extends into the flow along one of the grid directions, that covers some or all layers in the vertical (Deltares, 2018b). Its thickness is much smaller than the grid size in the direction normal to the porous plate. As a partially transparent structure, it allows for exchange of mass and momentum across its length (Deltares, 2018b). The porosity of the plate is controlled by friction with the resistance coefficient c_{loss-U} from Equation 4.2 as an input parameter. To approximate the current patterns through and around the permeable dams observed in the field similar to that depicted in Figure 4.4, the resistance coefficient was tested for values ranging from 1 to 1000. The residual and instantaneous depth-averaged current velocities across the porous plate in the test model for the different resistance coefficients are illustrated in Figure 4.5 and Figure 4.6 respectively. Values of resistance coefficient were chosen such that the porous plates were able to substantially reduce the current velocities through them, thereby inducing a proclivity for flow to traverse between the structures than through them. A value of 10 for the resistance coefficient simulates a reduction in residual current velocity of approximately 50% when compared to thin dams (see Figure 4.5). However, during rising tide at the location, a value of 20 for the resistance coefficient induces a

similar effect (see Figure 4.6). Hence, values in the range of 10-20 were chosen for the porous plates dependent on their location. Location of the structures implemented in the model is pictured in Figure 4.7. The values of resistance coefficient enforced for the different porous plates are provided in Table 4.1. Comparison of the residual and instantaneous current velocities across the six different plates are provided in Appendix B.

Figure 4.4: Streak lines of current patterns in the presence of permeable dams in Timbulsloko. Elevated flow velocities through the gaps between the structures can be ascertained from the darker lines accentuated by the yellow curves.

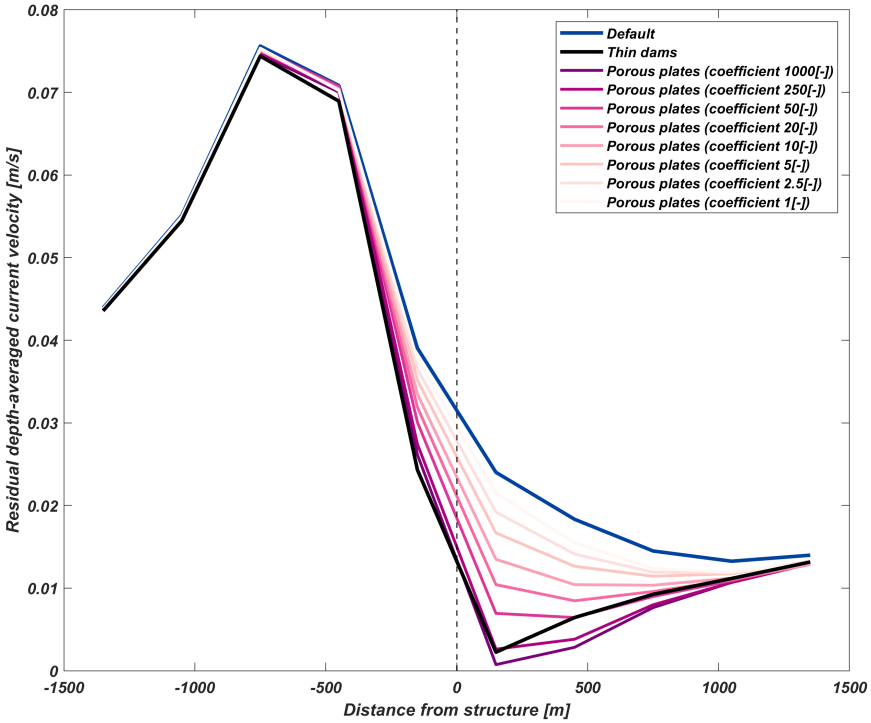

Figure 4.5: Residual depth-averaged currents over one month for the different cases of structural presence and values of resistance coefficient of the porous plates

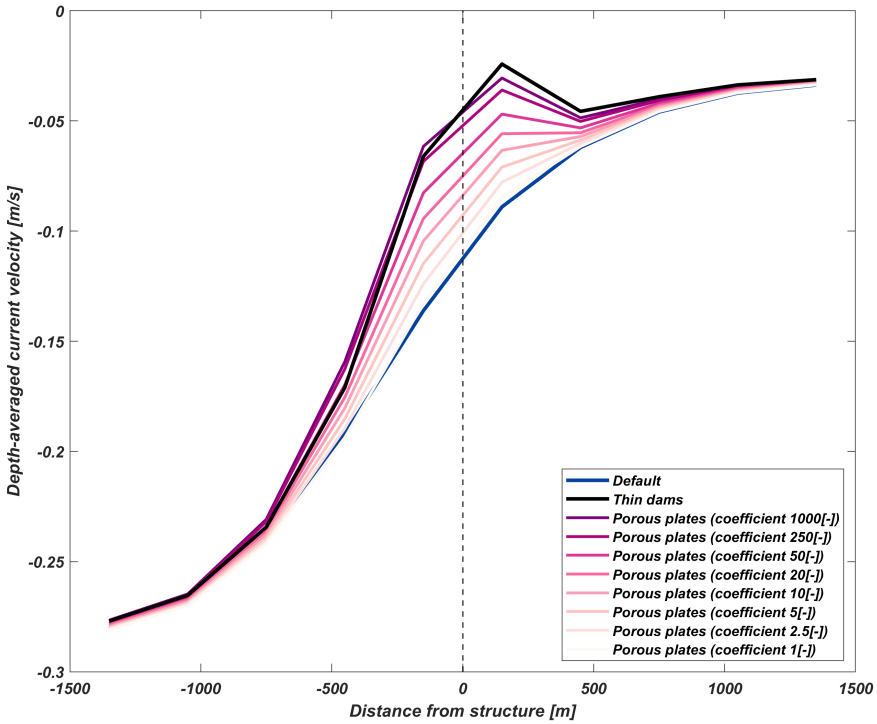

Figure 4.6: Depth-averaged currents during rising tide for the different cases of structural presence and values of resistance coefficient of the porous plates

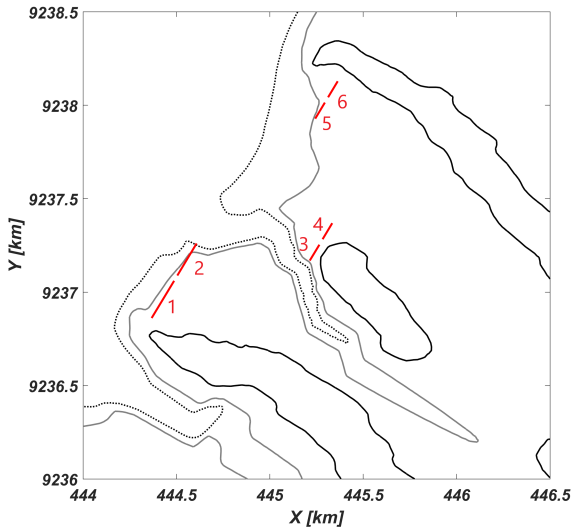

Figure 4.7: Location of the six structures implemented in the Delft3D models

Porous plate	1	2	3	4	5	6
Resistance coefficient [-]	15	10	20	10	10	10

Table 4.1: Values of resistance coefficient of the different porous plates implemented in the Delft3D models

Hard structures like the sea wall built using concrete cylinders in Timbulsloko (Winterwerp et al., 2020) were represented in the model using thin dams. Each dam acts as a closed boundary across a cell face preventing flow through it and is assumed to be of infinite height, making it impermeable. Similar to a porous plate, a thin dam is assumed to be negligible thickness in comparison to the grid size normal to the direction of the structure (Deltares, 2018b).

4.2.2. Model Calibration and Validation

Calibration is the tuning of a numerical model by adjusting parameter settings in order to reproduce physical phenomena as closely as possible. Validation of a model is proving that the model indeed accurately describes these physical phenomena using an additional data set (van Maren, 2004). To validate the results produced by the nested model, residual depth-averaged currents over the simulation period were compared with the results from the overall model and the reproducibility was evaluated. The overall model is used for validation since as an idealised model, it was previously validated by comparisons to existing models of the area, expert judgement, underlying principles and, literature (Bisschop, 2023). Residual currents were compared for different boundary conditions and, eddy viscosity and diffusivity values to validate and by way of which, to also calibrate the model.

Boundary Conditions

The boundary conditions for the nested model are obtained from the overall model using the tools Nesting(1) and Nesting(2) in Delft3D. Nesting(1) provides the observation points required in the overall model to produce the boundary conditions necessary for the nested model. Nesting(2) creates the flow and transport conditions using the results from monitoring stations of the overall model. The nesting tools in Delft3D can currently only generate hydrodynamic time-series boundary conditions of water level or perpendicular velocity type.

As the nested model domain covers a relatively small region of shallow water depths, the choice of type and composition of boundary conditions can particularly influence the model results. Hence, a range of configurations of the boundary conditions are tested:

(a) All water level boundaries (1, 2 and 3 in Figure 4.1)
(b) Cross-shore (1, 3) water level boundaries and offshore (2) current boundary
(c) Cross-shore (1, 3) current boundaries and offshore (2) water level boundary
(d) Current - offshore (2) and North (3) boundaries and water level South (1) boundary

For each configuration listed above, the residual depth-averaged currents over a period of one month of the simulation period are compared to those from the overall model run to determine the optimal type for each boundary section. Comparison of the residual currents is shown in Figure 4.8. Residual depth-averaged currents from the overall model show a general flow direction from the South to North offshore which is replicated in all nested model configurations except for all boundaries of water level. A residual inflow is observed at a small section of the North boundary for configuration (b), deviating from negligible, mostly parallel to the boundary currents there seen from the overall model. Currents from the overall model are best replicated for the (d) set of boundary types as shown in Figure 4.8 (d). However, implementing a water level boundary for a relatively smaller grid size in shallow water depths in the South boundary led to unreliably high velocities closer to land. Hence, the configuration (c) of cross-shore current boundaries and offshore water level boundary is chosen which produces a considerably similar pattern and magnitude of currents to the overall model.

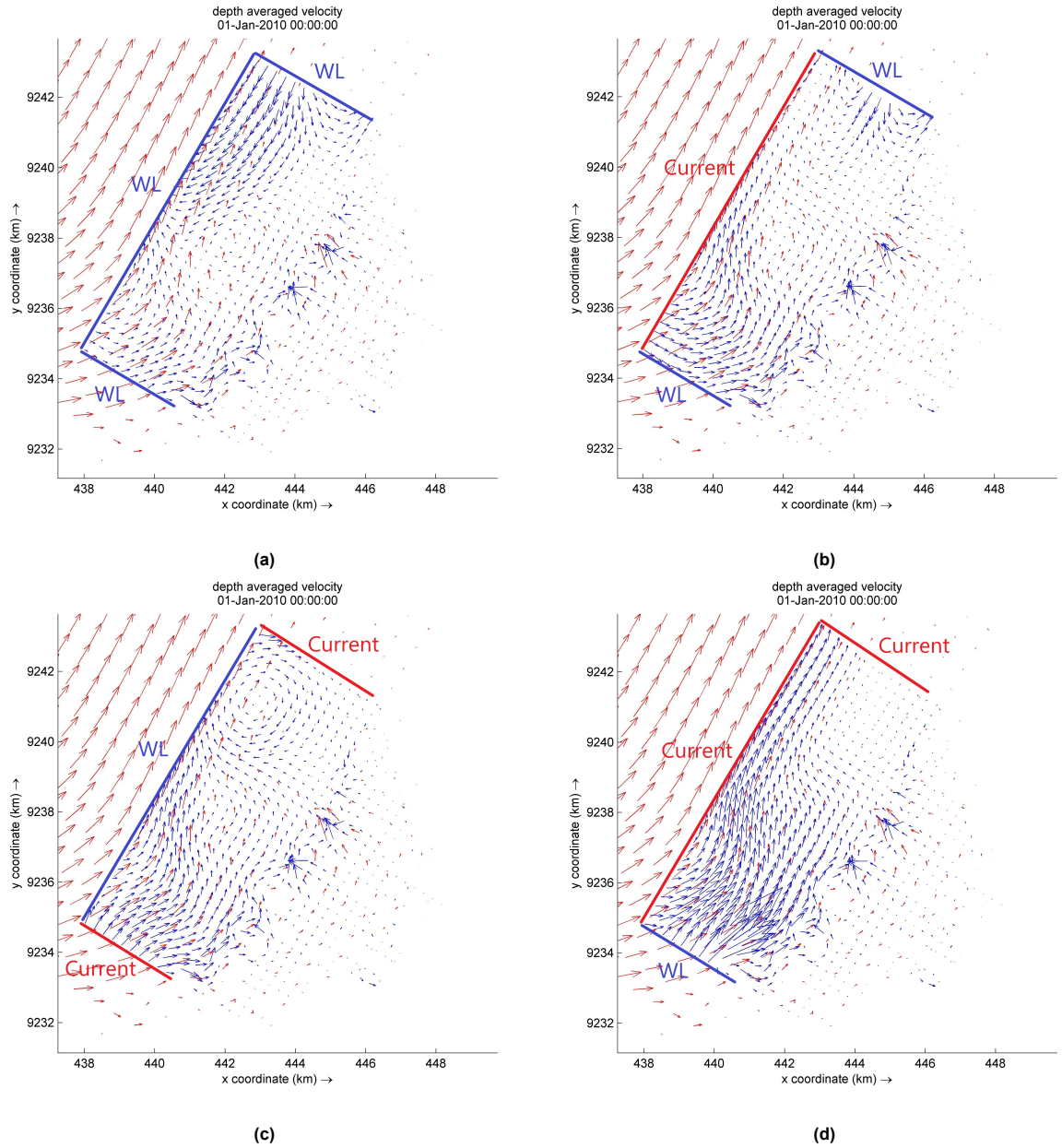

Figure 4.8: Residual depth-averaged currents for one month from overall model (in red) and nested model (in blue) for a) all water level boundaries b) cross-shore water level boundaries and offshore current boundary c) cross-shore current boundaries and offshore water level boundary (final configuration implemented in the model) d) current - offshore and North boundaries and water level South boundary

Eddy Viscosity

A uniform horizontal eddy viscosity value of 1 m^2/s (default value for Delft3D-4) provided as input in the nested model produced residual depth-averaged current patterns for a one-month simulation period in the monsoon season as shown in Figure 4.9 (a). A circulatory current near the offshore boundary can be seen in Figure 4.9 (a), not found in the residual current pattern of the overall model in Figure 4.9 (c). Therefore, a gradually varying viscosity from 10 m^2/s to 1 m^2/s near the offshore boundary depicted in Figure 4.10, is provided as input to ascertain if the change in viscosity can eliminate the circulation to the North. As can be seen from Figure 4.9 (b), the circulation is not eliminated but pushed landward instead. However, the current magnitude near the North boundary correlate better to that from the overall model when compared to the case with constant eddy viscosity.

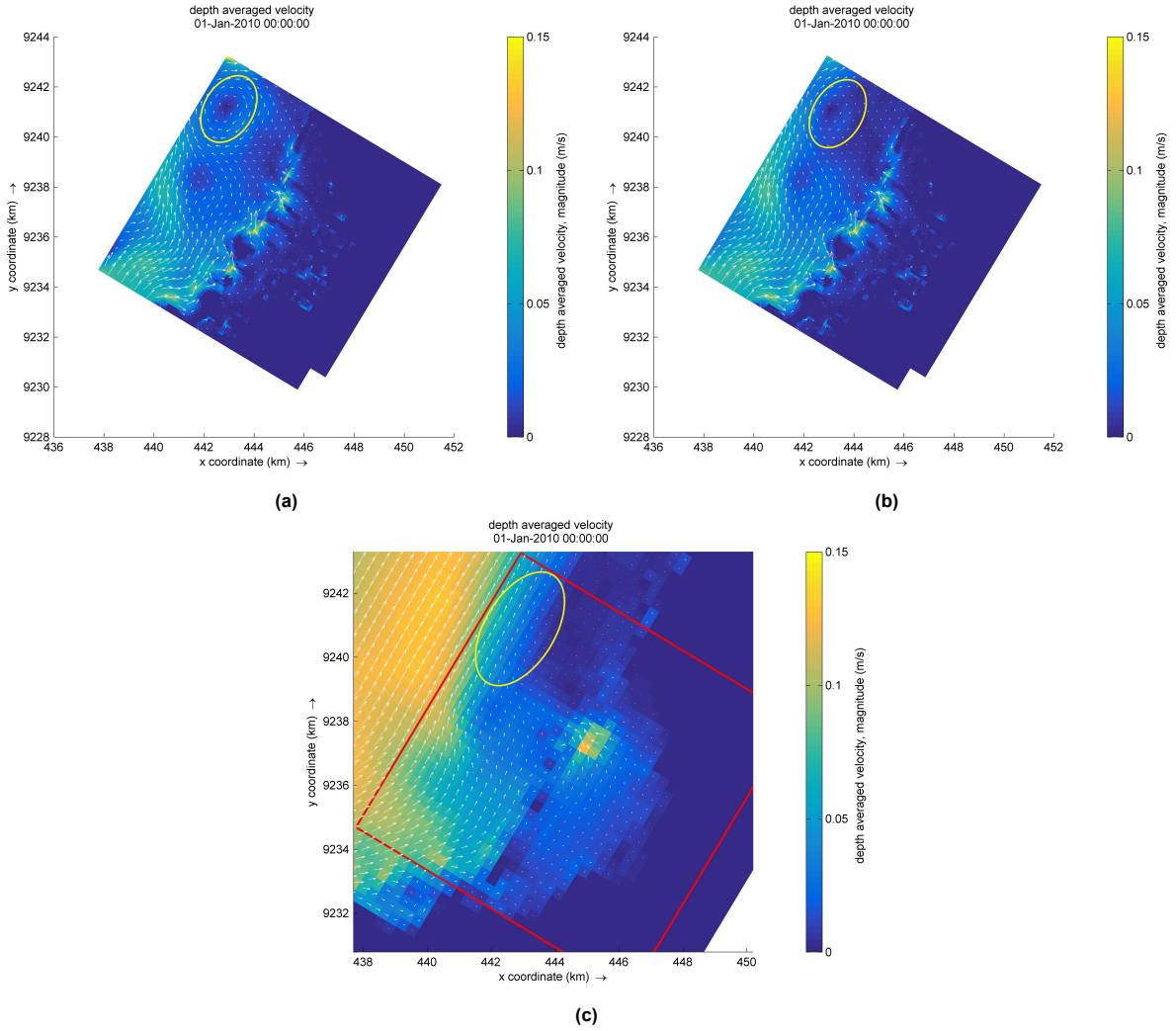

Figure 4.9: Residual depth-averaged currents from a) nested model for horizontal eddy viscosity of 1 m^2/s b) nested model for gradually varying horizontal eddy viscosity near the offshore boundary and c) overall model zoomed in to the nested model domain (outlined in red). The circulatory currents are highlighted in yellow.

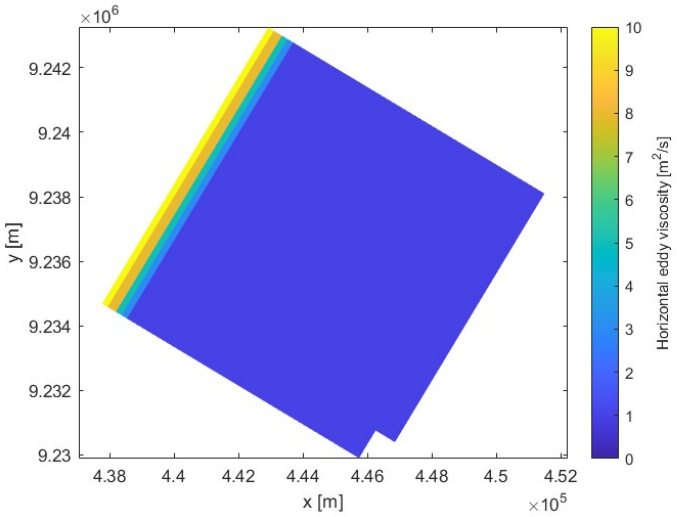

Figure 4.10: Horizontal eddy viscosity input to the nested model with gradually decreasing viscosity near the offshore boundary

Though the horizontal eddy viscosity and diffusivity are listed as calibration parameters, care must be taken to not provide as input unreasonably high values for the parameters. This is especially true for the model domain with low tidal current velocities in shallow regions, as eddy viscosity is prescribed in models as the product of a velocity and a length scale. The Delft3D-FLOW manual states that for detailed models of grid sizes in the range of tens of metres, the values for eddy viscosity and diffusivity are typically in the range of 1 to 10 m^2/s (Deltares, 2018b). Hence, a uniform horizontal eddy viscosity of 1 m^2/s is chosen for the model run.

4.2.3. Wave Model Set-Up

A nested stand-alone wave model in Delft3D was set up using the same grids used in the flow model with the finer grid nested in the overall grid. During the NW monsoon season modelled with Delft3D-FLOW, waves are assumed to approach the shoreline from NW with a directional spreading of 15° and significant height of 0.7 m (Smits, 2016). Processes of depth-induced breaking and bottom friction are modelled with wind growth and whitecapping. Wave-driven currents are excluded from the study as they are computationally expensive.

For a stand-alone wave model computation, water levels for which waves are to be modelled should be provided as input by the user. Since the emphasis of this thesis is on the sediment and propagule movement in the intertidal areas of Timbulsloko, characterized by consistently elevated water levels beyond MSL in contrast to offshore regions, a set of five water levels ranging between MSL and HW, equidistantly spaced, was designated as discrete temporal increments for computational purposes. This selection was undertaken with the objective of ensuring a constant presence of wave activity and consequently, sediment mobility within the designated area of interest.

Permeable dams were represented in the wave model by means of sheet type obstacle with a reflection coefficient of zero and a constant transmission coefficient. The appropriate value for the transmission coefficient was obtained from Gijón Mancheño (2022). For storm waves, a reasonable assumption of 60% transmission through the dams is made. From Figure 4.11, it can be ascertained that for an incoming wave height of 0.13 m, a wave height of approximately 0.08 m was recorded behind the permeable dam, resulting in a transmission coefficient of 0.6.

Hard structures were also implemented as sheet type obstacles in the wave model albeit with a transmission coefficient of zero and a reflection coefficient of one. Reflection of specular type with the angle of reflection equal to the angle of incidence was enforced.

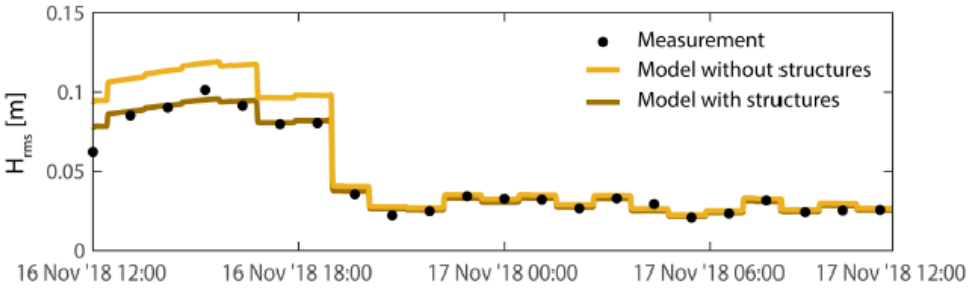

Figure 4.11: Significant wave heights measured (black dots) behind permeable dams with predictions by XMgrove model of wave transformation through the structures (from Gijón Mancheño, 2022)

4.3. SedTRAILS

To facilitate a meaningful interpretation of the current vector fields and bed shear stress data generated by the Delft3D-FLOW and Delft3D-WAVE models, SedTRAILS (Sediment TRAnsport vIsualisation and Lagrangian Simulator) is used as a post-processing tool. It is used to derive the sediment and propagule pathways within the study area using the output from the Delft3D models. SedTRAILS is a Lagrangian sediment transport model and visualisation tool, developed for efficient and high-resolution computation of sediment transport pathways (Pearson et al., 2021). The post-processing tool was originally developed for coral larvae, which was then extended to sandy sediment and in recent past to compute mangrove propagules (Storlazzi et al., 2017; Bisschop, 2023).

Lagrangian particle tracking has found extensive application in evaluating connectivity within the realm of oceanography and marine ecology (Hufnagl et al., 2017; van Sebille et al., 2018). This prominence arises from the models' capacity to simulate the complete trajectory history of particles, and not just their points of origin and final destination. Particle tracking models are also relatively fast and lend themselves well to parallel computing (Paris et al., 2013). This approach thus allows for a faster and more detailed analysis of sediment connectivity than existing Eulerian approaches (e.g., Pearson et al., 2020). Despite the existence of several Lagrangian models for sediment transport (MacDonald and Davies, 2007; Soulsby et al., 2011), their use in supporting connectivity investigations has been limited. Hence, there is a need for Lagrangian sediment particle tracking tools tailored to predicting sediment transport pathways and determining connectivity of complex coastal systems. To meet this need, the Lagrangian sediment transport model of SedTRAILS was developed (Pearson et al., 2021). Furthermore, visualisation of complex transport pathways help enable effective communication of sophisticated numerical model results to a non-scientific community and stakeholders to generate meaningful discussions.

SedTRAILS proves particularly useful where the execution of computationally expensive process-based models like Delft3D is confined to a concise simulation period to obtain the representative transport vector fields and other scalar output such as bed shear stress. Thus, acquired output are subsequently used in SedTRAILS to analyse the sediment and propagule connectivity in the model domain for a much shorter computation time while not sacrificing model resolution and accuracy.

4.3.1. Domain

Both Delft3D-FLOW and -WAVE models output to two separate grids: a coarser grid covering the larger area of Demak coastal system and a finer grid encompassing the intertidal areas of Timbulsloko. In order to achieve a comprehensive understanding of sediment and propagule trajectories, encompassing connectivity across the entirety of the coastal system, it becomes imperative to merge the output derived from the two grids. This merging process is executed using MATLAB employing a polygon file that can be used to include output from nested grid within its bounds and merge it with the results from the overall grid outside its bounds, as shown in Figure 4.12. Using a polygon file can be particularly helpful when combining results excluding part of the output from a grid that is better represented in the output from the other grid. For this research, output near the boundaries of the nested model is omitted to disregard a circulation current near the Northern boundary seen in Figure 4.8 (c).

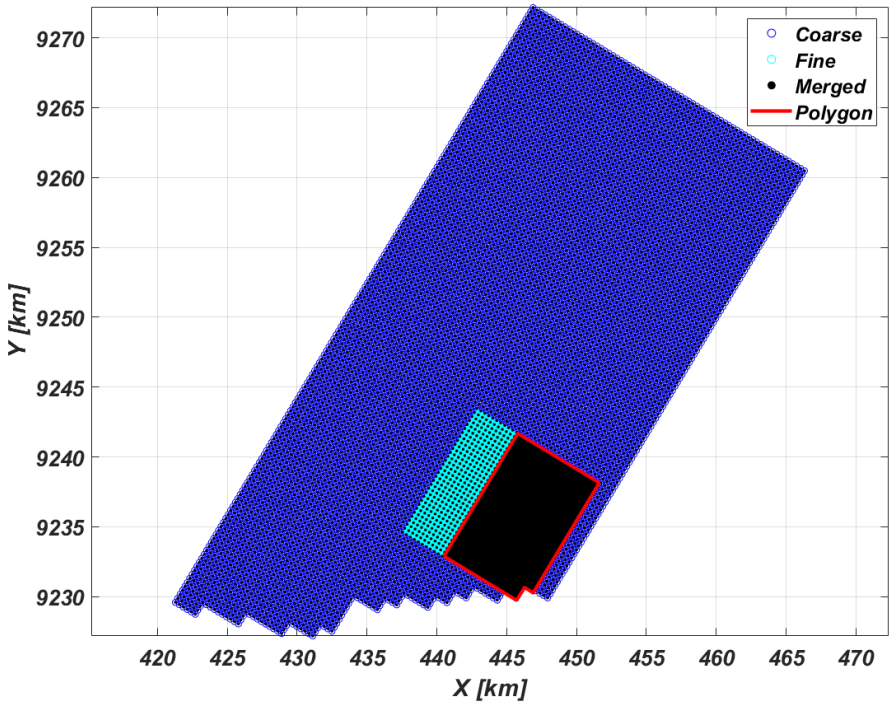

Figure 4.12: Domain used for trajectory computations in SedTRAILS merging part of output from the nested grid with output from overall grid in rest of the area

4.3.2. Structures

The effect of thin dams implemented in Delft3D-FLOW model on the flow field did not translate to the particle trajectories in SedTRAILS. In the presence of thin dams for which case flow should have ideally been blocked by the structures, the particles pass through, although they do slow down. To replicate the true effect of such structures on the different particle pathways, the expected behaviour of particles upon encountering the structures was explicitly coded into SedTRAILS. In the presence of thin dams, a particle that makes contact with the structures is directed algorithmically to reflect back at an angle normal to the angle of incidence. With such a modification, particles could no longer go through the structures but were entrapped instead. Subsequently, they are either transported along and out through the gap between the structures or align with the prevailing current, moving away from the structures. This can be seen in Figure 4.13.

To model the trapping behaviour of propagules behind the porous plates, a trapping probability per input timestep in SedTRAILS, $prob_{trap}$ is used wherein, any time a particle makes contact with the dam, the probability it traverses through the dam is computed as $prob_{traverse}$ = 1 - $prob_{trap}$. Consequently, for a sufficiently large trapping probability, only a minor fraction of particles manage to pass through the dam while the rest are trapped behind it during each ebb and flood cycle.

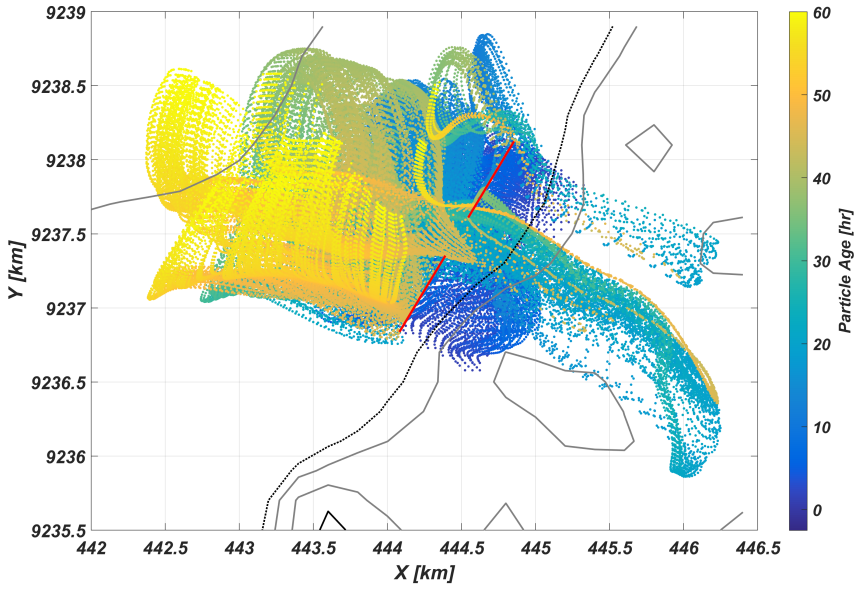

Figure 4.13: Trajectories of 540 flow particles around the thin dams for a period of 2.5 days. Reflection of particles when interacting with the structures is coded explicitly into SedTRAILS thus allowing no passage of particles through the thin dams

4.3.3. Sediment Module

The computation of sediment pathways in SedTRAILS requires the output from Delft3D-FLOW and -WAVE models. Current velocities and mean and maximum bed shear stress are extracted from the flow model runs. Since the wave model provides outputs at the grid corners, while the flow model calculates parameters at the grid centres, the mean of the output parameters at the corners is calculated for the former to derive the outputs at the grid centres.

Wave-induced maximum bed shear stress is computed using the output parameters from the -WAVE model as,

$$\hat{\tau}_w = 0.5\rho f_w \hat{u}_0^2 \tag{4.3}$$

with orbital velocity, $\hat{u_0}$ and friction factor, f_w (Bosboom and Stive, 2021). The friction factor is computed as,

$$f_w = exp\left[-5.977 + 5.213\left(\frac{\hat{\xi_0}}{r}\right)^{-0.19}\right] \tag{4.4a}$$

$$f_{w,max} = 0.3 \tag{4.4b}$$

with particle excursion amplitude, $\hat{\xi_0}$ and roughness r (Swart, 1974; Soulsby, 1994). Roughness is computed as the Nikuradse roughness, k_s of $2.5D_{50}$ and the particle excursion amplitude is given by,

$$\hat{\xi_0} = \frac{\hat{u}_0 T}{2\pi} \tag{4.5}$$

where, T is the wave period. Since the stand-alone wave model computations provide stationary result parameters, the time-varying maximum bed shear stress was computed based on the water levels from

an observation point in the intertidal region. The total maximum bed shear stress is then determined by adding the maximum bed shear stresses induced by both the current and the waves, without considering the non-linear enhancement of bed shear stress. The mean bed shear stress is equated to that due to currents as wave-induced bed shear stress tends to zero when averaged over time.

The pathways are computed based on the grain velocity defined by Soulsby et al. (2011) as in Equation (4.6). The freedom factor F indicates if the grain is trapped ($F = 0$) or is free to move ($F = 1$). F is set to 1 in the simulations with the grain always free to move thereby disregarding its interactions with the bed. P establishes the probability that a free grain moves as bedload or in suspension. R is a reduction factor for the speed of a mobile grain compared to the current velocity and, U_c is the current velocity averaged over the bottom 1 m of the water column. However, since the area in focus is the intertidal basins near and of Timbulsloko due to the presence of structures there, where the water depths are always below 1 m, the depth-averaged currents are used to compute the sediment pathways. Nevertheless, a few simulations with average current speeds over the bottom half of the water profile are executed to obtain a better representation of the trajectories of sediments offshore.

$$U_{gr} = F \cdot P \cdot R \cdot U_c \tag{4.6}$$

Pathways are computed for sediment particles from 1000 clusters in the region shown in Figure 4.14. Sediment trajectories are also modelled for source particles equidistantly spaced in the vicinity of the structures as depicted in Figure 4.15 to better understand the local trapping efficiency of such structures. Since sediment of varying grain sizes are observed in the study domain (see section 3.2.3), simulations for two different grain sizes are carried out. Sediment in the domain is assumed to be muddy with grain size of D_{50} = 18 µm to model large-scale pathways (Bisschop, 2023). At the location of structures about 100 m from the mangrove fringe in eroding transects, sediment of size D_{50} = 58 µm is observed and is hence modelled, to discern the local effects of structures on the sediment pathways.

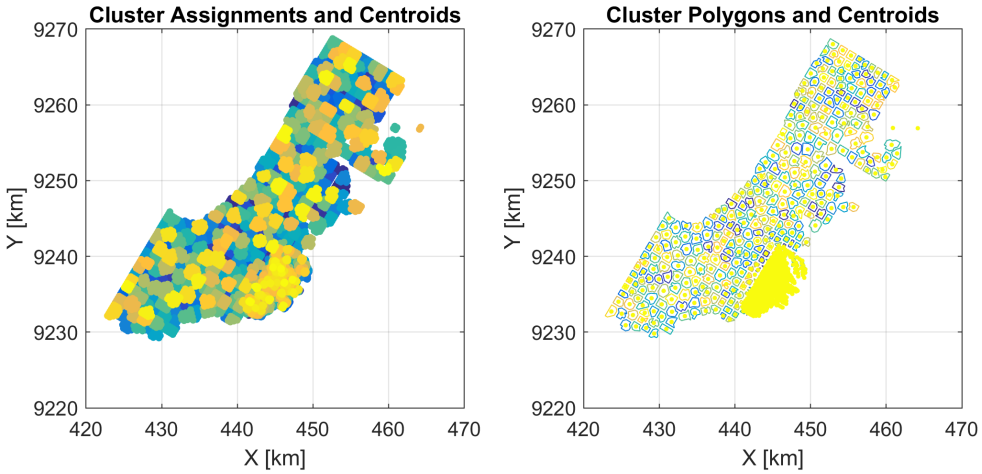

Figure 4.14: 1000 clusters in the model domain within a polygon outside which sediment movement is not observed. One sediment particle is released from each cluster at the start time of a simulation.

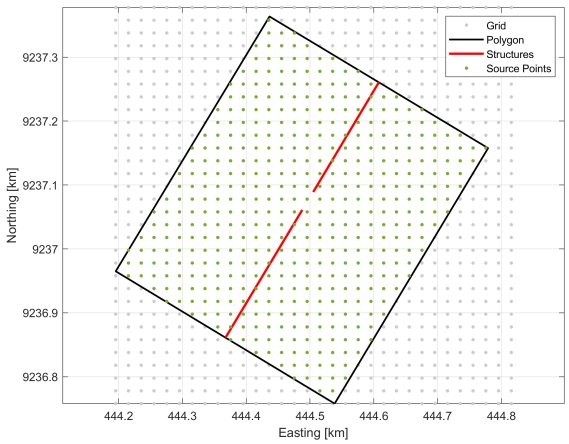

Figure 4.15: Source particles equidistantly spaced at 20 m around the structures

4.3.4. Propagule Module

Dispersal of propagules is heavily dependent on wind as discussed in section 2.1.2. For propagules floating on the surface or with a part above the surface, a windage factor can be introduced to enhance the influence of wind. However, observations by A. Gijón Mancheño have found that the *Avicennia Marina* propagules found on site float just below the surface (Bisschop, 2023). Hence, their trajectories are modelled using the current velocity of the surface layer from the Delft3D-FLOW model.

Unlike sediment, there are a number of other factors to consider when modelling the pathways of propagules such as their viability, depth of establishment, etc. A concept of ”sticky depth” is used in the SedTRAILS model, where floating propagules establish in their current location if the water depth in that area is shallower than the sticky depth specified by the user. For the simulations, a sticky depth of 2 cm is implemented based on the length of *Avicennia Marina* propagules which are typically 2-3 cms long (Yun et al., 2022). Another parameter of ”sticky time” is defined in the model as a period of time during which floating propagule cannot establish at any location. The parameter is introduced to replicate the obligate dispersal period (ODP) of the propagules which is the period for which propagules must remain floating once abscised to be able to establish as seedlings (Rabinowitz, 1978). An ODP of about 5-10 days is required for *Avicennia Marina* propagules (Clarke, 1993). Therefore, a sticky time of 5 days is implemented in the model.

The lifespan of propagules is determined by their viability and buoyancy periods. Rabinowitz (1978) found that *Avicennia Marina* propagules could remain viable in seawater for a period of up to 6 months. The propagules were found to sink within a few days when exposed to seawater but nonetheless, tend to refloat (Clarke, 1993; Clarke et al., 2001). The buoyancy period is thus disregarded for the study. Since the simulation period of the models is one month, which is shorter than the viability period of the propagules, their lifespan was neglected for the SedTRAILS simulations.

Propagule source polygons were generated using Google Earth images (see Figure 4.16) with which 300 sources were modelled with SedTRAILS. With the introduction of structures, interaction of propagules with the structures was coded in explicitly with a trapping probability as stated in section 4.3.2, since observations by A. Gijón Mancheño found that propagules tend to be trapped behind the permeable dams in the region. The windows of opportunity for successful establishment of propagules discussed in section 2.1.3 were not modelled, as the focus of this study is on the influence of structures on propagule pathways. With morphostatic model simulations, the change in bed elevations required for the creation of the windows of opportunity behind the structures is not captured. Modelling the criteria for successful establishment of the propagules without the appropriate change in the bed levels would therefore prove to be inaccurate.

Figure 4.16: Mangrove source patches shown as white polygons based on mangrove forest populations near the coastline within the model domain

5

Results

This chapter showcases the main results from the Delft3D model and subsequently from the Sed-TRAILS simulations with and without the different structures.

5.1. Hydrodynamics

This section elaborates on the results from the nested Delft3D-FLOW and -WAVE models.

5.1.1. Currents

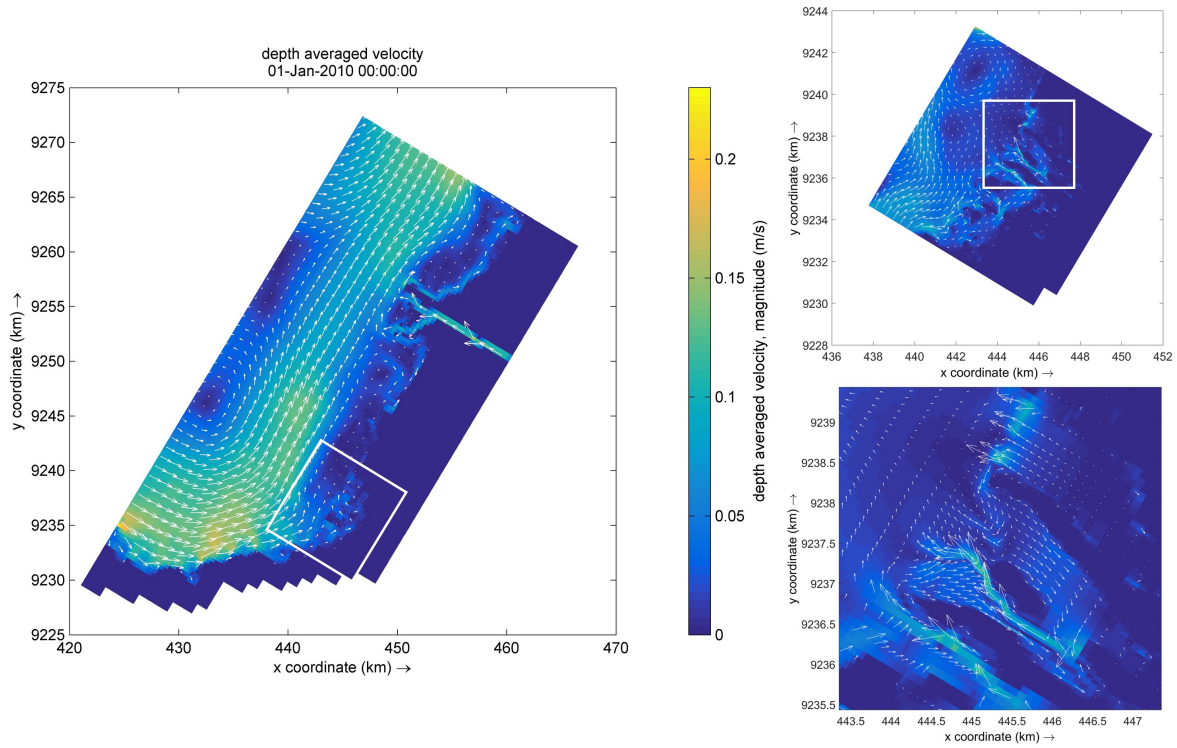

Figure 5.1: Residual depth-averaged currents over a month in the wet season in the overall model domain (left), nested model domain (top right) and, near Timbulsloko (bottom right)

The sediment pathways in the study area are modelled based on primarily the depth-averaged currents as showcased in section 5.2. The residual depth-averaged currents over one month in the NW monsoon season shown in Figure 5.1, in the study area offshore, are toward NE, in agreement with model results of Deltares (2020) and Bisschop (2023). Flow discharge from the Wulan River creates a freshwater plume near the mouth of the delta extending a few kilometres along the coastline. This plume, and thereby the riverine sediment, remains in close proximity to the coast due to the prevailing WNW winds during the wet season. The presence of stratification induced by freshwater discharge results in reduced depth-averaged current velocities within the plume area due to the prevention of mixing. In the intertidal basin, tidal flow is ebb-dominant in the channels and flood-dominant with alongshore components in the flats as (see Figure 5.1).

In the presence of thin dams, the flow is blocked by the structures resulting in currents of negligible magnitude behind them (see Figure 5.2 (a)). This flow blockage causes also creates a discontinuity in the current direction behind the barriers. Tidal inflow and therefore sediment input into the area behind the dams occurs via the openings between the structures. In the case of porous plates, current velocities are reduced as they pass through the structure (see Figure 5.2 (b)). The resistance to flow induces larger flow velocities through the gaps between the structures. In addition, the flow reduction behind the structures and acceleration through the gaps is less pronounced for porous plates compared to thin dams. The structures produce a similar effect on the instantaneous currents which can be ascertained from Figure B.3 and Figure B.4 in Appendix B.

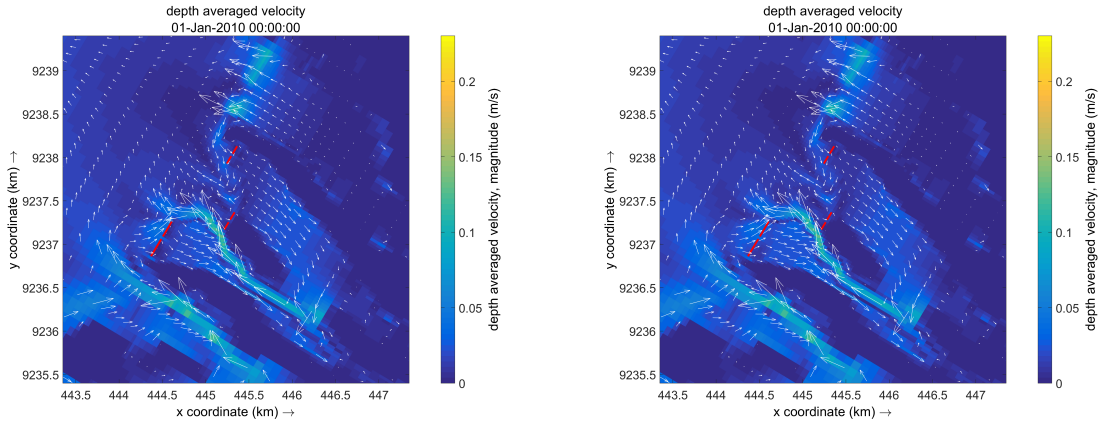

Figure 5.2: Residual depth-averaged currents over a month in the wet season near Timbulsloko in the presence of a) thin dams and b) porous plates

Comparison of the residual depth-averaged currents over a month in the wet season for the case without any structures, in the presence of thin dams and with porous plates, is depicted in Figure 5.3. The residual tidal flow is uninhibited in the absence of structures. When thin dams are introduced, the flow blockage causes a change in the direction of both instantaneous (not pictured) and residual currents behind the dams when compared to the default case without any barriers to the flow. Just behind the thin dams, the residual current vectors are infinitesimally small, indicating negligible velocities. When porous plates are present, current velocities behind the barriers become lower. Moreover, the direction of residual current vectors with porous plates exhibits a slight variation when compared to the default scenario. This phenomenon can be attributed to the spatial alterations in water levels between the two cases, which arise from the resistance offered to the flow by the porous plates. The changes manifested in the currents are however, restricted to a radius of less than one kilometre in the proximity of the structures in all scenarios. Beyond this range, there is no perceptible variation in the flow vectors.

The pathways taken by propagules in the region are modelled based on the surface layer currents, whose residuals over a month in the wet season are shown in Figure 5.4. Currents in the surface layer are predominantly governed by the wind and are hence directed onshore for the majority of the time in the intertidal regions, and along the coastline, as a consequence of modelling the NW monsoon

season, as can be seen from Figure 5.4. However, offshore, the flow is still governed by tides with the residual currents directed toward NE similar to the residual depth-averaged currents.

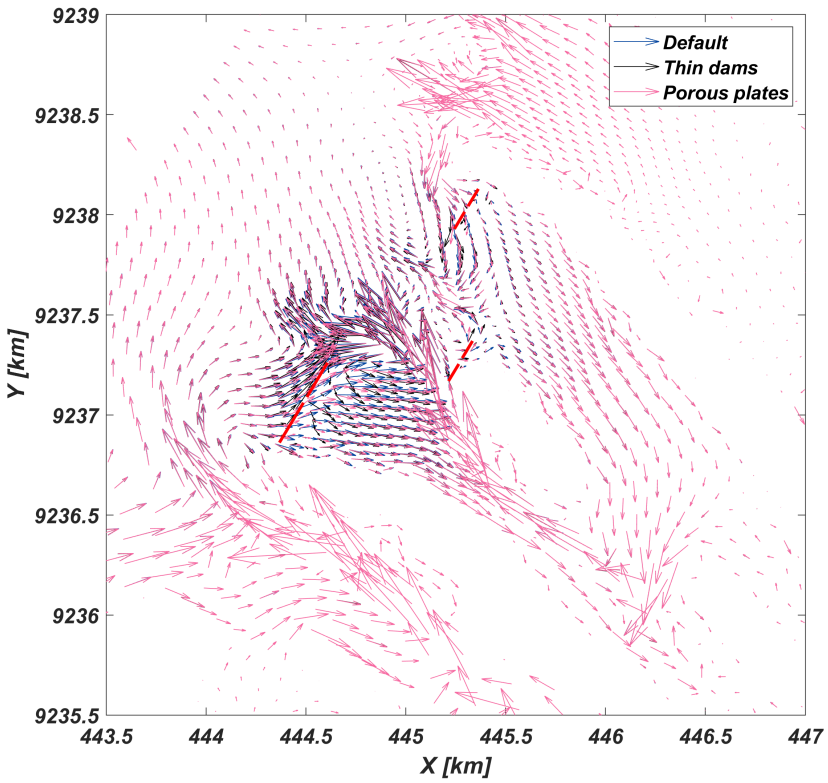

Figure 5.3: Residual depth-averaged current vectors over one month for the default case, in the presence of thin dams and in the case of porous plates

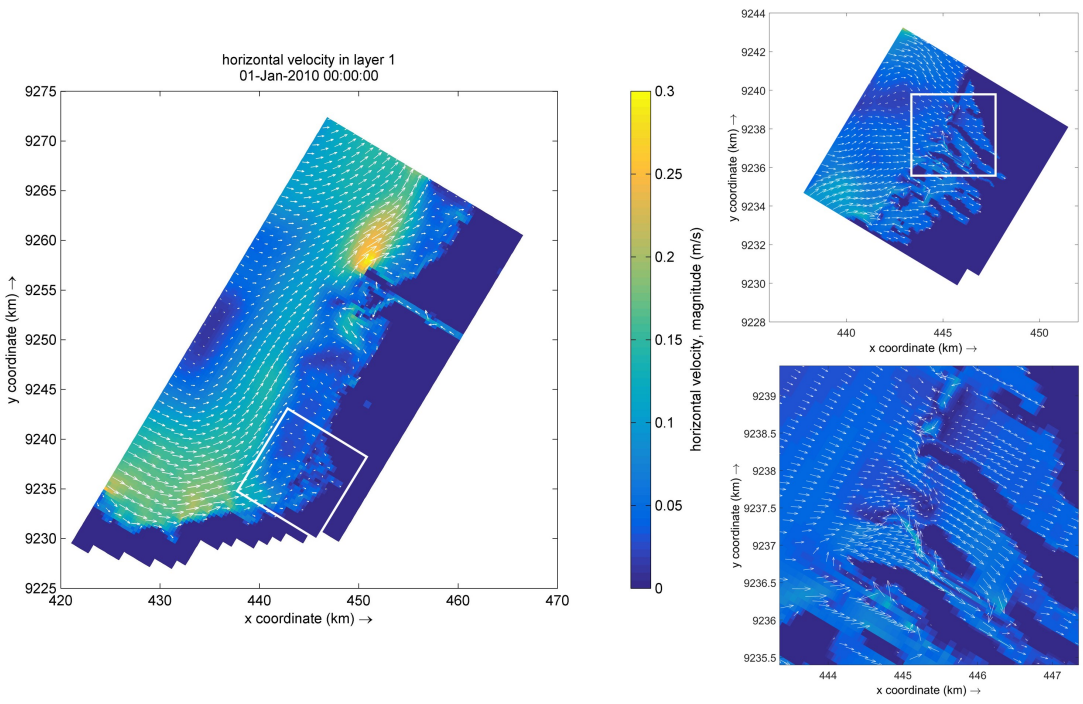

Figure 5.4: Residual currents over a month in the surface layer in the wet season in the overall model domain (left), nested model domain (top right) and, near Timbulsloko (bottom right)

5.1.2. Waves

The wave-induced maximum bed shear stress computed for a water level of 0.4 m (MHW) is shown in Figure 5.5 for the three scenarios of structural presence. The average maximum bed shear stress over the simulation period is illustrated in Figure C.1 in Appendix C. The hard structures induce complete wave reflection with no transmission, consequently leading to the most significant reduction in shear stress behind them. Moreover, due to wave reflection, it is also noticeable that shear stress in front of the structures is higher when compared to the scenario without any barriers. In the case of permeable dams modelled with a transmission coefficient of 0.6, a decrease in bed shear stress can be discerned, as illustrated in Figure 5.5 (b). However, this reduction is notably less pronounced than what is observed with hard structures. Considering the southernmost barrier, the introduction of a hard structure results in a maximum bed shear stress of 0.014 N/m^2 behind it. Conversely, a permeable dam situated in the same location induces a higher bed shear stress of 0.34 N/m^2 at that position, which escalates to 0.65 N/m^2 in the absence of barriers. However, since no reflection is considered for the permeable dams, shear stress in front of the dams is not enhanced as in the case with hard structures.

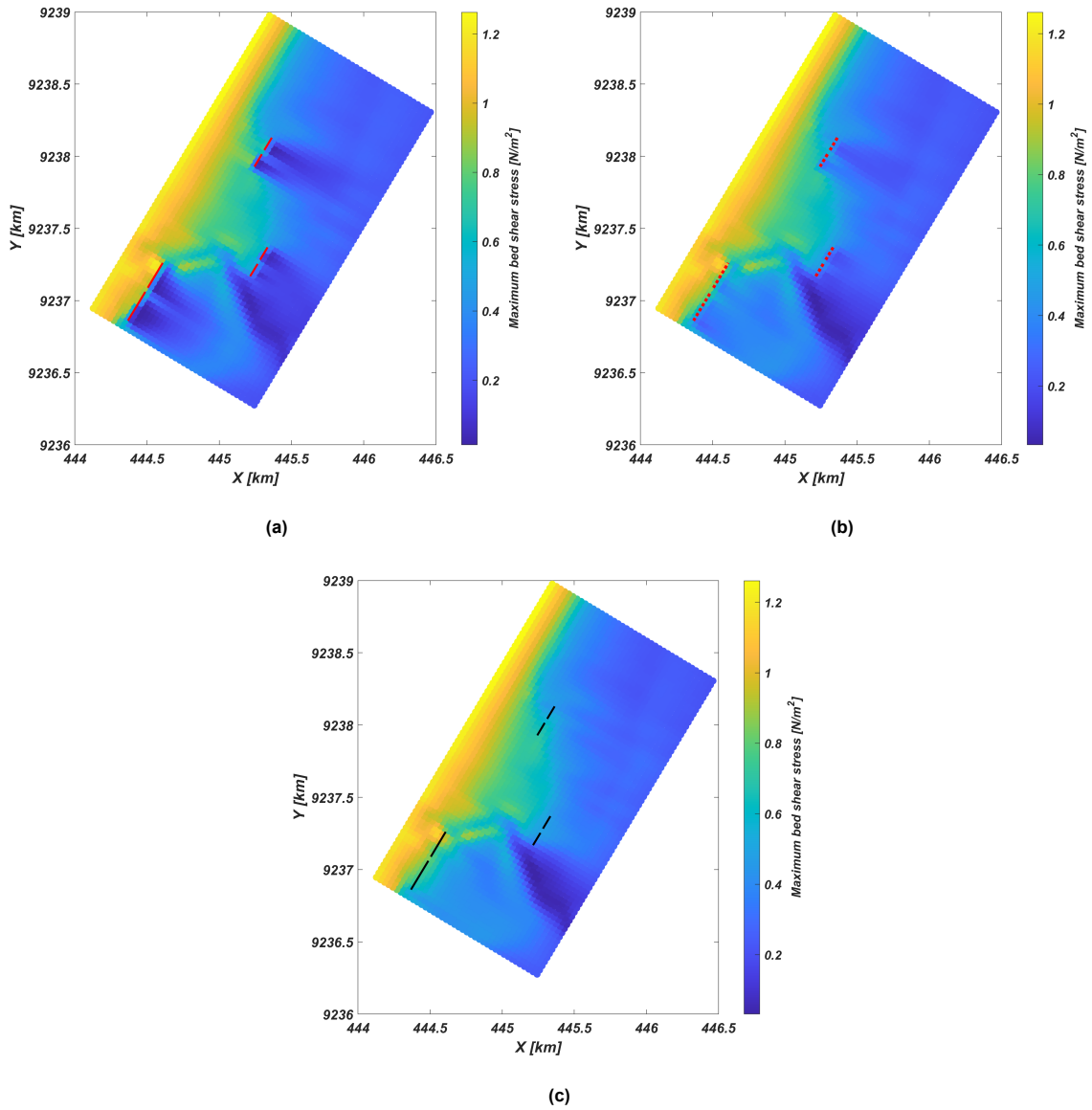

Figure 5.5: Maximum bed shear stress due to waves for MHW (0.4 m) in the a) vicinity of hard structures (shown as solid red lines) b) presence of permeable dams (dotted red lines) and, c) absence of structures (location indicated using black lines)

5.2. Sediment Pathways

This section showcases the results of sediment pathways and related parameters modelled using SedTRAILS. It should be noted that the results presented in this section do not represent the actual trajectories followed by the sediment particles. The formulation utilised in the SedTRAILS model, as described in Soulsby et al. (2011), was originally designed for non-cohesive, sand-sized sediment and therefore, does not account for mud-related processes such as flocculation, hindered settling, etc. Such processes are likely to be relevant at the muddy coastline of Demak. Therefore, these results should be regarded as a qualitative indication of potential sediment transport routes.

5.2.1. Large-scale Pathways

The trajectories taken by sediment particles in the Demak coastal region based on depth-averaged currents and on average currents of the bottom half of the vertical profile are shown in Figure 5.6 and Figure 5.7 respectively. While the pathways based on depth-averaged currents better represent sediment movement in the intertidal regions, those based on average currents of the lower half of the vertical profile might afford a better representation of sediment movement in the offshore region, since the formulation by Soulsby et al. (2011) used in the model prescribes the usage of current velocity averaged over the lowest 1 m of the water column. However, since the model is designed for sand-sized particles with a different sediment concentration profile compared to mud, accuracy of using current velocity of the lower half of the vertical profile is presently unknown.

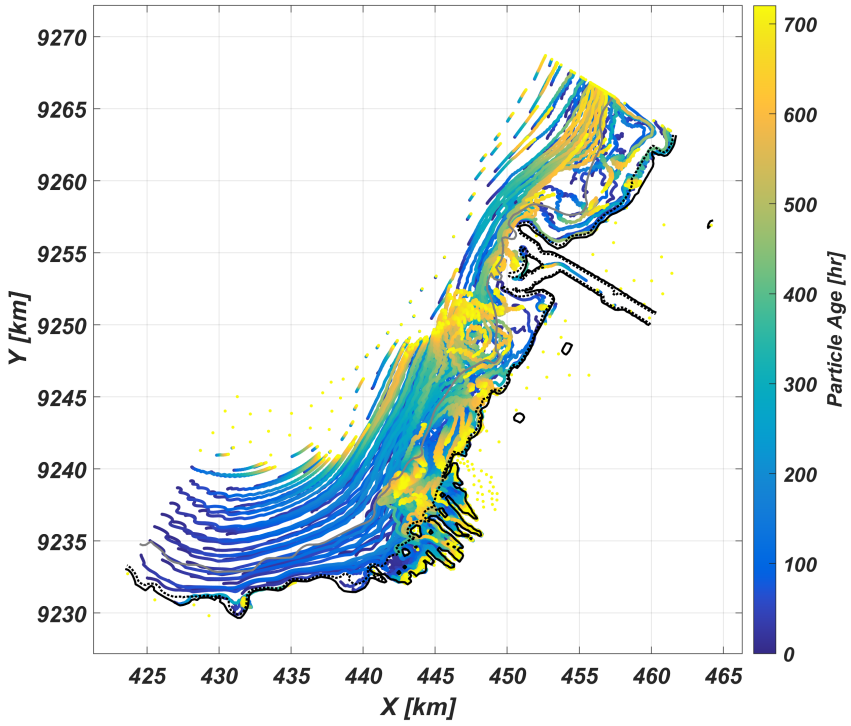

Figure 5.6: Pathways of 1000 sediment particles of size D_{50} = 18 µm based on depth-averaged currents during a month in the wet season. Three depth contours for -5 m below MSL, mean low water (MLW) and mean high water (MHW) are depicted as grey, dotted black and solid black lines respectively.

Sediment particles, especially offshore, in both cases, predominantly move along the coast toward NE. This resembles the residual depth-averaged current pattern in the area seen in Figure 5.1, so the sediment transport offshore can hence be said to be tide-dominant. Close to the coastline however, the

freshwater plume acts a barrier both to offshore sediment transport thereby trapping riverine sediment close to the coast, and possible inflow. Nevertheless, north of the Wulan Delta, sediment near the coastline, is transported offshore, by the average currents of the lower half of the profile. This could explain the observations by Septiangga and Mutaqin (2021) who found the northern shoreline to be retreating presently.

The protruding Wulan Delta also blocks some of the alongshore transport of sediment. This phenomenon is more apparent from Figure 5.7 where fewer particles are able to bypass the delta. Near the intertidal basins of Timbulsloko, export of sediment from the basins can be observed. Even so, the exported sediment does not travel far offshore and is trapped within the plume. Furthermore, no movement of sediment is observed far offshore, more than approximately 10 kilometres from the shoreline, as the maximum bed shear stress in the area is not large enough to initiate motion of the sediment particles.

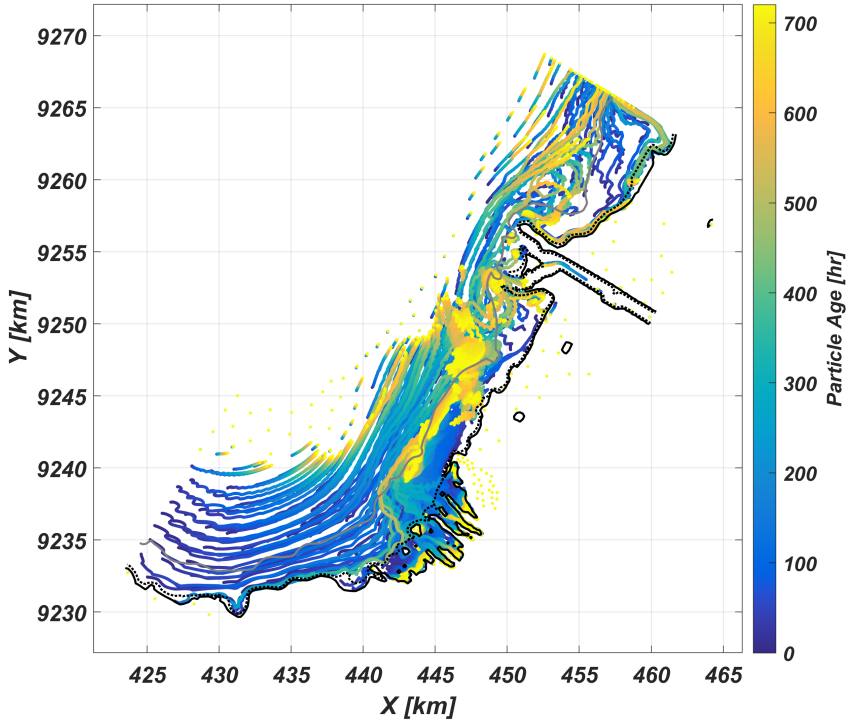

Figure 5.7: Pathways of 1000 sediment particles of size D_{50} = 18 µm based on average currents of the bottom half of the vertical profile during a month in the wet season. Three depth contours for -5 m below MSL, MLW and MHW are also depicted in the figure.

To better visualise the source of sediment traversing through the region, the sediment pathways are mapped based on the distance of the source particles from the back of the intertidal basin as shown in Figure 5.8. It is noticeable from the figure that sediment from offshore travels along the coastline before being barricaded by the freshwater plume and pushed offshore, where they continue parallel to the shoreline. Sediment near the coast is trapped within the plume where they circulate slowly due to the eddies formed in the area. The plume extends halfway to the intertidal basin, south of which there is an opportunity for sediment inflow through tidal infilling. However, it can be observed from Figure 5.8 (b) that sediment from offshore does not contribute to inflow into the basin. Most sediment within the basin is however transported landward, signifying local retention. Towards the north-eastern end of the basin near the coastline, a notable sediment recruitment process is observed occurring in the sheltered area behind the chenier, drawing sediment from the region located in front of the chenier. Caution should be exercised when interpreting the observations in the intertidal region, as the bathymetry in the area,

particularly the section immediately seaward of the intertidal basin, has been modified to allow for smooth transition between two sets of bathymetric datasets (see Appendix A). As a result, it exhibits a steeper profile compared to what is typically observed in eroding mud-mangrove coastal environments. The limitation is further discussed in Chapter 6.

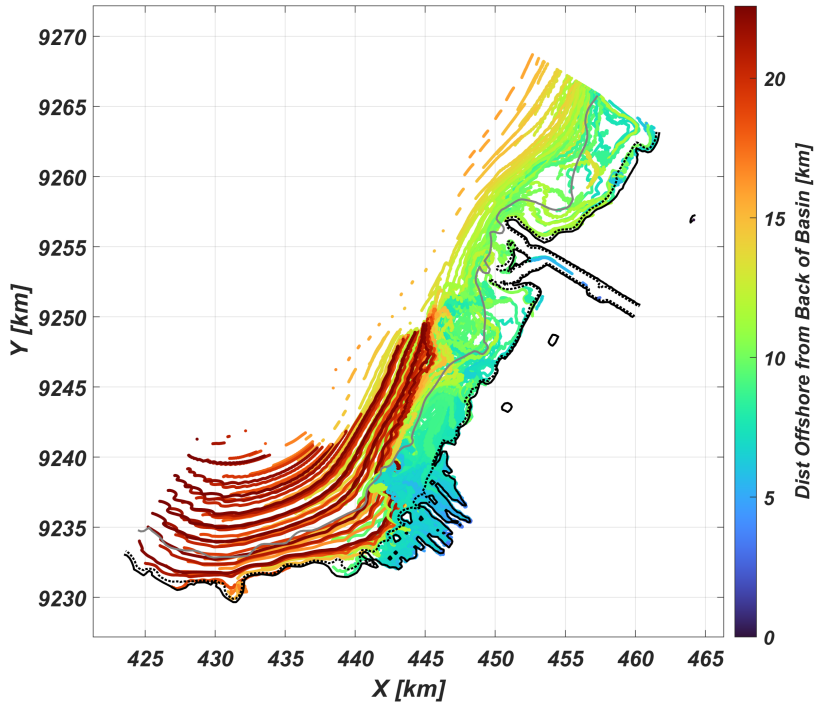

(a)

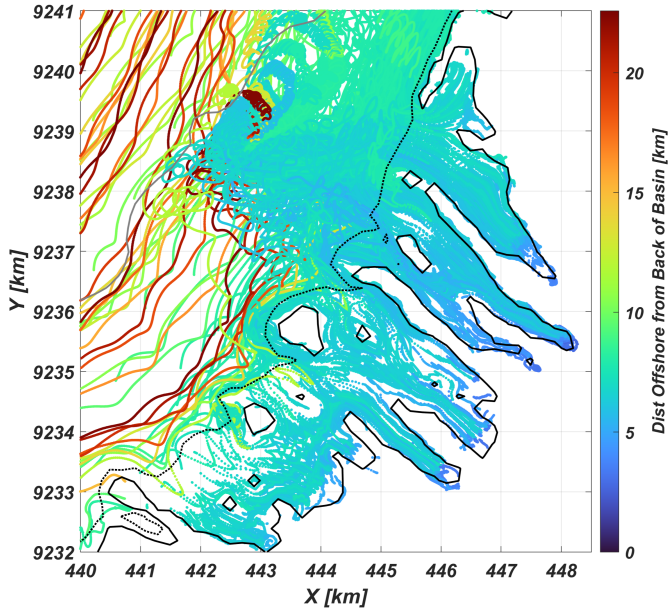

(b)

Figure 5.8: Pathways of sediment particles of size D_{50} = 18 µm based on distance offshore from back of the intertidal basin for a) Demak coastal region and, b) intertidal basin of Timbulsloko. Three depth contours for -5 m below MSL, MLW and MHW are also depicted in the figures.

5.2.2. Influence of Structures on Pathways

Sediment pathways in the presence of structures both hard and permeable are modelled to better understand the influence of such structures on the pathways and sediment-structure interactions. Trajectories taken by sediment in the Demak coastal region in the vicinity of hard structures are depicted in Figure 5.9 for sediment of D_{50} both 18 µm and 58 µm. Sediment in both cases does not pass through the structures as prescribed in SedTRAILS. More movement of sediment is observed for particles of smaller size with a smaller critical Shields parameter. The structures at the southern end (1 and 2 from Figure 4.7) are able to slow down the sediments travelling behind them, and even trap them when they are of the larger size. However, most particles are still either carried farther into the basin through the channel nearby or transported alongshore, outside the influence of the structure, and out of the basin due to change in tidal current direction in the area. The residual currents behind the structure near the channel are also slightly alongshore corresponding to the sediment pathways in the region (see Figure 5.2 (a)). The structures farther into the basin (3 and 4 from Figure 4.7) seem to be more efficient in trapping sediment of the larger size due to their placement closer to the mangrove fringe, where the currents are already negligible (Figure 5.2 (a)). Structures at the northern end (5 and 6 from Figure 4.7) seem to be the least effective in their ability to trap sediment, as the sediments imported through the gap between the structures and behind the structures themselves are transported out of the region in the subsequent ebb cycle. However, near the obstruction at the northern end, sediments are more sheltered and slowly move into the intertidal basin.

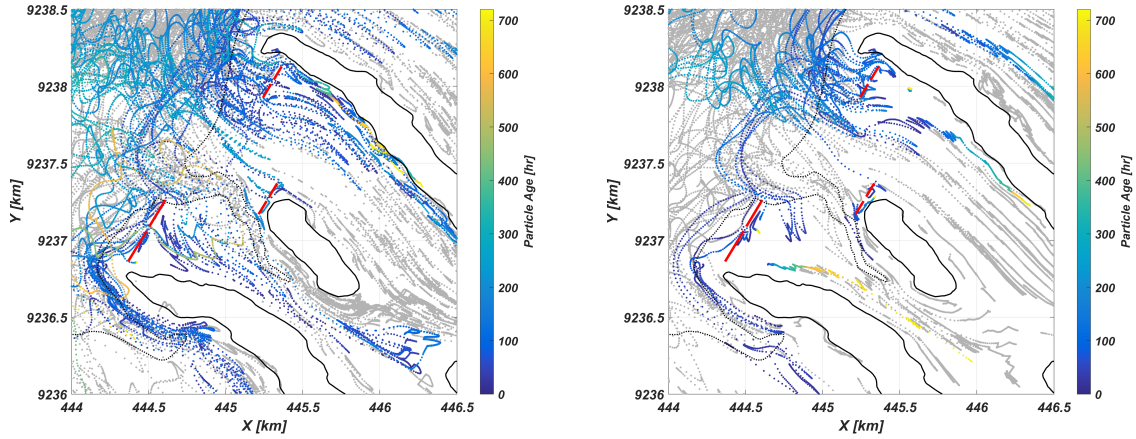

Figure 5.9: Sediment pathways of 500 source particles in the Demak coastal region based on depth-averaged currents zoomed into the area near the thin dams for particles of a) size D_{50} = 18 µm and, b) size D_{50} = 58 µm. Sediment particles traversing through the area about half a kilometre behind the structures (shown as purple dotted polygons in Figure 5.11) are mapped in colour according to their age (time elapsed since the particles were released), with the pathways of other sediment particles in the region in grey. Two depth contours for MLW and MHW are also depicted in the figure.

Sediment pathways in the Demak coastal region near the permeable dams are shown in Figure 5.10. In the presence of permeable dams, more movement of the sediment can be observed near the structures. This can be attributed to a relatively smaller reduction in currents and wave heights by the dams in comparison to the impact of hard structures. However, more import of sediment by the structures can also be noted in the case of permeable dams. This is also supported by Winterwerp et al. (2013) who found that hard structures like seawalls reduce the tidal prism and hence reduce sediment import. Winterwerp et al. (2020) and Smits (2016) also hypothesised that when permeable dams are implemented, tidal flow will be primarily through the openings between the structures with negligible flow through the dams themselves. From Figure 5.10 it can be seen that the hypothesis is not supported by the model results, since the permeable dams are modelled as porous plates, and therefore allow for substantial sediment movement though the structures. Observations by Borsje (2017) in Demak also confirm current flow through the dams, although the field study was conducted during the dry season. The alongshore transport and eventual export of sediment behind the structures at the southern end (1 and 2 from Figure 4.7) is evident from Figure 5.10 (b), more so than in the case with hard structures. The dams farther into the basin (3 and 4 from Figure 4.7) however, seem to still be capable of sediment import and retention behind them even with reduced impact on currents and waves. Nevertheless, in both structure types and at all locations, whatever small amount of sediment is imported is all sourced locally from within the basin itself and not from offshore. This could have major impact on other locations within the basin and could trigger coastline retreat in the area.

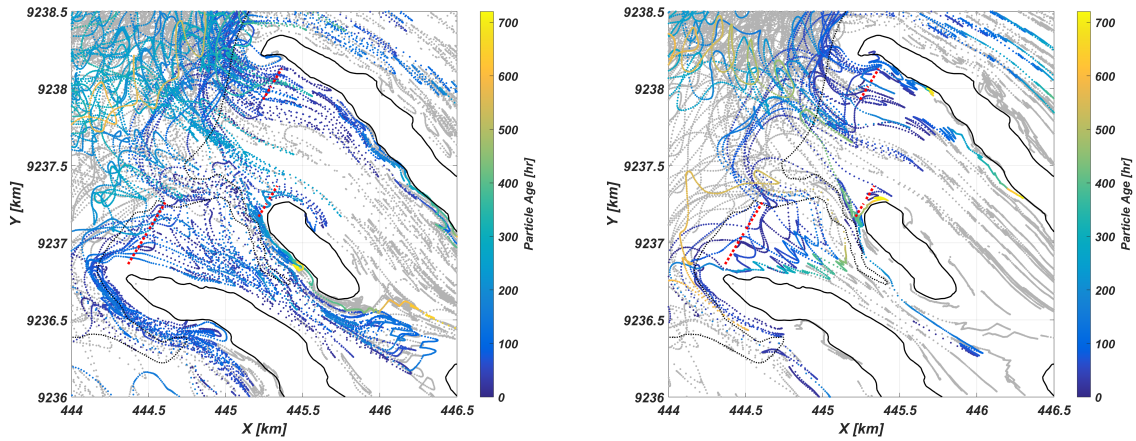

Figure 5.10: Sediment pathways of 500 source particles in the Demak coastal region based on depth-averaged currents zoomed into the area near the porous plates for particles of a) size D_{50} = 18 µm and, b) size D_{50} = 58 µm. Sediment particles traversing through the area about half a kilometre behind the structures (shown as purple dotted polygons in Figure 5.11) are mapped in colour according to their age (time elapsed since the particles were released), with the pathways of other sediment particles in the region in grey. Two depth contours for MLW and MHW are also depicted in the figure.

5.2.3. Structure Characteristics

In order to quantify the effect of structures and their characteristics such as their type (hard or permeable), length, etc., on the sediment pathways, the retention ability is measured by counting the number of particles behind the structure at each time step over the entire simulation. The count is then normalised by the number of sediment particles that were present initially before the start of the simulation to serve as a measure of the trapping efficiency of the structure. For this purpose, sources just in the vicinity of the structure spaced equally at 20 m resolution are used (see Figure 5.11).

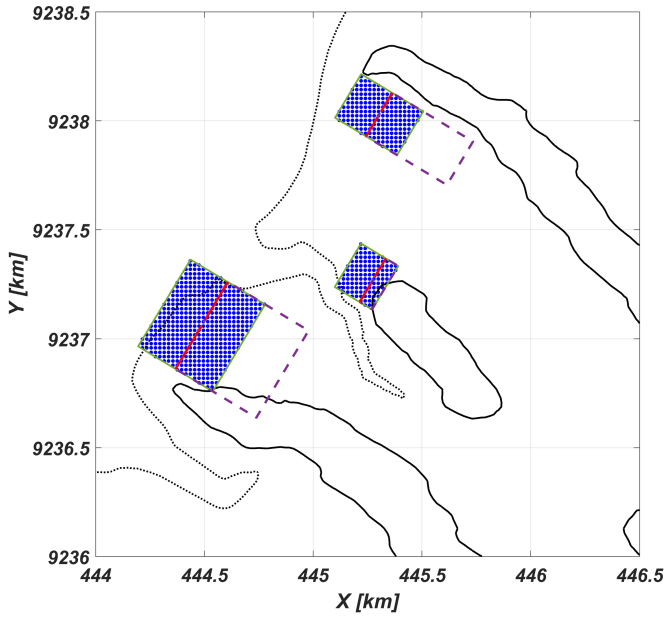

Figure 5.11: Sources of sediment particles in the vicinity of the structures with the dotted purple lines representing the polygons within which particles are counted to quantify the retention ability of each set of structures. The purple polygons are larger to include counting of the sediment particles in the seaward side of the mangrove patches behind the structures. Two depth contours for MLW and MHW are also depicted in the figure.

Type of Structure

The normalised number of particles behind the set of structures farther into the basin (3 and 4 from Figure 4.7) for the three cases of structural presence is showcased in Figure 5.12. The number of sediment particles is normalised as the fraction of particles at each timestep to the initial number of particles behind the structures.

It is evident from the figure that even without the presence of any structure to combat erosion, some retention behaviour is exhibited at the location as the normalised number of particles do not reach zero during the simulation time. With the presence of permeable dams, the retention capacity is slightly increased wherein approximately 20% of the particles behind the dams is retained. When hard structures are implemented however, the trapping efficiency is increased considerably where 80% of the sediment particles present initially behind the dams stay there through the month. Nonetheless, both temporary and hard structures are unable to retain the sediment imported during the initial flood cycles and eventually end up losing sediment behind them. The rate of loss of sediment from behind the structures however can be improved most by implementing hard structures.

A note of caution here however, is that SedTRAILS was developed as a visualisation tool for qualitatively assessing the source-to-sink movement of sediment. Quantification of the amount of sediment transport is not the main purpose of the tool with the existence of a major supply limitation. Results shown in Figure 5.12 for instance, consider only a thin, uniform surface layer of sediment. Though the thin dams supposedly retain 80% of the sediment particles, the model computes the number of particles based solely on the initial single layer of prescribed sediment sources. Consequently, the translation of these numbers into erosional or depositional characteristic of the region remains unknown and should not be interpreted as such.

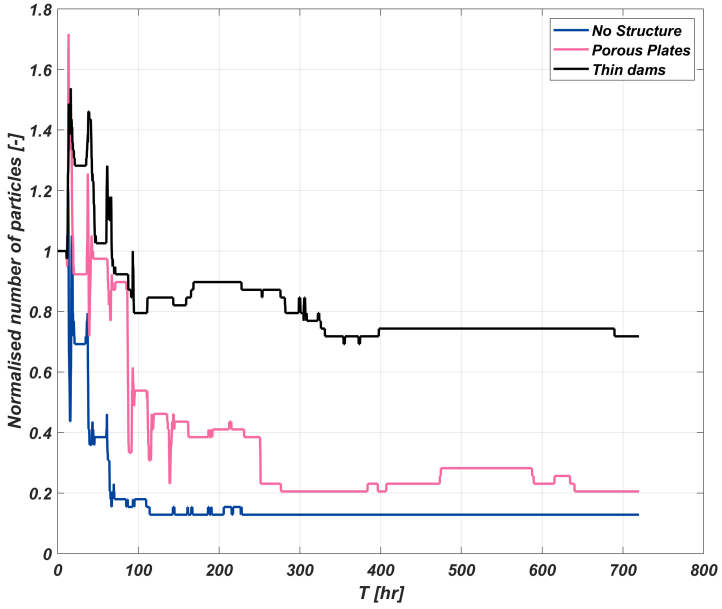

Figure 5.12: Normalised number of sediment particles behind the set of structures further behind in the basin, in the absence of structures, in the presence of porous plates and for thin dams during the simulation period

Structure Length

The effect of length of the structures on the retention capacity of the structures is studied by comparison of the normalised number of sediment particles behind the set of hard structures on the northern (5 and 6 from Figure 4.7) and southern (1 and 2) ends shown in Figure 5.13. The structures at the southern end of the basin are each 200 to 250 m long with a 33 m opening between them whereas the structures at the northern end are 100 m long each with the same 33 m gap between them.

Both sets of structures are present at locations with similar residual current patterns with small alongshore components near one end and sheltering due to obstruction at the other end (Figure 5.2 (a)). From the figure, it can be discerned that longer structures and larger structure length to opening size ratio can increase the trapping efficiency of the structure set-up. While the thin dams at the northern end lose almost all the sediment behind them, the longer ones at the southern end have a retention capacity of about 70%.

However, caution is warranted when interpreting these observations. While both types of structures are situated in areas with similar residual current patterns and sheltering, it is essential to note that the comparison of retention ability does not consider the lengths of structures at the same location. This oversight could introduce deviations in the assessment of retention ability. Therefore, the natural retention ability at the three locations of structural presence is compared in Figure 5.14. Here, zero retention is observed at the northern and southern locations of the structures, whereas approximately 18% natural retention is noted at the location farther into the basin. Thus, when comparing the sediment retention capacity at the different locations, especially structures at the northern and southern ends (1, 2, 5 and 6 from Figure 4.7) to structures mid-basin (3 and 4), regional differences must be acknowledged. To disentangle the influence of structure characteristics from the location of the structures, a preliminary sensitivity analysis is performed (see Appendix D), revealing the superior retention capability of longer structures. Nevertheless, it is worth noting that longer structures could produce larger shadow zones from waves and hence better protect sediment in the area from resuspension and eventual transport away from the region.

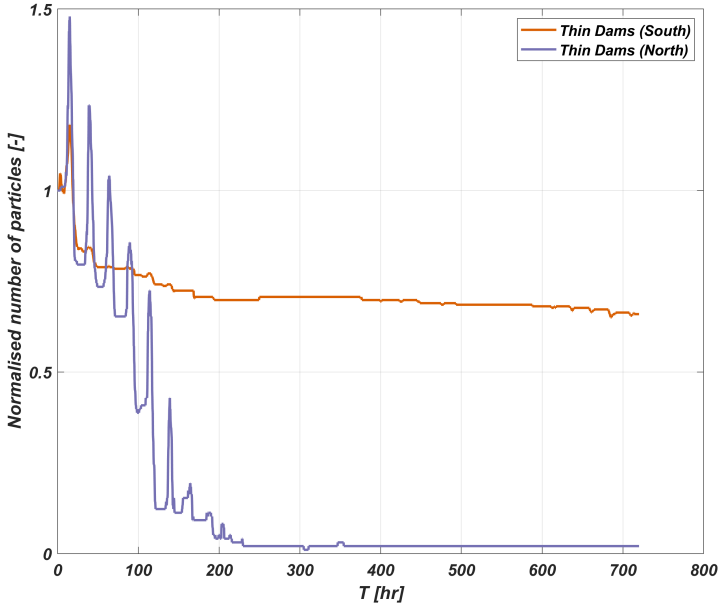

Figure 5.13: Normalised number of sediment particles during the simulation period behind the thin dams at the southern and northern ends. The number of sediment particles is normalised as the fraction of particles at each timestep to the initial number of particles behind the structures.

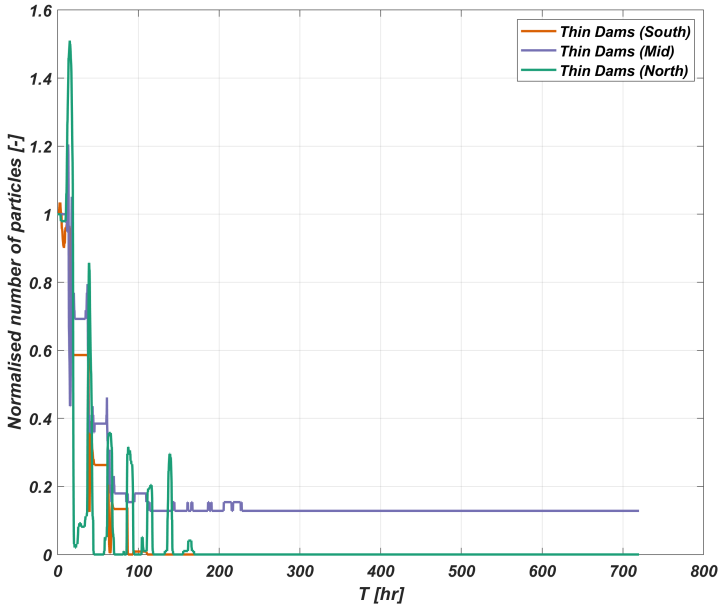

Figure 5.14: Normalised number of sediment particles during the simulation period behind the location of thin dams at the southern, mid and northern ends when no structures are present. The number of sediment particles is normalised as the fraction of particles at each timestep to the initial number of particles behind the structures.

Distance of Placement from Mangrove Fringe

Another characteristic of distance of placement of the structure from the mangrove fringe is tested for its influence on the trapping efficiency of the structures. Two sets of structures, one farther into the intertidal basin (3 and 4 from Figure 4.7) closer, at about 50 m from the mangrove fringe, and another, at the northern end of the basin (5 and 6 from Figure 4.7) placed at approximately 150 m offshore from the nearest mangrove population, are compared on the basis of the normalised number of sediment particles behind them throughout the simulation period of one month as depicted in Figure 5.15. Both sets of structures are of the same length with equal sizes of gaps between them.

It can be observed from the figure that structures placed closer to the mangrove fringe or elevated bathymetry can retain sediment better than those placed far from it. The structures placed closer to the mangroves could retain up to almost 80% of the sediment initially present behind them compared to less than 5% by the structures placed further from the mangroves. Here too, caution must be exercised in direct interpretation of the observations as the structures compared are placed at different locations within the system. However, from the analysis presented in Appendix D, the higher retention capacity of structures placed closer to the mangrove fringe can be ascertained. It is worth noting that, structures when placed closer to the mangroves are helped by the reduced current velocities and wave action at the location which are further enhanced with the structures themselves thereby helping them better retain the sediment behind them.

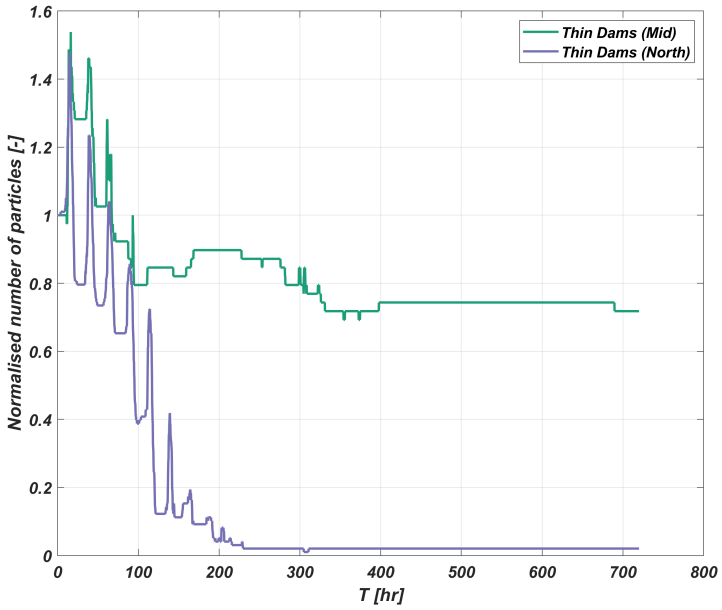

Figure 5.15: Normalised number of sediment particles during the simulation period behind the thin dams farther into the basin and at the northern end. The number of sediment particles is normalised as the fraction of particles at each timestep to the initial number of particles behind the structures.

5.3. Propagule Pathways

This section presents the results of propagule pathways modelled using SedTRAILS in the NW monsoon season.

5.3.1. Large-scale Pathways

The trajectories taken by propagules with sources at the mangrove patches observed from Google Earth images (see Figure 4.16), during the NW monsoon season, are mapped in Figure 5.16. The pathways of propagules are dominated by wind and are therefore all moving toward the coastline. Within the intertidal basin, due to the added complexity of the obligate dispersal period (ODP), during which propagules cannot get stuck, some traverse alongshore before eventually moving landward and getting stuck within the basin. Without the ODP, not as much movement of the propagules can be observed. Nevertheless, from examining the colour of the pathways in Figure 5.16, it becomes apparent that although propagules cannot get stuck during the first five days of the simulation and are free to move, they ultimately settle in locations from where they cannot move within the subsequent two days and are effectively immobilised. In the intertidal basin, most propagules get stuck at the pond bunds (Figure 5.17) in the regions as they move toward the coastline. This observation is supported by van Bijsterveldt et al. (2022) whose findings indicate that more propagules were observed in the pond zone than in the coastal zone during the NW monsoon season.

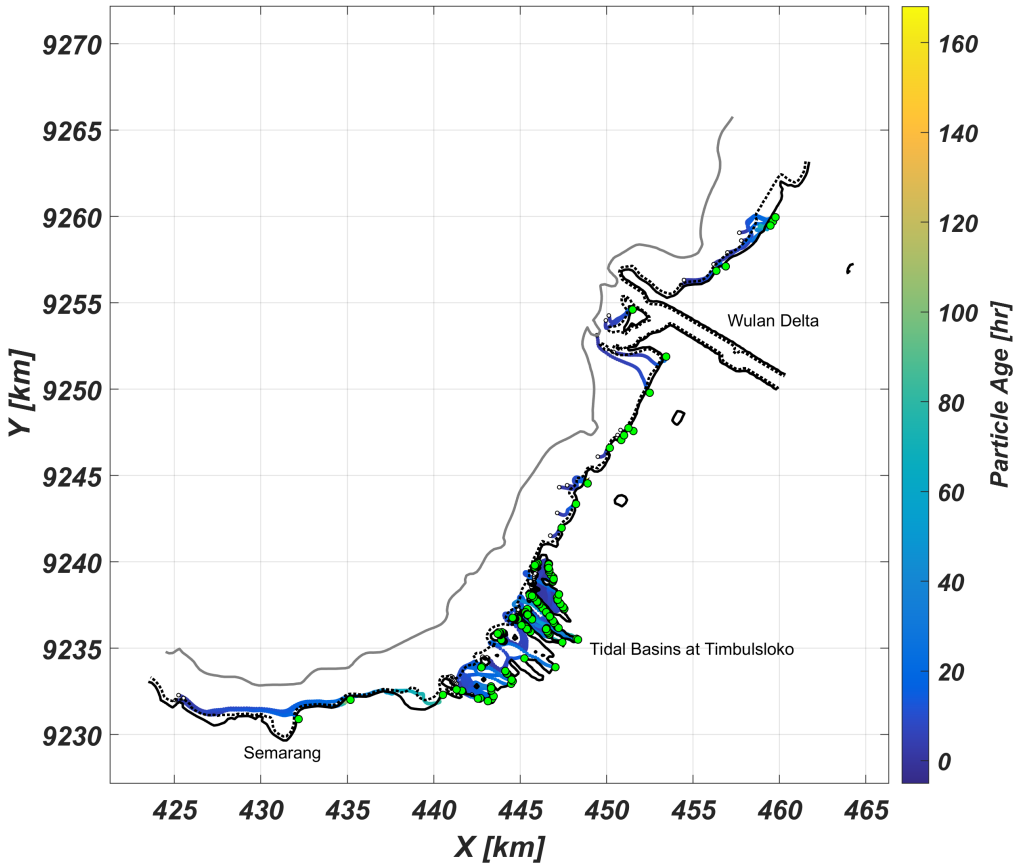

Figure 5.16: Pathways of propagules over a week with an obligate dispersal period (ODP) of five days and based on surface current velocity. The green dots represent the location where the propagules get stuck while the smaller white dots represent the sources of the propagules. Cross marks, if any, indicate end points of propagules that are not stuck within the simulation period of seven days. Three depth contours for -5 m below MSL, MLW and MHW are also depicted in the figure.

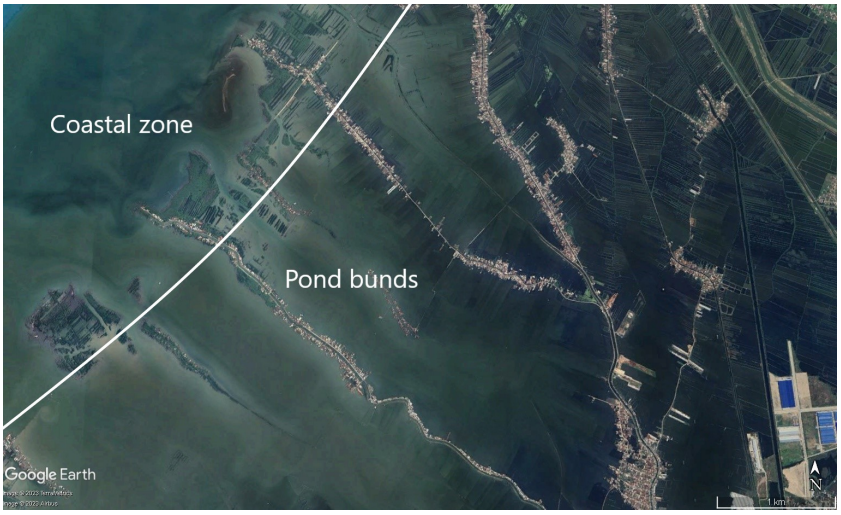

Figure 5.17: Coastal and pond zones demarcated from a Google Earth image

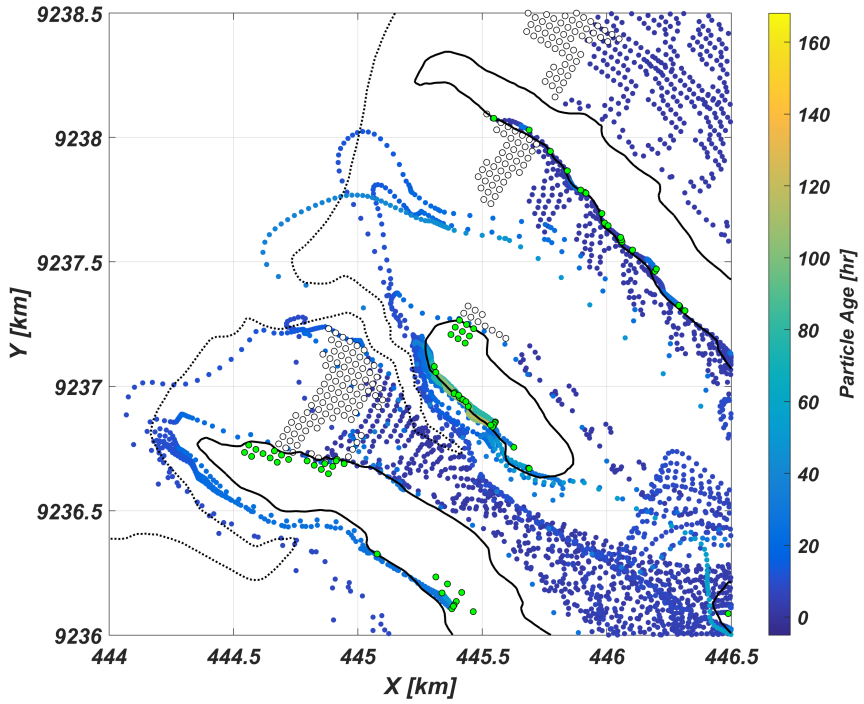

Figure 5.18: Pathways of propagules over a week with an ODP of five days and based on surface current velocity near the structural locations. The green dots represent the location where the propagules get stuck while the smaller white dots represent the sources of the propagules. Two depth contours for MLW and MHW are also depicted in the figure.

Near the location of the structures, propagules from the mangrove patches in the region are also transported onshore and therefore do not feed the region behind the structures. In any case, a few propagules from other sources within the basin are transported to the location of the structures and eventually get stuck near the mangrove patches landward of the structures as shown in Figure 5.18. However, since the model is implemented with a constant wind in the region without possible daily variation, local propagules in reality could serve more as a source for the region behind the structures than depicted through these pathways.

5.3.2. Influence of Structures on Pathways

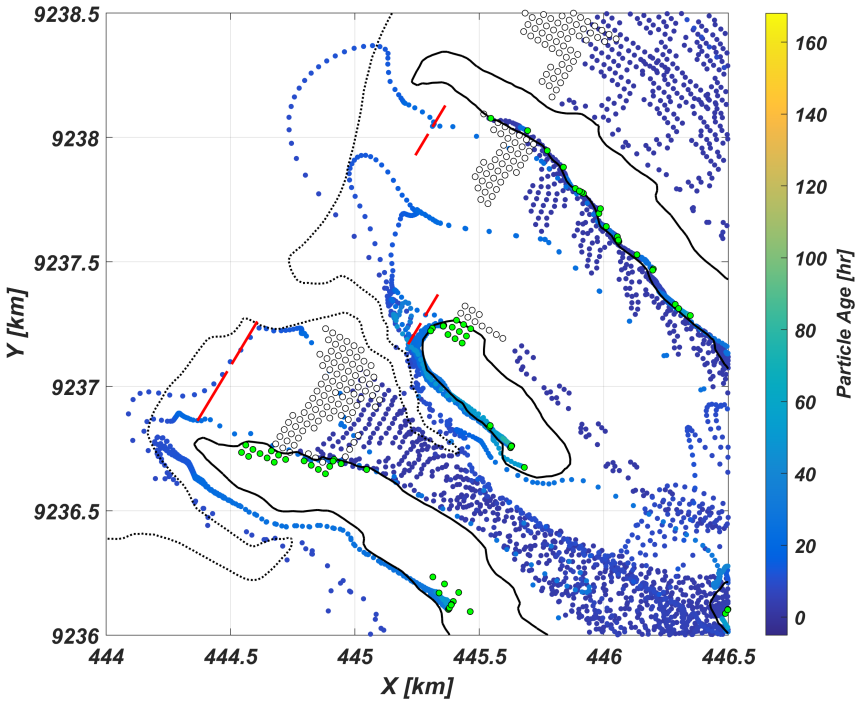

(a)

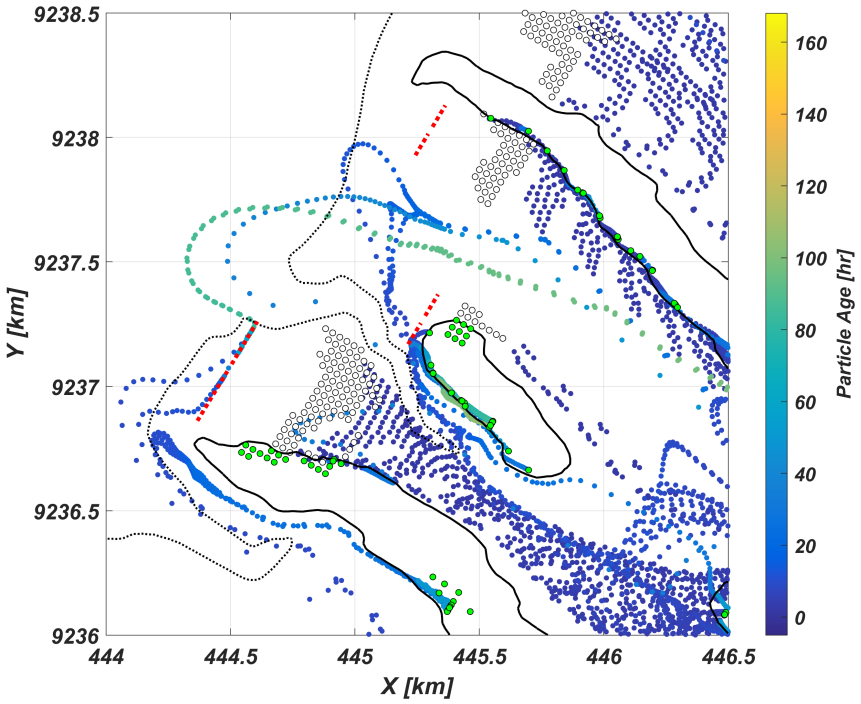

(b)

Figure 5.19: Pathways of propagules over a week with an ODP of five days and based on surface current velocity in the presence of a) thin dams and, b) porous plates. The green dots represent the location where the propagules get stuck while the smaller white dots represent the sources of the propagules. Two depth contours for MLW and MHW are also depicted in the figure.

The effect of structures both hard and temporary, if any, on the propagule pathways is portrayed in Figure 5.19. In the presence of thin dams, propagules that are approaching the area behind the structures are blocked by the structures at the northern (5 and 6 from Figure 4.7) and southern (1 and 2) ends until eventually transported along the structures and into the basin. In case of porous plates, the propagules are trapped in front of the same structures until the current can carry them away and to another location within the basin.

When propagules approach from behind the structures like in the case of the barriers further into the basin (3 and 4 from Figure 4.7), they are trapped by the structures in the site behind them and could contribute to mangrove growth there. It should be noted nonetheless that, as stated previously, when time-varying wind is taken into account, the structures might be able to help trap more propagules behind them.

6

Discussion

This chapter mounts a discussion of the results showcased in Chapter 5 in the context of model limitations, generalisations made, contribution to literature and possible future applications.

6.1. Methodological Limitations

This section elaborates on the constraints associated with the Delft3D-FLOW and -WAVE hydrodynamic models as well as the Lagrangian model SedTRAILS, and other assumptions made for modelling of the study region, and their influence on the outcomes derived from them.

6.1.1. Delft3D Model Limitations

Bathymetry

The bathymetry used for both the flow and wave models is a combination of two different datasets, one relatively coarse (Bisschop, 2023) and another more refined (Smits, 2016) near the coastline. The coarser dataset was used for the large-scale model while the refined set was used for the nested model. Since the boundary conditions for the nested model are obtained from the large-scale model, the bathymetry near the open boundaries of the nested model needed to closely resemble that of the large-scale model to obviate unrealistic current velocities near the boundaries. Hence, bathymetry for the nested model was constructed with the coarser dataset offshore of the intertidal region and with the refined dataset in the basin. However, the difference in both datasets was substantial, which was smoothed over a small distance of nearly 600 m in front of the basin. This produced a steep foreshore in the region (with slopes of about 1:400), as depicted, in Figure 6.1 with contour lines close together in front of the intertidal region. van Bijsterveldt et al. (2020) found that mangrove retreat occurred in steeper foreshores due to concentrated wave energy in the hollow profiles. This implies that the very steep foreshore modelled in this thesis may not be representative of the whole coastal region, as both eroding and accreting transects were found in Demak (van Domburg, 2018). The accreting transects however, were found to be expanding due to the presence of cheniers, which are not modelled in the morphostatic model of Delft3D used for this research (van Bijsterveldt, van Der Wal, et al., 2023). In addition, the identified eroding transects in the area exhibited slopes ranging from approximately 1:600 to 1:500, milder than the slope of 1:400 modelled (Deltares, 2020; van Domburg, 2018). The much steeper foreshores could result in larger waves near the intertidal basin, thereby affecting sediment import due to the enhanced bed shear stresses.

Furthermore, although a more refined bathymetric dataset is employed for the intertidal zone, it is noteworthy that data points across much of the basin exhibited the same elevation of MSL. Although channels were introduced manually using Google Earth images (see Appendix A), the flats are still mostly equally elevated. This observation raises concerns, particularly in areas with mangrove vegetation, where elevations might reasonably be expected to be higher owing to the sediment trapping ability of the mangroves (Walters et al., 2008). Field studies in the region to measure the bed levels are therefore recommended, to obtain a robust dataset of the bathymetry in the intertidal area.

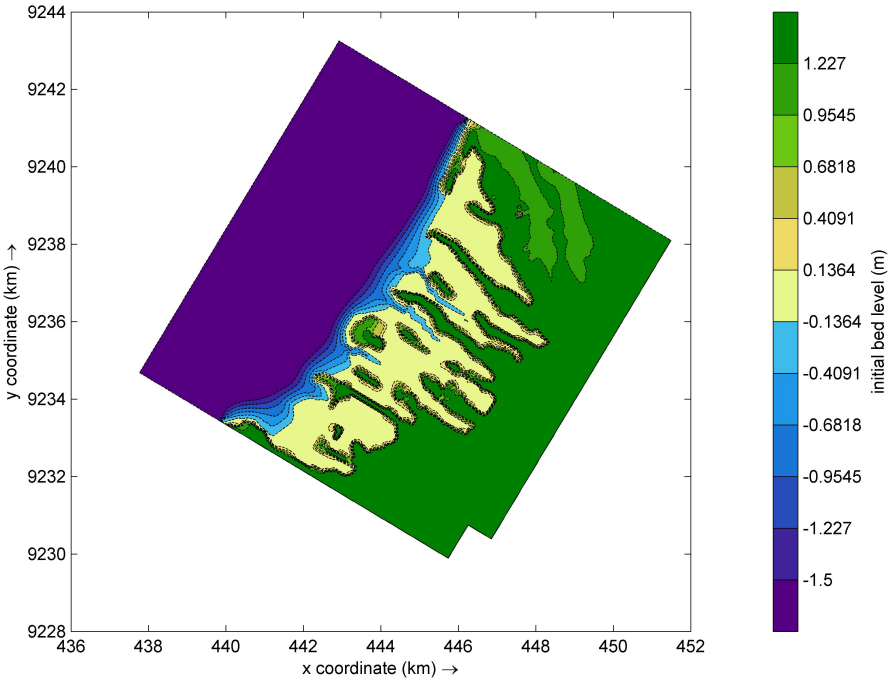

Figure 6.1: Bathymetry of nested model mapped with colour limits of -1.5 to +1.5 with respect to MSL with contour lines

Boundary Conditions for Nested Model

Various configurations of boundary conditions were tested for the nested model to find the ideal set such that the processes are well-represented by the model as discussed in section 4.2.2. Out of all possible boundary conditions for the nested model, cross-shore current boundaries and offshore water level boundaries provided the residual current patterns that were most similar to those of the large-scale model, and were hence chosen. However, a residual circulation current not present in the large-scale model persists near the northern bound of the nested model. Influence of the eddy on sediment and propagule pathways is however avoided by combining the results from large-scale and nested models, disregarding the output from nested model in the region near the boundaries, as depicted in Figure 4.12. The resultant current patterns near the bounds of the nested model are therefore not expected to have a substantial effect on the results derived from SedTRAILS. Nonetheless, utilising a more appropriate set of boundary conditions for the model would help in its future applications. Presently, Delft3D-FLOW exclusively supports the use of hydrodynamic time-series as boundary conditions for the nested model, specifically pertaining to water level or current velocity data types (Deltares, 2018b). Novel techniques such as the one proposed by Ye et al. (2012) are being developed for implementation of boundary conditions of other types for nested models. Ye et al. (2012) proposed a new boundary condition of a combination of Riemann and tangential velocity components. This combination allows the representation of oblique incoming flows at open boundaries, facilitating a smooth transition between inflow and outflow in the nested modelling domain. Exploring such techniques in future studies could contribute to the development of a more robust model.

Vegetation

Mangrove stands in the intertidal region are not modelled in this study to avoid over-complicating the model. Consequently, their influence on the hydrodynamics in the region is neglected. Mangroves exhibit the capacity to dampen waves and decelerate water flow as the tides and waves traverse through them (see section 2.1.1). This capability endows mangroves with the potential to amplify the sediment trapping efficiency of the structures erected in front of them. Consequently, the current model may underestimate the sediment-trapping capabilities of these structures.

Furthermore, the complex root systems of mangroves can also affect propagule pathways by restricting their movement out of the mangrove stand, thereby reducing the number of propagules reaching open water. However, this phenomenon is not expected to affect the modelled propagule pathways, as only the propagules exported out of the stand are currently modelled.

Mangrove vegetation can be implemented in the Delft3D-FLOW model either through trachytopes or as rigid 3D vegetation (Deltares, 2018b). The former approximates the vegetation through variation in roughness while the latter imitates vegetation with the help of various parameters describing vertical plant structure and spatial distribution of the plants. However, when the required parameters are unknown, the effect of mangroves on currents can be imitated using a grid of porous plates. Such an implementation has been successfully tested previously by Gan (2014) to mimic temporary breakwaters.

6.1.2. SedTRAILS Model Limitations

Transport Formulation

The transport formulation used in the SedTRAILS model is based on the Lagrangian particle tracking model of Soulsby et al. (2011) for sand-sized non-cohesive sediment. The formulation is thus not intended for the modelling of mud transport, and does not account for transportation processes related to muddy sediment, such as flocculation, hindered settling, etc. Since flocculation is ignored, the associated increase in sediment size and thus the increased possibility of deposition is not manifested in the sediment pathways modelled using SedTRAILS. In particular, when freshwater discharge and associated baroclinic effects are already found to play a substantial role in the sediment transport in the system, inclusion of the behaviour of flocculation would lead to the formation of flocs at the plume front, enhancing deposition there (Eisma, 1986).

Hindered settling signifies a reduction in settling velocities of suspended sediment when the concentration of sediment in the water column reaches a significant level (Winterwerp et al., 2021). Incorporation of the effect would provide more realistic depositional rates of suspended sediment. Furthermore, the 3D motion of mud particles, incorporating settling velocities is not simulated with the current formulation.

Morphostaticity

SedTRAILS is developed as a Lagrangian model to compute sediment pathways for a fixed bathymetry. While working with a constant bathymetry saves computation time, it nevertheless introduces a distinct set of challenges. When the bed levels are not updated, the bed shear stress, water depths, currents etc., do not vary as they would in reality. Therefore, the sediment pathways that could vary as the bed is elevated behind the structures are not modelled. Consequently, the sediment retention capacity obtained for the various structure characteristics is valid for the initial stages after the construction of the structures at the location, during which time the bed levels do not vary considerably. By implementing a morphostatic model, the consolidation effects of mud are also discarded which could overestimate the mobility of sediment in the area.

For propagules, survival of those that are trapped behind the structures is not modelled, since the bed levels, and consequently the windows of opportunity at the location remain unchanged. When the bed levels are not updated, it leads to inaccuracies in reflecting the true requirements of the mini-

mum inundation-free period and reduced bed shear stress behind the structures, thereby providing an inaccurate assessment of the survivability of trapped propagules.

6.1.3. Other Assumptions

Wind

In both the Delft3D-FLOW and -WAVE models, wind of a constant speed and direction is implemented. The constant onshore wind results in an almost constant onshore surface layer velocity near the coastline and regular onshore waves. The unvarying onshore wave direction does not influence the sediment pathways as the wave-induced currents are neglected in the study. However, near-constant onshore directed currents in the surface layer mean that the propagules are always moving landward. Since the structures are present offshore of mangrove stands, this assumption of invariable wind leads to negligible propagule movement and consequent establishment in the area behind the structures while van Bijsterveldt et al. (2022) observed sufficient establishment of propagules behind the structures during the wet season.

Waves

The bed shear stress from the wave model computations are used in SedTRAILS to obtain the relevant sediment pathways. For this research, the maximum bed shear stress due to currents and waves are added linearly, neglecting the non-linear interactions between the two processes. However, it can be gleaned from Figure 6.2 that the non-linear effects could be substantial (Bosboom and Stive, 2021). Underestimating the maximum bed shear stress could therefore have a considerable influence on the sediment pathways due to the underestimation of sediment mobility.

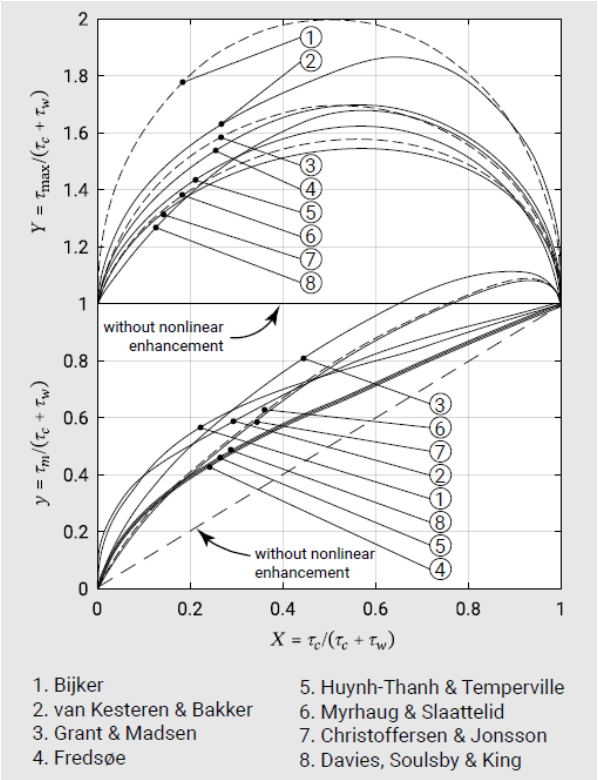

Figure 6.2: Maximum and mean bed shear stress based on different models, accounting for non-linear interactions between currents and waves (from Bosboom and Stive, 2021)

Implementation of permeable dams in the wave model is done using a sheet-type obstacle with a constant transmission coefficient. However, research done by Gijón Mancheño (2022) established the relation between incident wave height and the transmission coefficient also shown in Figure 4.11. Hence, a constant transmission coefficient chosen for storm waves could potentially be mispredicting the wave heights behind the structures. However, wave model simulations for larger water depths result in wave heights above 0.2 m near the structures surpassing the storm wave heights for which the transmission coefficient was calculated. Hence, employing a constant transmission coefficient of 0.6 may not be entirely unrealistic.

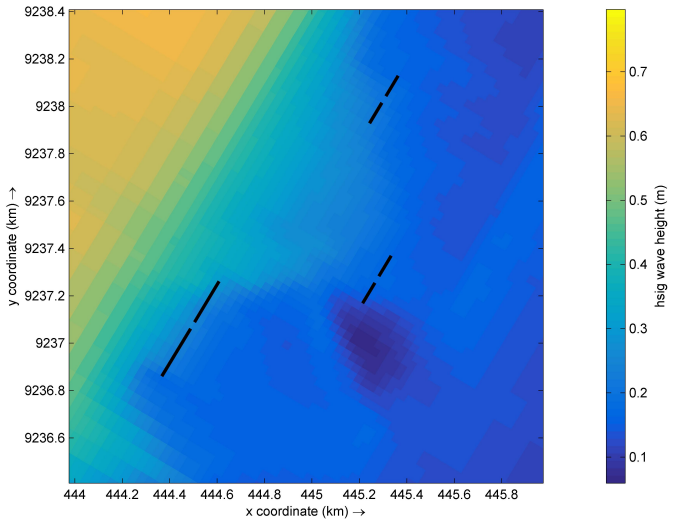

Figure 6.3: Significant wave heights near the location of the structures (indicated as solid black lines) for tidal elevation of MHW

The time series of maximum bed shear stress used in SedTRAILS for the computation of sediment pathways, is constructed based on the water level time series at an observation point in the intertidal region. This also means that the wave-induced bed shear stresses for water levels below MSL are ignored which could have potential consequences in the sediment pathways in regions outside the intertidal zone. However, since the focus of this thesis is on the effect of structures in the intertidal basin on the sediment and propagule pathways, the main conclusions of this research will not be altered by this assumption.

Porous Plate

The porous plates implemented in the Delft3D-FLOW model to approximate the effect of permeable dams used in field employ the usage of a resistance coefficient that determines the reduction in current velocities. The coefficient is chosen qualitatively to simulate a current reduction of approximately 50% of that brought about by the hard structures. For a more precise implementation of the dams to thereby obtain more accurate sediment pathways, field measurements of current velocities in the vicinity of the dams are required.

6.2. Knowledge Contribution

The literature gap is stated in section 2.4.3 as a lack of an understanding of the systemic implications of using permeable dams to rehabilitate mangroves. This research has tried bridging the gap by estimating the effect of coastal structures, both permeable (temporary brushwood structures) and impermeable (permanent hard structures), on the sediment and propagule pathways. Firstly, the impact of structures on currents and waves within their proximity and beyond was studied. Subsequently,

the effect of structures and their various characteristics on sediment and propagule trajectories was researched. Ultimately, it was examined if the sediment and propagule pathways correspond to help rehabilitate mangroves behind the structures. Through this process, the first step toward gaining a systemic understanding of using structures to rehabilitate mangroves is taken. Below, a few important results from the research are discussed in the context of the available literature.

6.2.1. River Plume

Previous research by Bisschop (2023) found the river plume to act as a barrier to sediment transport in the Demak coastal system. The freshwater plume traps the riverine sediment close to the coast, and blocks possible inflow of sediment from offshore. Wolanski (1992) also observed that sediments outwelled from mangrove forests can be retained in a coastal boundary layer formed by estuarine circulation. However, the sediment pathways presented in Figure 5.8 (b) in the previous chapter show the plume to also act as a barrier of sediment import to the intertidal basin. The lack of import is further enhanced by the steep foreshores modelled with Delft3D. Therefore, the hypothesis by Winterwerp et al. (2013) that large waves could be a potential importer of sediment to the coastline possibly depends on estuarine circulation, if any.

6.2.2. Structure Permeability

The results showcased in Chapter 5 assert the influence of structure permeability on both the hydrodynamics and sediment pathways in the region. While the impermeable structures reduce sediment movement with better efficacy than permeable dams, they also allow for comparatively less import as predicted by Winterwerp et al. (2013). However, the sediment retention capacity of the impermeable structures was found to be much higher in comparison and could therefore, better retain sediment behind them. Although installation of hard structures is more expensive, extensive and frequent shipworm induced damage to permeable dams result in substantial maintenance costs (Deltares (2021b)). Therefore, using hard structures to enhance sediment accretion could be a favourable alternative, keeping in mind the risks related to their usage in muddy environments discussed in Chapter 2.

The effect of permeability of structures on the hydrodynamics and sediment transport has not previously been modelled for a quasi-3D system. Research previously done by Gijón Mancheño (2022) provided insights into the effect of structures on the morphodynamics using a 1D cross-sectional model. Smits (2016) explored the influence of permeable dams on the hydrodynamics and morphodynamics of the Demak coastal system with a 2D model, but implemented the structures as impermeable thin dams within the model. Results from this study therefore provide useful distinction between the hard and permeable structures and their influence on the processes in a coastal system.

6.2.3. Sediment Sources

The sediment pathways in the presence of structures depicted in Figure 5.9 and Figure 5.10 show reduced movement of sediment travelling behind the structures. However, the sediment that traverses in the region is sourced from within the basin and not from offshore as hypothesised by Winterwerp et al. (2013). Nevertheless, the steeper than normal foreshores could be a reason behind the lack of sediment import from offshore into the basin.

6.2.4. Propagule Dispersal

Propagule pathways modelled in the region show negligible movement indicating dispersal of propagules up to a maximum of about 10 kms within the system. Observations of *Avicennia Marina* propagule dispersal by Clarke (1993) found most propagules to disperse for less than 1 km with very few dispersing for distances larger than 10 kms, supporting the model results.

To ensure long-term survival of mangrove forests, genetic diversity of the population is imperative as discussed in section 2.1.4. A bio-diverse forest requires the coastal system to be a recipient of propagules from sources far away. Receiving such propagules and their eventual establishment is possible in the region due to the onshore winds during the wet season pushing available propagules toward the coastline.

6.2.5. Mangrove Restoration

Worthington and Spalding (2018) mention that as a starting point for mangrove restoration, it is prudent to consider locations where mangroves have recently been lost, as such areas are highly likely to possess the necessary conditions for successful restoration. Structures in the study area, especially those modelled for this thesis, are located close to the existing mangrove patches and can therefore said to be ideally located. However, the sediment and propagule pathways correlate at only select locations, thereby highlighting the importance of other factors such as structure length, type, direction of wind, etc. Pathways of both sediment and propagules, large-scale and in the vicinity of the structures, vary widely. This can be attributed to their driving forces. While the sediment pathways are modelled with depth-averaged currents, the propagule pathways are modelled based on currents in the surface layer which is predominantly forced by the wind. Nevertheless, at locations were both sediment and propagule pathways correlate, possibly leading to restoration of mangroves there, long-term survival is a challenge, with high subsidence rates in the region (Deltares, 2021b).

6.3. Application

The results obtained from this research can in principle, be applied directly to similar systems with comparable hydrodynamic processes, for instance other micro-tidal mud-mangrove systems with extensive degradation by shrimp farming and/or ground water extraction. However, the morphostatic modelling approach used for this study may not be ideal when the relative timescale of morphodynamic change is significantly smaller than the duration of the model run. For the study region of Demak coastal system, a mean bed level increase of 0.5 cm was observed over four months in the wet season behind the permeable dams at a certain location (Winterwerp et al. (2020)). With a simulation period of one month, and an average bed level change of 0.13 cm, validity of the morphostatic approach can be ascertained by modelling the sediment pathways for the initial bed level and for with an increase of 0.13 cm, and comparing the results obtained. At regions with rapidly migrating mudbanks (celerity of 1.5 km/year) like Suriname (Augustinus, 2004), a morphostatic modelling approach might not be ideal. Nonetheless, the small-scale interactions of sediment and propagules with the structures can be universal such as reduction in movement of sediment behind the structures. The modelling approach and the methodology remains mostly universal wherein the structures can be implemented in the model of other systems using the methodology described in Chapter 4.

When considering the various structure characteristics, longer structures, placed closer to the mangrove fringe show a high sediment retention capacity. Additionally, the location of the structures also play a significant role in their retention capabilities. When currents in the region have a significant alongshore component, shore-perpendicular dams are advised to be constructed to slow sediment transport in the direction and thereby promote accretion. Without the cross-shore dams, the sediment transported behind the shore-parallel structures are eventually carried out of their region of influence as showcased in Figure 5.9.

The propagule pathways depend on specific local characteristics such as the wind direction, propagule species, etc. The modelled *Avicennia Marina* propagules have intrinsic properties such as buoyancy and viability periods that inform their lifespan in the model, and the obligate dispersal period (ODP) that dictates the ”sticky time”. Therefore, when this approach is utilised for other systems, the site-specific properties need to altered to suit the target system.

7

Conclusions and Recommendations

This chapter concludes the thesis work and suggests recommendations for further research.

7.1. Conclusions

This section presents the conclusions for the research question posed in Chapter 1.

7.1.1. Primary Research Objective

The main research question posed at the start of the study was:

How do coastal structures affect sediment and propagule pathways for mangrove restoration?

Coastal structures used to rehabilitate mangroves affect the sediment and propagule pathways by altering currents and transforming waves in the region. Additionally, structures of varying types and characteristics affect the pathways in different ways. This is further expounded up on by answering the research sub-questions posed in Chapter 1.

- How are currents affected by the presence of structures used to trap sediment and thereby help rehabilitate mangrove systems?

In the presence of hard structures, flow is blocked, thereby deflecting the currents. Just behind the structures, current velocities are negligible. In case of permeable dams, current velocities are reduced as flow passes through the dams. Currents are also slightly deflected by the presence of the dams due to the resistance exerted on the flow by the structures. The changes induced by both types of structures on the flow are however, restricted to a radius of less than one kilometre in the proximity of the structures for the site modelled.

- What is the effect on wave transformation by the structures present in the region?

The hard structures exhibit complete wave reflection with no transmission, consequently leading to the most significant reduction in wave action behind them. In addition, due to wave reflection, wave-induced bed shear stress in front of the structures is enhanced. Permeable dams too, induce a reduction in

wave heights, although not to the extent of the hard structures. However, with the current approach, the permeable dams reflect negligible wave energy, due to which, the shear stress in front of the dams are not enhanced as in the case with hard structures.

- How do structures and their implementation in the model influence sediment pathways in the study area?

Hard structures block sediment transport through them, allowing inflow through the gaps between the structures. The structures are able to slow down the sediment transported behind them and trap a fraction of the sediments, the rest of which are either carried farther into the basin, or transported alongshore, outside the influence of the structure, and out of the basin. In the presence of permeable dams, more movement of the sediment can be observed near the structures. However, the dams also allow for more influx of sediment when compared to hard structures. Nevertheless, in both structure types and at all locations, whatever small amount of sediment is imported is all sourced locally from within the basin itself and not from offshore. This could have major impact on other locations within the basin and could trigger coastline retreat in the area.

- How do structures influence mangrove propagule pathways in the study area?

In the presence of hard structures, propagules that approach from in front of the structures are blocked by them until eventually transported along the structures and into the basin. In case of porous plates, the propagules are trapped in front of the same structures until the current can carry them away and to another location within the basin. However, propagules approaching from behind the structures are trapped by them at the required region. Therefore, whether the propagules are blocked transport into the area behind the structures, or are trapped there, depends on whether from which relative direction they approach the structures.

- How do different characteristics of the structures affect the sediment pathways?

The permeable dams exhibit a greater sediment retention capacity compared to a scenario with no structures in place. In contrast, hard structures demonstrate even higher sediment retention capabilities when compared to permeable dams. However, both permeable and hard structures are unable to retain the sediment imported during the initial flood cycles and eventually end up losing sediment behind them. The rate of loss of sediment from behind the structures however can be improved most by implementing hard structures. Longer structures and larger structure length to opening size ratio can increase the trapping efficiency of the structure set-up. Longer structures are able to produce more pronounced shadow zones from waves and hence better protect sediment in the area from resuspension and eventual transport away from the region. Finally, structures placed closer to the mangrove fringe or elevated bathymetry are able to retain sediment better than those placed far from it. When placed closer to the mangroves, structures are helped by the reduced current velocities and wave action at the location which are further enhanced with the structures themselves thereby helping them better retain the sediment behind them.

- Do the pathways of sediment and propagules correlate to contribute to mangrove restoration?

Structures can help trap sediment behind them through reduction of currents and wave action thus creating a shadow zone behind them where movement of sediment is restricted. The efficacy of the structures depend on where they are located, what type is used and how long they are in comparison to the size of the openings between the structures. In case of propagules, the trapping behaviour of the structures is less apparent as the sources of propagules are mostly behind the structures and are pushed landward due to the persistent onshore wind during the wet season. However, when propagule sources are available relatively landward from the structures, the barriers are able to trap propagules, thereby creating a possibility for mangrove rehabilitation.

7.2. Recommendations

This section propounds a few recommendations for further research based on discussion in Chapter 6 of the results obtained from the various models.

7.2.1. Bathymetry

The bathymetry utilised in the flow and wave nested models is a combination of two datasets: a coarser one offshore of the intertidal basin and a more refined dataset for the basin itself. However, a significant disparity between these datasets resulted in a steep foreshore in front of the basin. Furthermore, in the intertidal zone, a notable issue arises as many data points across the basin are reported at the same elevation of MSL. This uniformity in elevations, especially in areas with mangrove vegetation, is a cause for concern, as one would expect higher elevations due to the sediment trapping capacity of mangroves. To address these concerns and improve accuracy, field studies to measure bed levels in the region are recommended to obtain a more comprehensive and precise dataset of the bathymetry in the intertidal area. Using such a dataset can result in a more accurate prediction of the hydrodynamics and hence the sediment pathways in the region. However, the refined dataset could be implemented in both the large-scale and nested models as a first step to improving the model.

7.2.2. Vegetation

Mangrove stands and their impact on the hydrodynamics in the study area are not explicitly modelled in this research. However, mangroves have the potential to enhance the sediment-trapping efficiency of the structures placed in front of them by reducing current velocities and attenuating wave energy. Therefore, mangrove vegetation could be incorporated into the Delft3D-FLOW model using methods such as trachytopes or rigid 3D vegetation. Alternatively, when the necessary parameters are unknown, the effect of mangroves on currents can be approximated using a grid of porous plates.

7.2.3. Transport Formulation

The SedTRAILS model employs a transport formulation based on a Lagrangian particle tracking model originally designed for sand-sized non-cohesive sediment. However, this formulation was not intended for muddy sediment and therefore, does not account for processes such as flocculation and hindered settling. The absence of flocculation in the model results in the neglect of increased sediment size and deposition possibilities. Hindered settling, representing reduced settling velocities with higher sediment concentrations, is another process not considered. Incorporating this effect could yield more realistic depositional rates of the sediment. Furthermore, the 3D motion of mud particles, incorporating settling velocities is not simulated with the current formulation. Therefore, using a Lagrangian sediment transport model developed for mud or implementation of muddy processes in SedTRAILS is recommended, with the inclusion of a 3D component such that settling velocities are included in the computations.

7.2.4. Morphodynamic Approach

SedTRAILS is designed as a Lagrangian model for computing sediment pathways within a fixed bathymetry. Without updating bed levels, factors such as bed shear stress, water depths, and currents remain static, deviating from real-world variability. Consequently, the model does not account for potential variations in sediment pathways resulting from elevated beds behind structures. As a first step, sediment pathways are recommended to be computed for the initial bed levels, and for bed levels expected at the end of the simulation period for a preliminary comparison. When a substantial difference is noted, a morphodynamic approach might be better suited.

References

Abidin, H. Z., Andreas, H., Gumilar, I., Sidiq, T. P., & Fukuda, Y. (2013). Land subsidence in coastal city of semarang (indonesia): Characteristics, impacts and causes. *Geomatics, Natural Hazards and Risk*, *4*(3), 226–240.

Abidin, H. Z., Andreas, H., Gumilar, I., Yuwono, B. D., Murdohardono, D., & Supriyadi, S. (2016). On integration of geodetic observation results for assessment of land subsidence hazard risk in urban areas of indonesia. *IAG 150 Years: Proceedings of the IAG Scientific Assembly in Postdam, Germany, 2013*, 435–442.

Alongi, D. M. (2002). Present state and future of the world's mangrove forests. *Environmental Conservation*, *29*(3), 331–349.

Alongi, D. M. (2008). Mangrove forests: Resilience, protection from tsunamis, and responses to global climate change. *Estuarine Coastal and Shelf Science*, *76*(1), 1–13.

Alongi, D. M. (2012). Carbon sequestration in mangrove forests. *Carbon management*, *3*(3), 313–322.

Anthony, E. J., & Gratiot, N. (2012). Coastal engineering and large-scale mangrove destruction in guyana, south america: Averting an environmental catastrophe in the making. *Ecological Engineering*, *47*, 268–273.

Augustinus, P. G. (2004). The influence of the trade winds on the coastal development of the guianas at various scale levels: A synthesis. *Marine Geology*, *208*(2-4), 145–151.

Balke, T., Bouma, T. J., Horstman, E. M., Webb, E. L., Erftemeijer, P. L., & Herman, P. M. (2011). Windows of opportunity: Thresholds to mangrove seedling establishment on tidal flats. *Marine Ecology Progress Series*, *440*, 1–9.

Barbier, E. B., Hacker, S. D., Hacker, S. D., Kennedy, C. J., Koch, E. W., Stier, A. C., & Silliman, B. R. (2011). The value of estuarine and coastal ecosystem services. *Ecological Monographs*, *81*(2), 169–193.

Bayong Tjasyono, H., Gernowo, R., Sri Woro, B., & Ina, J. (2008). The character of rainfall in the indonesian monsoon. *The International Symposium on Equatorial Monsoon System, Yogyakarta*.

Bayraktarov, E., Saunders, M. I., Abdullah, S., Mills, M., Beher, J., Possingham, H. P., Mumby, P. J., & Lovelock, C. E. (2016). The cost and feasibility of marine coastal restoration. *Ecological Applications*, *26*(4), 1055–1074.

Besset, M., Gratiot, N., Anthony, E. J., Bouchette, F., Goichot, M., & Marchesiello, P. (2019). Mangroves and shoreline erosion in the mekong river delta, viet nam. *Estuarine, Coastal and Shelf Science*, *226*, 106263.

Bisschop, F. (2023). Modelling sediment and propagule pathways to improve mangrove rehabilitation: A case study of the pilot project in demak, indonesia.

Biswas, S. R., Mallik, A. U., Choudhury, J. K., & Nishat, A. (2009). A unified framework for the restoration of southeast asian mangroves—bridging ecology, society and economics. *Wetlands Ecology and Management*, *17*, 365–383.

Borsje, R. (2017). Assessing current patterns behind hybrid dams: Demak, indonesia.

Bosboom, J., & Stive, M. J. (2021). Coastal dynamics.

Bunting, P., Rosenqvist, A., Hilarides, L., Lucas, R. M., Thomas, N., Tadono, T., Worthington, T. A., Spalding, M., Murray, N. J., & Rebelo, L.-M. (2022). Global mangrove extent change 1996–2020: Global mangrove watch version 3.0. *Remote Sensing*, *14*(15), 3657.

Ceddia, M. G. (2019). The impact of income, land, and wealth inequality on agricultural expansion in latin america. *116*(7), 2527–2532.

Clarke, P. J. (1993). Dispersal of grey mangrove (avicennia marina) propagules in southeastern australia. *Aquatic Botany*, *45*(2-3), 195–204.

Clarke, P. J., Kerrigan, R. A., & Westphal, C. J. (2001). Dispersal potential and early growth in 14 tropical mangroves: Do early life history traits correlate with patterns of adult distribution? *Journal of Ecology*, 648–659.

delos Santos, K. A., Avtar, R., Salmo III, S., & Fujii, M. (2022). Assessment of mangrove colonization of aquaculture ponds through satellite image analysis: Implications for mangrove management. In *Assessing, mapping and modelling of mangrove ecosystem services in the asia-pacific region* (pp. 31–50). Springer.

Deltares (Ed.). (2018a). *Delft3d functional specifications*.

Deltares (Ed.). (2018b). *Delft3d-flow user manual*.

Deltares (Ed.). (2018c). *Delft3d-wave user manual*.

Deltares. (2020). *Effectiveness of ecosystem-based adaptation measures subject to sea level rise and land subsidence* (tech. rep.). 1220476-004-ZKS-0011.

Deltares. (2021a). *Economic assessment of subsidence in semarang and demak* (tech. rep.). 1220476-002-ZKS-0009.

Deltares. (2021b). *Monitoring of ecological mangrove restoration by use of permeable structures* (tech. rep.). 1220476-000-ZKS-0010.

Di Nitto, D., Erftemeijer, P., van Beek, J., Dahdouh-Guebas, F., Higazi, L., Quisthoudt, K., Jayatissa, L., & Koedam, N. (2013). Modelling drivers of mangrove propagule dispersal and restoration of abandoned shrimp farms. *Biogeosciences*, *10*(7), 5095–5113.

Duke, N. C. (1995). Genetic diversity, distributional barriers and rafting continents—more thoughts on the evolution of mangroves. *Asia-Pacific Symposium on Mangrove Ecosystems: Proceedings of the International Conference held at The Hong Kong University of Science & Technology, September 1–3, 1993*, 167–181.

Ecoshape. (2015). *Building with nature indonesia: Securing eroding delta coastlines: Design and engineering plan* (tech. rep.).

Eisma, D. (1986). Flocculation and de-flocculation of suspended matter in estuaries. *Netherlands Journal of sea research*, *20*(2-3), 183–199.

Enwright, N. M., Griffith, K. T., & Osland, M. J. (2016). Barriers to and opportunities for landward migration of coastal wetlands with sea-level rise. *Frontiers in Ecology and the Environment*, *14*(6), 307–316.

Eong, O. J. (1993). Mangroves-a carbon source and sink. *Chemosphere*, *27*(6), 1097–1107.

Etminan, V., Lowe, R. J., & Ghisalberti, M. (2017). A new model for predicting the drag exerted by vegetation canopies. *Water Resources Research*, *53*(4), 3179–3196.

Fadlillah, L. N., Widyastuti, M., Geottongsong, T., Sunarto, & Marfai, M. A. (2019). Hydrological characteristics of estuary in wulan delta in demak regency, indonesia. *Water Resources*, *46*, 832–843.

Feller, I. C., Lovelock, C. E., Berger, U., McKee, K. L., Joye, S. B., & Ball, M. (2010). Biocomplexity in mangrove ecosystems. *Annual review of marine science*, *2*, 395–417.

FLOW-3D. (2022). *Grid systems*. Retrieved May 21, 2023, from https://www.flow3d.com/resources/cfd-101/general-cfd/grid-systems/

Friess, D. A., Adame, M. F., Adams, J. B., & Lovelock, C. E. (2022). Mangrove forests under climate change in a 2 c world. *Wiley Interdisciplinary Reviews: Climate Change*, *13*(4), e792.

Furukawa, K., Wolanski, E., & Mueller, H. (1997). Currents and sediment transport in mangrove forests. *Estuarine, Coastal and Shelf Science*, *44*(3), 301–310.

Gan, S. (2014). Hydrodynamic modelling for mangrove reforestation at tanjung piai, west coast peninsular malaysia.

Gijón Mancheño, A. (2022). Restoring mangroves with structures: Improving the mangrove habitat using local materials.

Gijón Mancheño, A., Jansen, W., Uijttewaal, W., Reniers, A., van Rooijen, A., Suzuki, T., Etminan, V., & Winterwerp, J. (2021). Wave transmission and drag coefficients through dense cylinder arrays: Implications for designing structures for mangrove restoration. *Ecological Engineering*, *165*, 106231.

Gijón Mancheño, A., Jansen, W., Winterwerp, J. C., & Uijttewaal, W. S. (2021). Predictive model of bulk drag coefficient for a nature-based structure exposed to currents. *Scientific reports*, *11*(1), 3517.

Gilman, E. L., Ellison, J., Duke, N. C., & Field, C. (2008). Threats to mangroves from climate change and adaptation options: A review. *Aquatic botany*, *89*(2), 237–250.

Giri, C., Ochieng, E., Tieszen, L. L., Zhu, Z., Singh, A., Loveland, T. R., Masek, J. G., & Duke, N. (2011). Status and distribution of mangrove forests of the world using earth observation satellite data. *Global Ecology and Biogeography*, *20*(1), 154–159.

Glaser, M. (2003). Interrelations between mangrove ecosystem, local economy and social sustainability in caeté estuary, north brazil. *Wetlands Ecology and Management*, *11*, 265–272.

Goldberg, L., Lagomasino, D., Thomas, N., & Fatoyinbo, T. (2020). Global declines in human-driven mangrove loss. *Global change biology*, *26*(10), 5844–5855.

Guo, Z., Li, X., He, Z., Yang, Y., Wang, W., Zhong, C., Greenberg, A. J., Wu, C.-I., Duke, N. C., & Shi, S. (2018). Extremely low genetic diversity across mangrove taxa reflects past sea level changes and hints at poor future responses. *Global Change Biology*, *24*(4), 1741–1748.

Hagger, V., Worthington, T. A., Lovelock, C. E., Adame, M. F., Amano, T., Brown, B. M., Friess, D. A., Landis, E., Mumby, P. J., Morrison, T. H., et al. (2022). Drivers of global mangrove loss and gain in social-ecological systems. *Nature Communications*, *13*(1), 6373.

Hamilton, S. E., Casey, D., & Casey, D. C. (2016). Creation of a high spatiotemporal resolution global database of continuous mangrove forest cover for the 21st century (cgmfc-21). *Global Ecology and Biogeography*, *25*(6), 729–738.

Hatayama, T., Awaji, T., & Akitomo, K. (1996). Tidal currents in the indonesian seas and their effect on transport and mixing. *Journal of Geophysical Research: Oceans*, *101*(C5), 12353–12373.

Holl, K. D., Studies, E., & Cruz, S. (2020). Asian mangroves: Community involvement in mangrove restoration provides coastal hazard reduction and enhances human livelihoods. *Indonesia and Sri Lanka*.

Hufnagl, M., Payne, M., Lacroix, G., Bolle, L. J., Daewel, U., Dickey-Collas, M., Gerkema, T., Huret, M., Janssen, F., Kreus, M., et al. (2017). Variation that can be expected when using particle tracking models in connectivity studies. *Journal of sea research*, *127*, 133–149.

Ilman, M., Dargusch, P., Dart, P., et al. (2016). A historical analysis of the drivers of loss and degradation of indonesia's mangroves. *Land use policy*, *54*, 448–459.

Kamali, B., & Hashim, R. (2011). Mangrove restoration without planting. *Ecological Engineering*, *37*(2), 387–391.

Kathiresan, K., & Bingham, B. L. (2001). Biology of mangroves and mangrove ecosystems.

Kathiresan, K., & Rajendran, N. (2005). Coastal mangrove forests mitigated tsunami. *Estuarine, Coastal and shelf science*, *65*(3), 601–606.

Krauss, K. W., McKee, K. L., Lovelock, C. E., Cahoon, D. R., Saintilan, N., Reef, R., & Chen, L. (2014). How mangrove forests adjust to rising sea level. *New Phytologist*, *202*(1), 19–34.

Krauss, K. W., & Osland, M. J. (2020). Tropical cyclones and the organization of mangrove forests: A review. *Annals of Botany*, *125*(2), 213–234.

Lewis, R. R. (2001). Mangrove restoration-costs and benefits of successful ecological restoration. *Proceedings of the Mangrove Valuation Workshop, Universiti Sains Malaysia, Penang*, *4*(8).

Lewis III, R. R. (1990). Creation and restoration of coastal plain wetlands in florida. kusler and kentula, editors. wetland creation and restoration: The status of the science.

Lewis III, R. R. (2005). Ecological engineering for successful management and restoration of mangrove forests. *Ecological engineering*, *24*(4), 403–418.

Lewis III, R. R., Brown, B. M., & Flynn, L. L. (2019). Methods and criteria for successful mangrove forest rehabilitation. In *Coastal wetlands* (pp. 863–887). Elsevier.

Lovelock, C. E., Cahoon, D. R., Friess, D. A., Guntenspergen, G. R., Krauss, K. W., Reef, R., Rogers, K., Saunders, M. L., Sidik, F., Swales, A., et al. (2015). The vulnerability of indo-pacific mangrove forests to sea-level rise. *Nature*, *526*(7574), 559–563.

MacDonald, N. J., & Davies, M. H. (2007). Particle-based sediment transport modeling. In *Coastal engineering 2006: (in 5 volumes)* (pp. 3117–3128). World Scientific.

Marfai, M. A. (2011). The hazards of coastal erosion in central java, indonesia: An overview. *Geografia-Malaysian Journal of Society and Space*, *7*(3), 1–9.

Marfai, M. A., & King, L. (2007). Monitoring land subsidence in semarang, indonesia. *Environmental geology*, *53*, 651–659.

Mazda, Y., Magi, M., Ikeda, Y., Kurokawa, T., & Asano, T. (2006). Wave reduction in a mangrove forest dominated by sonneratia sp. *Wetlands Ecology and Management*, *14*, 365–378.

McKee, K. L., & Faulkner, P. L. (2000). Restoration of biogeochemical function in mangrove forests. *Restoration Ecology*, *8*(3), 247–259.

McKee, K. L., Rogers, K., & Saintilan, N. (2012). Response of salt marsh and mangrove wetlands to changes in atmospheric co2, climate, and sea level. In *Global change and the function and distribution of wetlands* (pp. 63–96). Springer.

Mitra, A. (2020). Ecosystem services of mangroves: An overview. *Mangrove Forests in India: Exploring Ecosystem Services*, 1–32.

Nagelkerken, I., Blaber, S., Bouillon, S., Green, P., Haywood, M., Kirton, L., Meynecke, J.-O., Pawlik, J., Penrose, H., Sasekumar, A., et al. (2008). The habitat function of mangroves for terrestrial and marine fauna: A review. *Aquatic botany*, *89*(2), 155–185.

Nathan, R., Schurr, F. M., Spiegel, O., Steinitz, O., Trakhtenbrot, A., & Tsoar, A. (2008). Mechanisms of long-distance seed dispersal. *Trends in ecology & evolution*, *23*(11), 638–647.

NHMI. (2000). *Mangrove reproduction*. Retrieved August 19, 2023, from https://www.nhmi.org/mangroves/rep.htm

Osborne, D. J., & Berjak, P. (1997). The making of mangroves: The remarkable pioneering role played by seeds of avicennia marina. *Endeavour*, *21*(4), 143–147.

Paris, C. B., Helgers, J., Van Sebille, E., & Srinivasan, A. (2013). Connectivity modeling system: A probabilistic modeling tool for the multi-scale tracking of biotic and abiotic variability in the ocean. *Environmental Modelling & Software*, *42*, 47–54.

Pautasso, M., Holdenrieder, O., & Stenlid, J. (2005). 13 susceptibility to fungal pathogens of forests differing in tree diversity. *Forest diversity and function: temperate and boreal systems*, *176*, 263.

Pearson, S. G., Elias, E., van Ormondt, M., Roelvink, F., Lambregts, P., Wang, Z., & van Prooijen, B. (2021). Lagrangian sediment transport modelling as a tool for investigating coastal connectivity. *Coastal Dynamics*.

Pearson, S. G., van Prooijen, B. C., Elias, E. P., Vitousek, S., & Wang, Z. B. (2020). Sediment connectivity: A framework for analyzing coastal sediment transport pathways. *Journal of Geophysical Research: Earth Surface*, *125*(10), e2020JF005595.

Prasetyo, Y., Bashit, N., Sasmito, B., & Setianingsih, W. (2019). Impact of land subsidence and sea level rise influence shoreline change in the coastal area of demak. *IOP Conference Series: Earth and Environmental Science*, *280*(1), 012006.

Primavera, J. H., & Esteban, J. M. A. (2008). A review of mangrove rehabilitation in the philippines: Successes, failures and future prospects. *Wetlands Ecology and Management*, *16*, 345–358.

Rabinowitz, D. (1978). Dispersal properties of mangrove propagules. *Biotropica*, 47–57.

Rajpar, M. N., & Zakaria, M. (2014). Mangrove fauna of asia. *Mangrove ecosystems of Asia: Status, challenges and management strategies*, 153–197.

Randy, A. F., Hutomo, M., & Purnama, H. (2015). Collaborative efforts on mangrove restoration in sedari village, karawang district, west java province. *Procedia Environmental Sciences*, *23*, 48–57.

Rönnbäck, P., Crona, B., & Ingwall, L. (2007). The return of ecosystem goods and services in replanted mangrove forests: Perspectives from local communities in kenya. *Environmental Conservation*, *34*(4), 313–324.

Saengsupavanich, C. (2013). Erosion protection options of a muddy coastline in thailand: Stakeholders' shared responsibilities. *Ocean & coastal management*, *83*, 81–90.

Saintilan, N., Khan, N., Ashe, E., Kelleway, J., Rogers, K., Woodroffe, C. D., & Horton, B. P. (2020). Thresholds of mangrove survival under rapid sea level rise. *Science*, *368*(6495), 1118–1121.

Schmitt, K., & Albers, T. (2014). Area coastal protection and the use of bamboo breakwaters in the mekong delta. In *Coastal disasters and climate change in vietnam* (pp. 107–132). Elsevier.

Schmitt, K., Albers, T., Pham, T., & Dinh, S. (2013). Site-specific and integrated adaptation to climate change in the coastal mangrove zone of soc trang province, viet nam. *Journal of Coastal Conservation*, *17*(3), 545–558.

Septiangga, B., & Mutaqin, B. W. (2021). Spatio-temporal analysis of wulan delta in indonesia: Characteristics, evolution, and controlling factors. *Geographia Technica*, *16*.

Smith III, T. J. (1992). Forest structure. *Tropical mangrove ecosystems*, *41*, 101–136.

Smits, B. (2016). Morphodynamic optimisation study of the design of semi-permeable dams for rehabilitation of a mangrove-mud coast: A case study of the building-with-nature project in demak, indonesia.

Soulsby, R. (1994). *Manual of marine sands*. HR Wallingford.

Soulsby, R., Mead, C., Wild, B., & Wood, M. (2011). Lagrangian model for simulating the dispersal of sand-sized particles in coastal waters. *Journal of waterway, port, coastal, and ocean engineering*, *137*(3), 123–131.

Sousa, W. P., Kennedy, P. G., Mitchell, B. J., & Ordóñez L, B. M. (2007). Supply-side ecology in mangroves: Do propagule dispersal and seedling establishment explain forest structure? *Ecological monographs*, *77*(1), 53–76.

Spalding, M. (2010). *World atlas of mangroves* (1st ed.). Routeledge.

Spalding, M., Mcivor, A., Tonneijck, F., Tol, S., & van Eijk, P. (2014). Mangroves for coastal defence.

Spalding, M., & Parrett, C. L. (2019). Global patterns in mangrove recreation and tourism. *Marine Policy*, *110*, 103540.

Storlazzi, C. D., Van Ormondt, M., Chen, Y.-L., & Elias, E. P. (2017). Modeling fine-scale coral larval dispersal and interisland connectivity to help designate mutually-supporting coral reef marine protected areas: Insights from maui nui, hawaii. *Frontiers in Marine Science*, *4*, 381.

Suzuki, T., Hu, Z., Kumada, K., Phan, L. K., & Zijlema, M. (2019). Non-hydrostatic modeling of drag, inertia and porous effects in wave propagation over dense vegetation fields. *Coastal Engineering*, *149*, 49–64.

Swart, D. H. (1974). Offshore sediment transport and equilibrium beach profiles.

Tas, S. (2022). Chenier dynamics.

Tas, S., van Maren, D., & Reniers, A. (2020). Observations of cross-shore chenier dynamics in demak, indonesia. *Journal of Marine Science and Engineering*, *8*(12), 972.

Thomas, N., Lucas, R., Bunting, P., Hardy, A., Rosenqvist, A., & Simard, M. (2017). Distribution and drivers of global mangrove forest change, 1996–2010. *PloS one*, *12*(6).

Trakhtenbrot, A., Nathan, R., Perry, G., & Richardson, D. M. (2005). The importance of long-distance dispersal in biodiversity conservation. *Diversity and Distributions*, *11*(2), 173–181.

Trégarot, E., Caillaud, A., Cornet, C. C., Taureau, F., Catry, T., Cragg, S. M., & Failler, P. (2021). Mangrove ecological services at the forefront of coastal change in the french overseas territories. *Science of the Total Environment*, *763*, 143004.

Van, T., Wilson, N., Thanh-Tung, H., Quisthoudt, K., Quang-Minh, V., Xuan-Tuan, L., Dahdouh-Guebas, F., & Koedam, N. (2015). Changes in mangrove vegetation area and character in a war and land use change affected region of vietnam (mui ca mau) over six decades. *Acta Oecologica*, *63*, 71–81.

Van Cuong, C., Brown, S., To, H. H., & Hockings, M. (2015). Using melaleuca fences as soft coastal engineering for mangrove restoration in kien giang, vietnam. *Ecological Engineering*, *81*, 256–265.

van der Stocken, T., Carroll, D., Menemenlis, D., Simard, M., & Koedam, N. (2019). Global-scale dispersal and connectivity in mangroves. *Proceedings of the National Academy of Sciences*, *116*(3), 915–922.

van der Stocken, T., De Ryck, D. J., Balke, T., Bouma, T. J., Dahdouh-Guebas, F., & Koedam, N. (2013). The role of wind in hydrochorous mangrove propagule dispersal. *Biogeosciences*, *10*(6), 3635–3647.

van der Stocken, T., Vanschoenwinkel, B., Carroll, D., Cavanaugh, K. C., & Koedam, N. (2022). Mangrove dispersal disrupted by projected changes in global seawater density. *Nature Climate Change*, *12*(7), 685–691.

van der Stocken, T., Vanschoenwinkel, B., De Ryck, D. J., Bouma, T. J., Dahdouh-Guebas, F., & Koedam, N. (2015). Interaction between water and wind as a driver of passive dispersal in mangroves. *PLoS One*, *10*(3), e0121593.

van der Stocken, T., Wee, A. K., De Ryck, D. J., Vanschoenwinkel, B., Friess, D. A., Dahdouh-Guebas, F., Simard, M., Koedam, N., & Webb, E. L. (2019). A general framework for propagule dispersal in mangroves. *Biological Reviews*, *94*(4), 1547–1575.

van Bijsterveldt, C. E., Debrot, A. O., Bouma, T. J., Maulana, M. B., Pribadi, R., Schop, J., Tonneijck, F. H., & van Wesenbeeck, B. K. (2022). To plant or not to plant: When can planting facilitate mangrove restoration? *Frontiers in Environmental Science*, *9*, 690011.

van Bijsterveldt, C. E., Herman, P. M., van Wesenbeeck, B. K., Ramadhani, S., Heuts, T. S., van Starrenburg, C., Tas, S. A., Triyanti, A., Helmi, M., Tonneijck, F. H., et al. (2023). Subsidence reveals potential impacts of future sea level rise on inhabited mangrove coasts. *Nature Sustainability*, 1–13.

van Bijsterveldt, C. E., van Der Wal, D., Gijón Mancheno, A., Fivash, G. S., Helmi, M., & Bouma, T. J. (2023). Can cheniers protect mangroves along eroding coastlines?–the effect of contrasting foreshore types on mangrove stability. *Ecological engineering*, *187*, 106863.

van Bijsterveldt, C. E., van Wesenbeeck, B. K., van der Wal, D., Afiati, N., Pribadi, R., Brown, B., & Bouma, T. J. (2020). How to restore mangroves for greenbelt creation along eroding coasts with abandoned aquaculture ponds. *Estuarine, coastal and shelf science*, *235*, 106576.

van Domburg, T. (2018). Identifying windows of opportunity for mangrove establishment on a mud coast: A case study for the biomanco project in demak, indonesia.

van Maren, D. (2004). *Morphodynamics of a cyclic prograding delta: The red river, vietnam*. Utrecht University.

van Ormondt, M., Nederhoff, K., & van Dongeren, A. (2020). Delft dashboard: A quick set-up tool for hydrodynamic models. *Journal of Hydroinformatics*, *22*(3), 510–527.

van Sebille, E., Griffies, S. M., Abernathey, R., Adams, T. P., Berloff, P., Biastoch, A., Blanke, B., Chassignet, E. P., Cheng, Y., Cotter, C. J., et al. (2018). Lagrangian ocean analysis: Fundamentals and practices. *Ocean modelling*, *121*, 49–75.

Verschure, S. (2013). Final report on applying hybrid engineering to restore a muddy coast in north java indonesia. *Wetlands International, Netherlands*.

Walsh, K. J., McBride, J. L., Klotzbach, P. J., Balachandran, S., Camargo, S. J., Holland, G., Knutson, T. R., Kossin, J. P., Lee, T.-c., Sobel, A., et al. (2016). Tropical cyclones and climate change. *Wiley Interdisciplinary Reviews: Climate Change*, *7*(1), 65–89.

Walters, B. B., Rönnbäck, P., Kovacs, J. M., Crona, B., Hussain, S. A., Badola, R., Primavera, J. H., Barbier, E., & Dahdouh-Guebas, F. (2008). Ethnobiology, socio-economics and management of mangrove forests: A review. *Aquatic Botany*, *89*(2), 220–236.

Wang, W., Li, X., & Wang, M. (2019). Propagule dispersal determines mangrove zonation at intertidal and estuarine scales. *Forests*, *10*(3), 245.

Winterwerp, J. C., Albers, T., Anthony, E. J., Friess, D. A., Gijón Mancheño, A., Moseley, K., Muhari, A., Naipal, S., Noordermeer, J., Oost, A., et al. (2020). Managing erosion of mangrove-mud coasts with permeable dams–lessons learned. *Ecological Engineering*, *158*, 106078.

Winterwerp, J. C., Borst, W. G., & De Vries, M. B. (2005). Pilot study on the erosion and rehabilitation of a mangrove mud coast. *Journal of Coastal Research*, *21*(2), 223–230.

Winterwerp, J. C., Erftemeijer, P., Suryadiputra, N., van Eijk, P., & Zhang, L. (2013). Defining eco- morphodynamic requirements for rehabilitating eroding mangrove-mud coasts. *Wetlands*, *33*(3), 515–526.

Winterwerp, J. C., van Kessel, T., van Maren, D. S., & van Prooijen, B. C. (2021). *Fine sediment in open water*. WORLD SCIENTIFIC.

Wodehouse, D. C., & Rayment, M. B. (2019). Mangrove area and propagule number planting targets produce sub-optimal rehabilitation and afforestation outcomes. *Estuarine, Coastal and Shelf Science*, *222*, 91–102.

Wolanski, E. (1992). Hydrodynamics of mangrove swamps and their coastal waters. *Hydrobiologia*, *247*, 141–161.

Worthington, T., & Spalding, M. (2018). Mangrove restoration potential: A global map highlighting a critical opportunity.

Wyrtki, K. (1961). Physical oceanography of the southeast asia waters. *NAGA report*, *2*, 1–195.

Ye, Q., Morelissen, R., Goede, E. d., Ormondt, M. v., & Kester, J. v. (2012). A new technique for nested boundary conditions in hydrodynamic modeling. In *Asian and pacific coasts 2011* (pp. 1368–1377). World Scientific.

Yun, W. Y., Yeok, F. S., Youshao, W., Lu, D., Limi, M., & Lai, G. T. (2022). Spatiotemporal dispersal study of mangrove avicennia marina and rhizophora apiculata propagules. *Sains Malaysiana*, *51*(8), 2351–2364.

Yusuf, M., & Yanagi, T. (2013). Numerical modeling of tidal dynamics in the java sea. *Coastal marine science*, *36*(1), 1–12.

A

Bathymetry of Nested Model

Bathymetry of the nested Delft3D model was built from two datasets, one relatively coarse in the offshore region (Bisschop, 2023) and another more refined in the intertidal basin (Smits, 2016). The combined bathymetry used in the model is shown in Figure A.1.

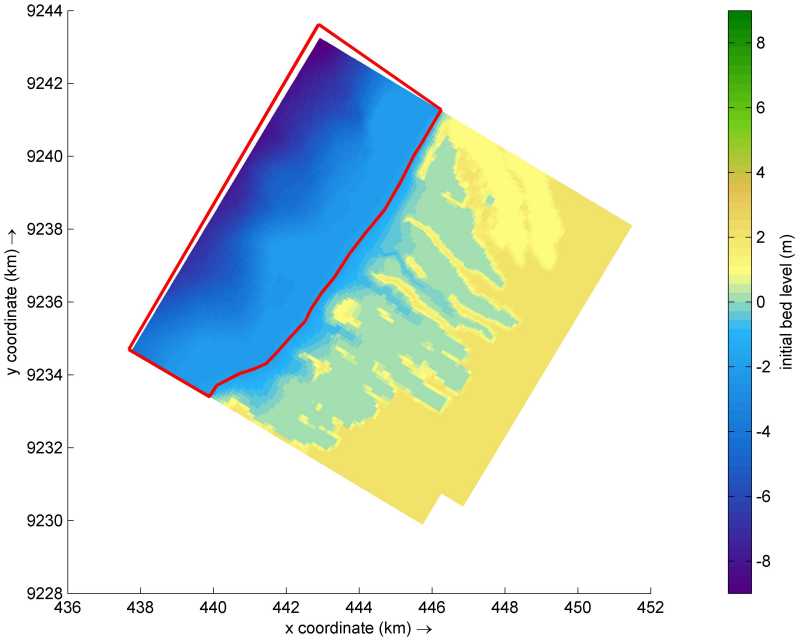

Figure A.1: Bathymetry of the nested model with the area where dataset from Bisschop (2023) was used indicated with a red polygon

Bathymetric datasets from Bisschop (2023) and Smits (2016) are shown in Figure A.2. When compared, it is evident that the dataset from Bisschop (2023) is not as detailed in the intertidal region. The datasets are therefore combined to result in the bathymetry depicted in Figure A.3.

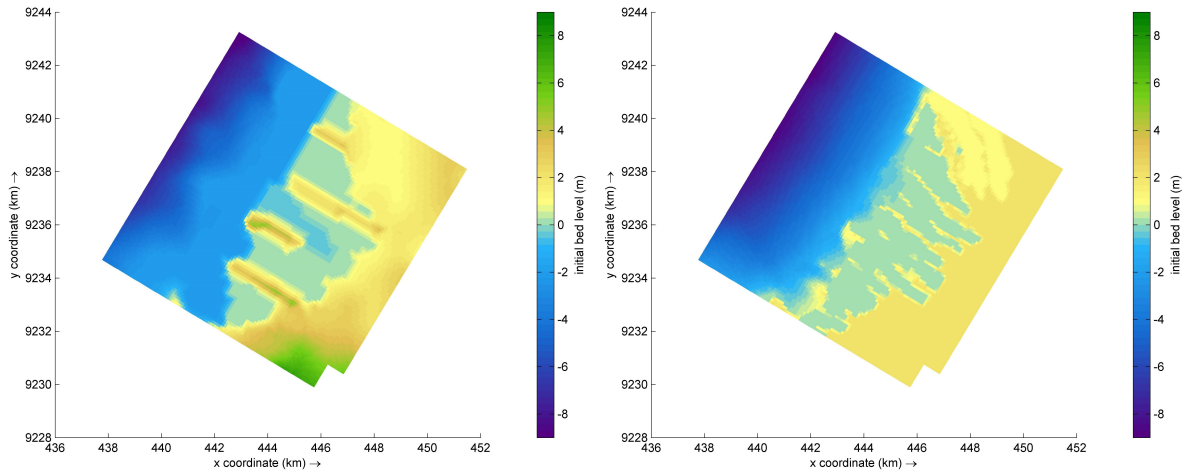

Figure A.2: Bathymetric datasets obtained from a) Bisschop (2023) and b) Smits (2016)

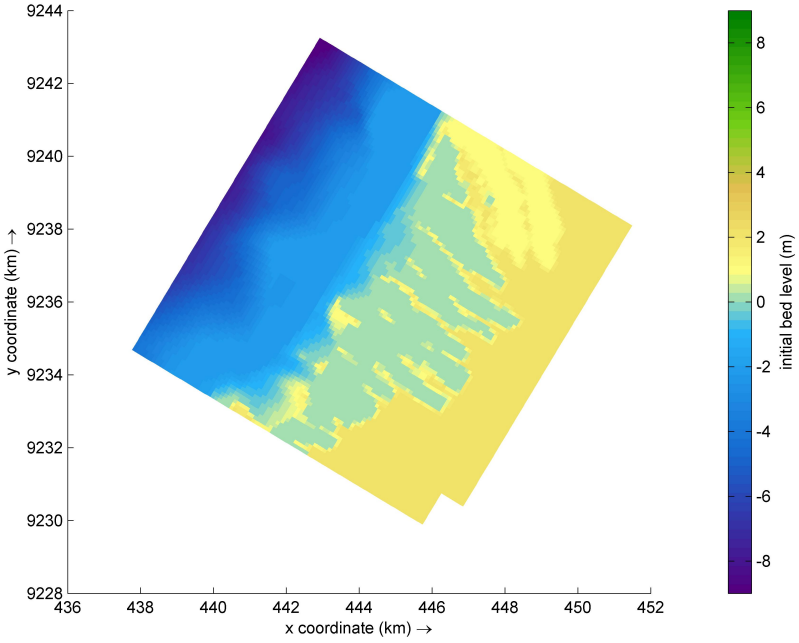

Figure A.3: Combined bathymetry built using the dataset of Bisschop (2023) in the offshore region and Smits (2016) in the intertidal basin

Although the dataset from Smits (2016) was comparatively more detailed, the intertidal region was elevated at the same level of MSL with the exception of the land strips. Therefore, channels were introduced based on past Google Earth images shown in Figure A.4 (a) and Figure A.4 (b). Additional modifications based on the current Google Earth image (Figure A.4 (c)) were also made to obtain the bathymetry of the nested model showcased in Figure A.5 (b).

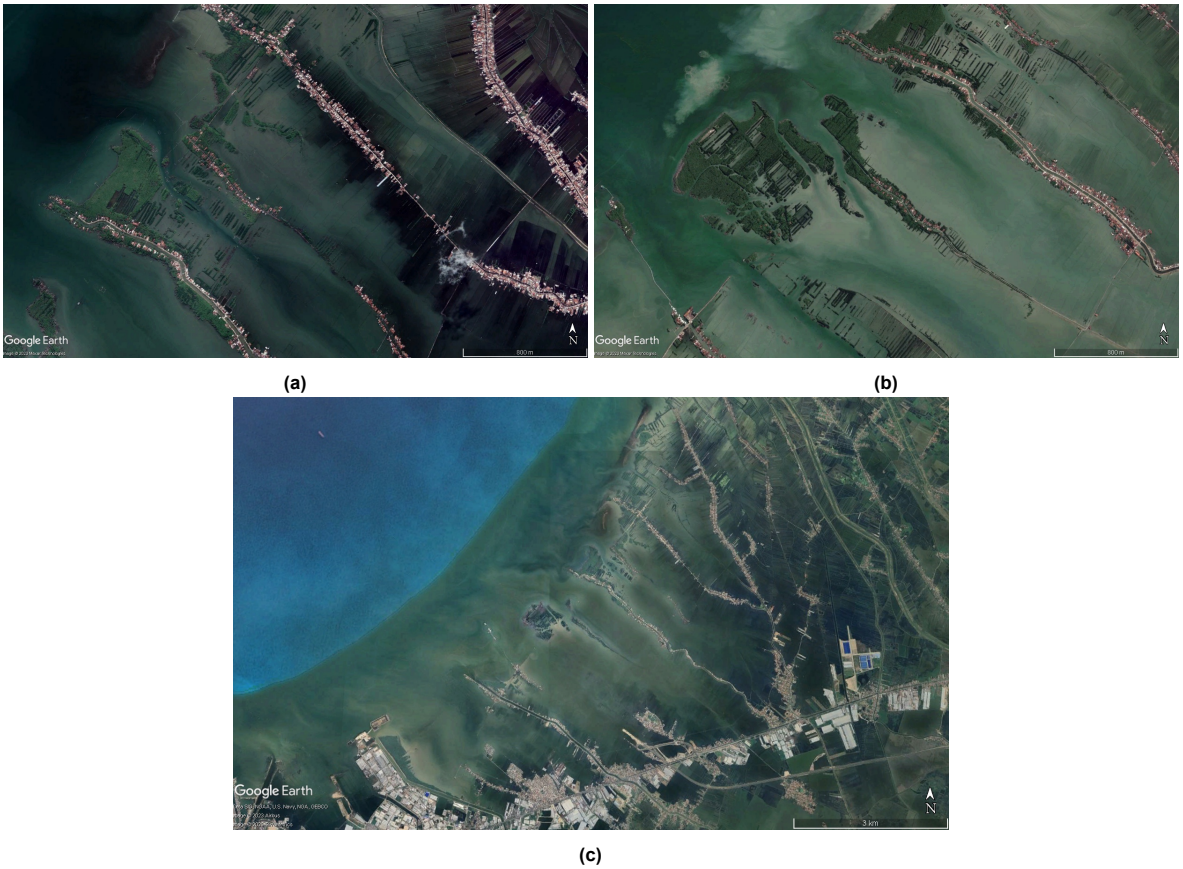

Figure A.4: Google Earth images of the intertidal basin a) at July 2021 with the channel depicted as a darker streak between two land strips, b) at May 2017 with two channels south and north of a mangrove patch, and c) at April 2023

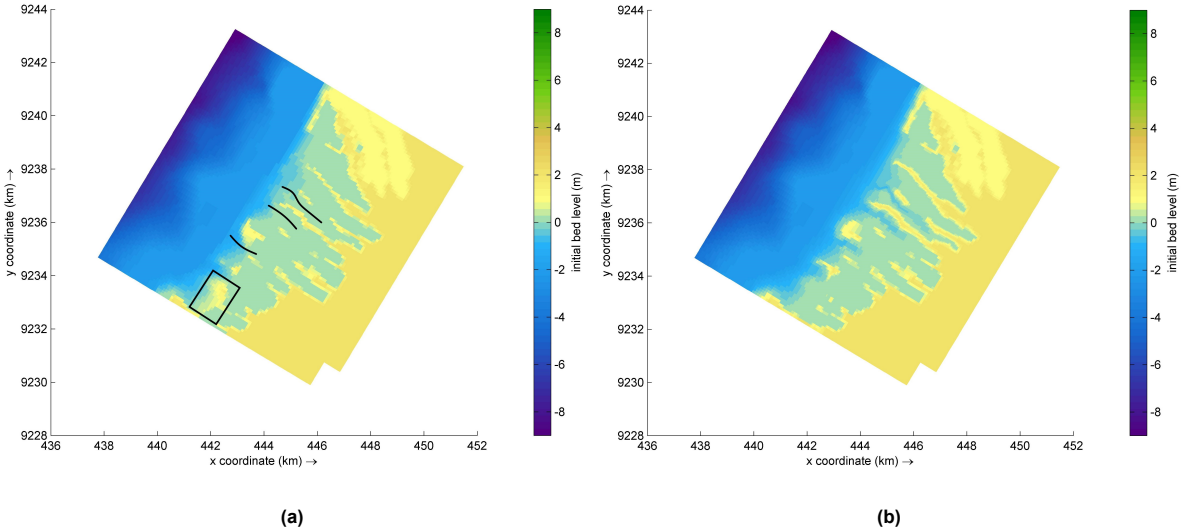

Figure A.5: Bathymetry of the nested model a) before adding channels (black lines) and lowering elevations at areas (black polygon) based on Google Earth images, and b) used in Delft3D

B

Porous Plates

Permeable dams constructed in the study area to trap sediment are replicated in the Delft3D model utilising an additional parameter of porous plate. Since the porous plate allows for restricted transfer of mass and momentum, the input parameter of resistance coefficient was tested for a range of values to find the one for which the flow patterns and current velocities correspond closely to those observed in the field and physical models constructed in laboratories to replicate a scaled-down version of the system. Residual and instantaneous current velocities across each of the six porous plates with the resistance coefficients implemented in the model are provided in the figures in this appendix.

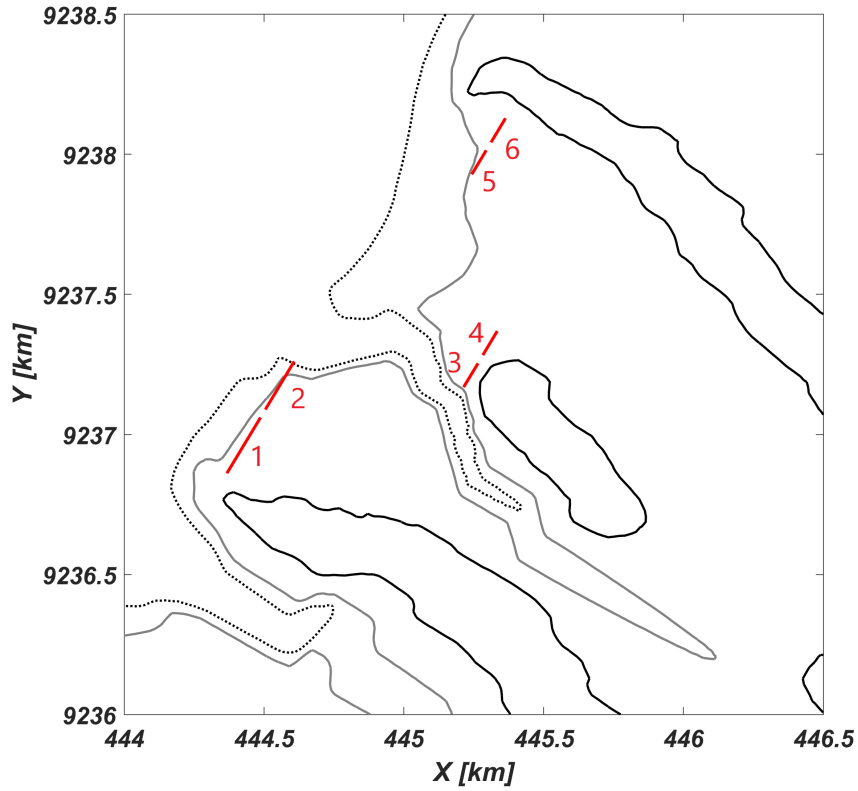

Figure B.1: Location of the six structures implemented in the Delft3D models

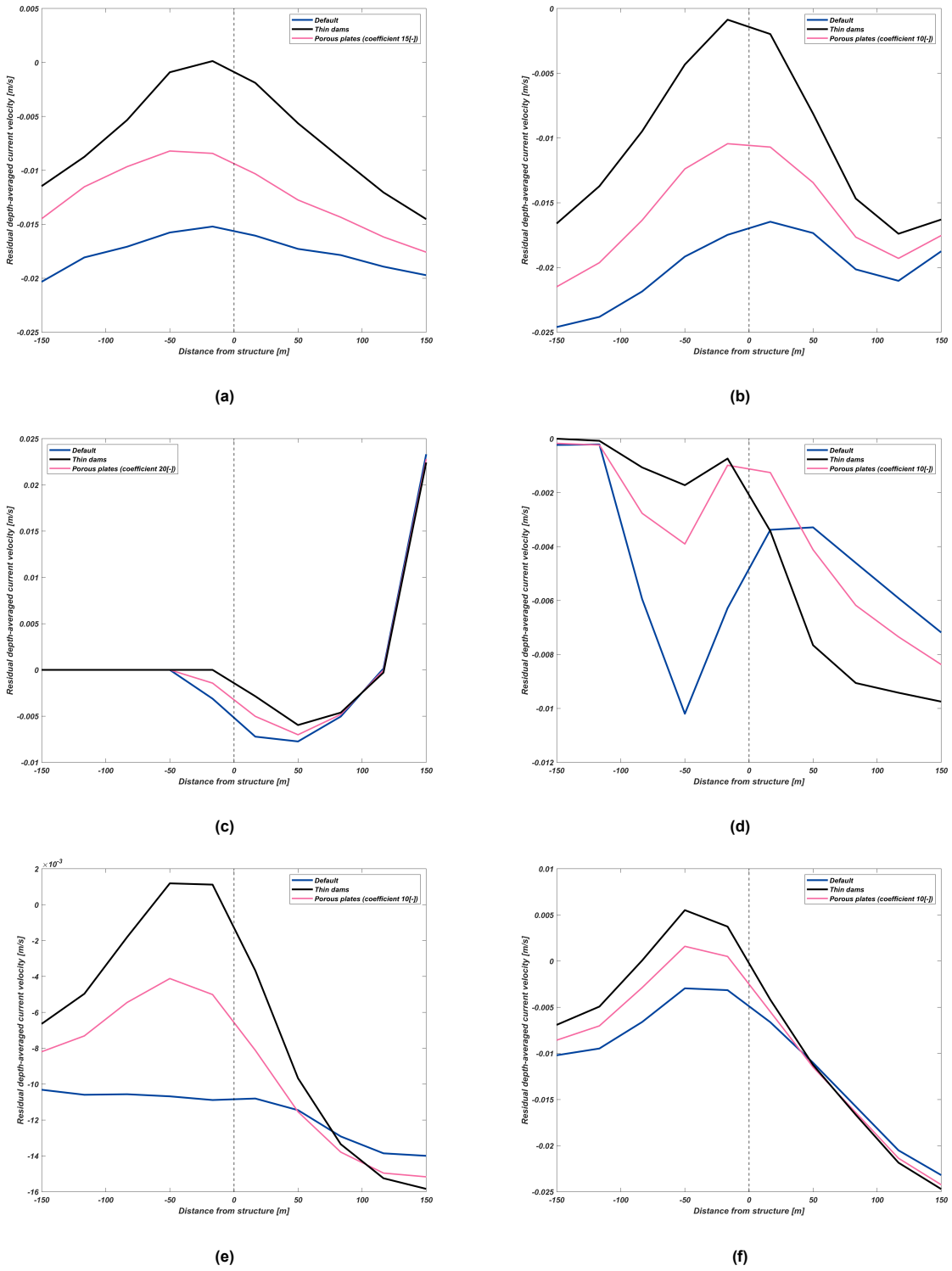

Figure B.2: Comparison of residual depth-averaged currents over a month in the absence of structures (blue), thin dams (black) and porous plates (pink) for structures a) 1 b) 2 c) 3 d) 4 e) 5 f) 6

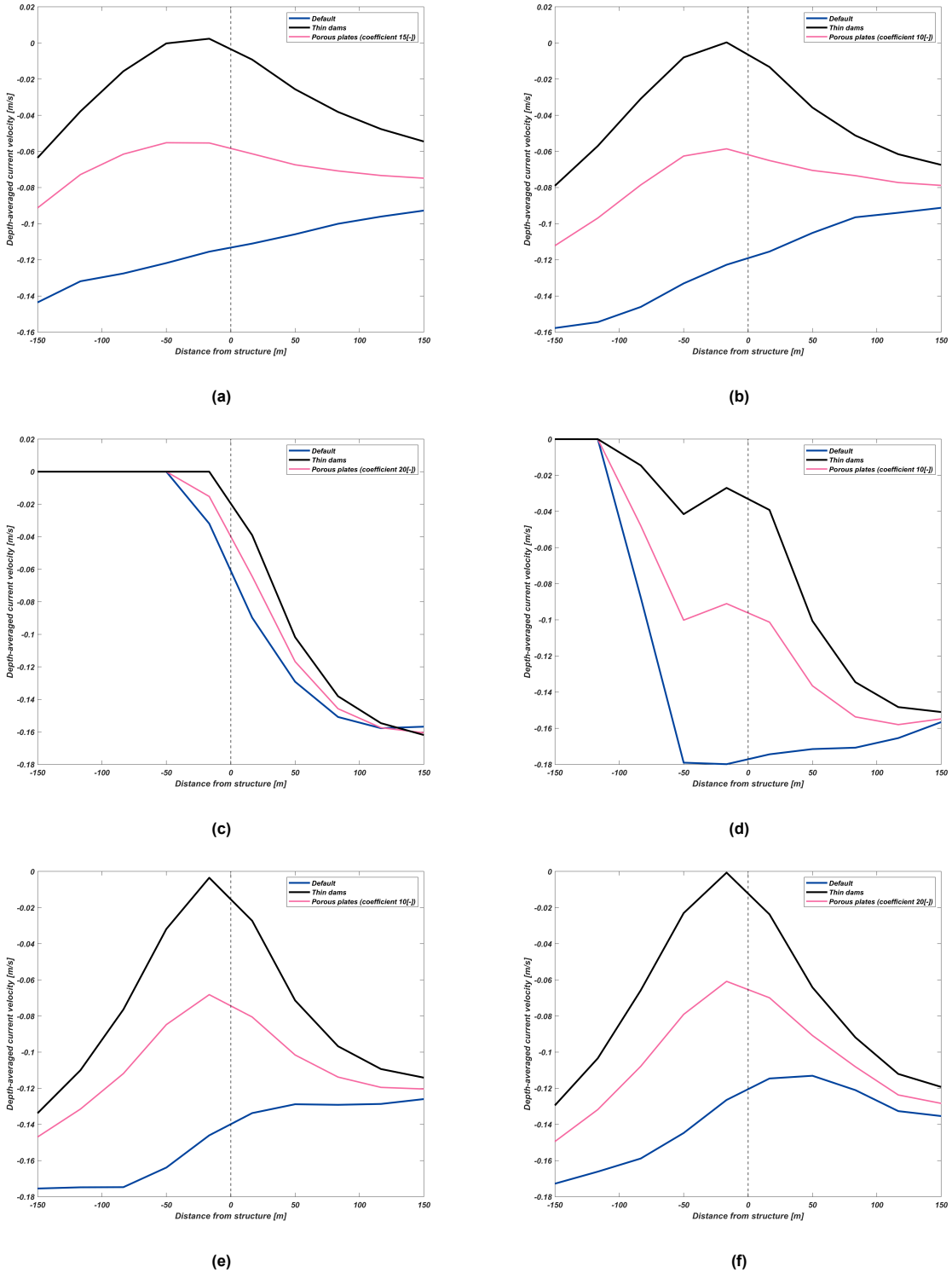

Figure B.3: Comparison of depth-averaged currents during rising tide in the absence of structures (blue), thin dams (black) and porous plates (pink) for structures a) 1 b) 2 c) 3 d) 4 e) 5 f) 6

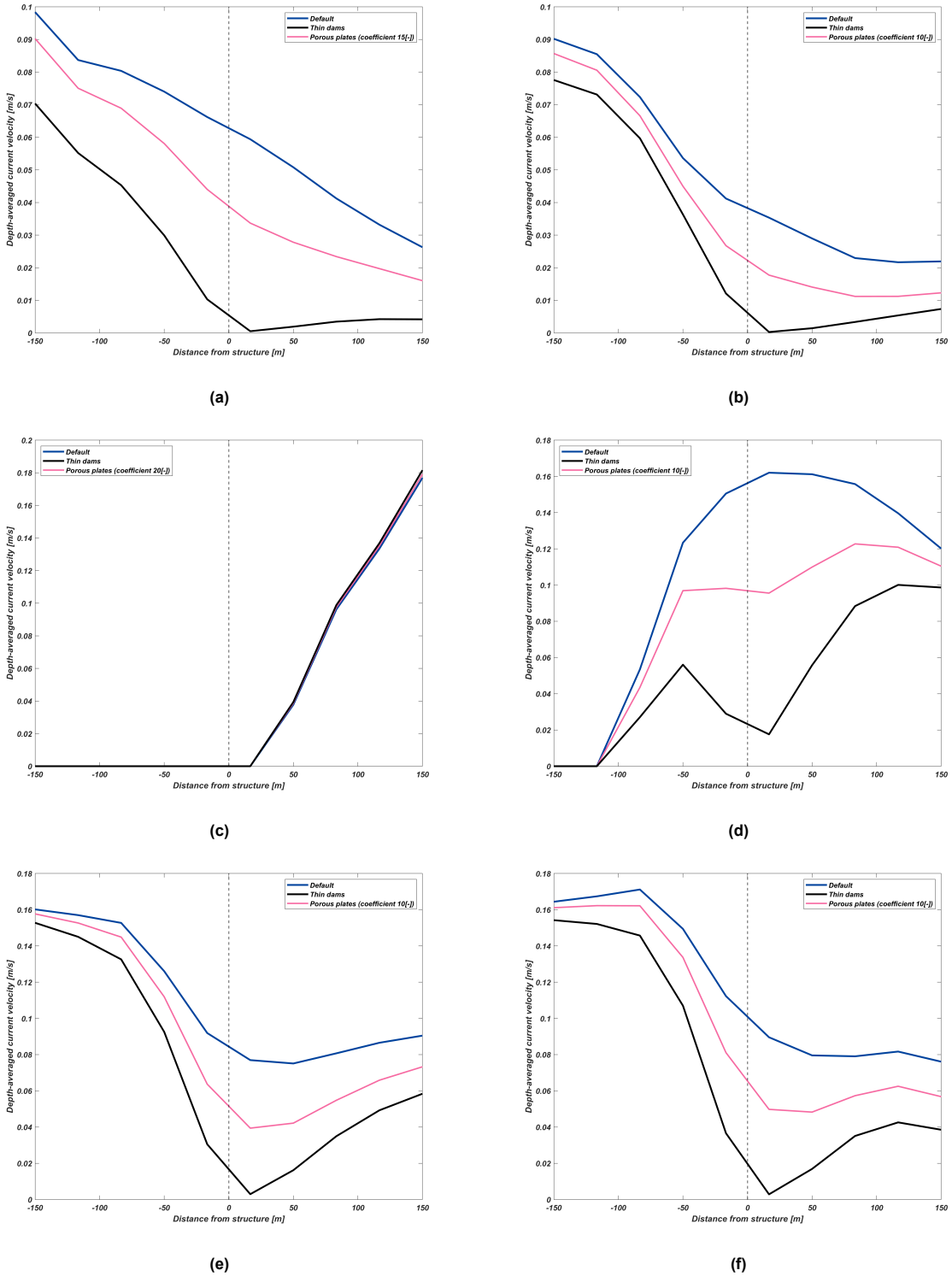

Figure B.4: Comparison of depth-averaged currents during falling tide in the absence of structures (blue), thin dams (black) and porous plates (pink) for structures a) 1 b) 2 c) 3 d) 4 e) 5 f) 6

C

Bed Shear Stress

The wave-induced maximum bed shear stress computed as the average over a month for water levels based on a observation point in the intertidal basin is shown in Figure C.1 for the three scenarios of structural presence.

The hard structures do not transmit the waves and are instead fully reflected. This leads to the most significant reduction in shear stress behind them. Additionally, due to wave reflection, shear stress in front of the structures is higher when compared to the scenario without any structures. In the case of permeable dams modelled with a transmission coefficient of 0.6, a decrease in bed shear stress can be observed. However, this reduction is notably less pronounced than what is observed with hard structures. When compared to Figure 5.5 based on MHW, effect of the structures on the maximum shear stress is less apparent when averaged over the simulation period.

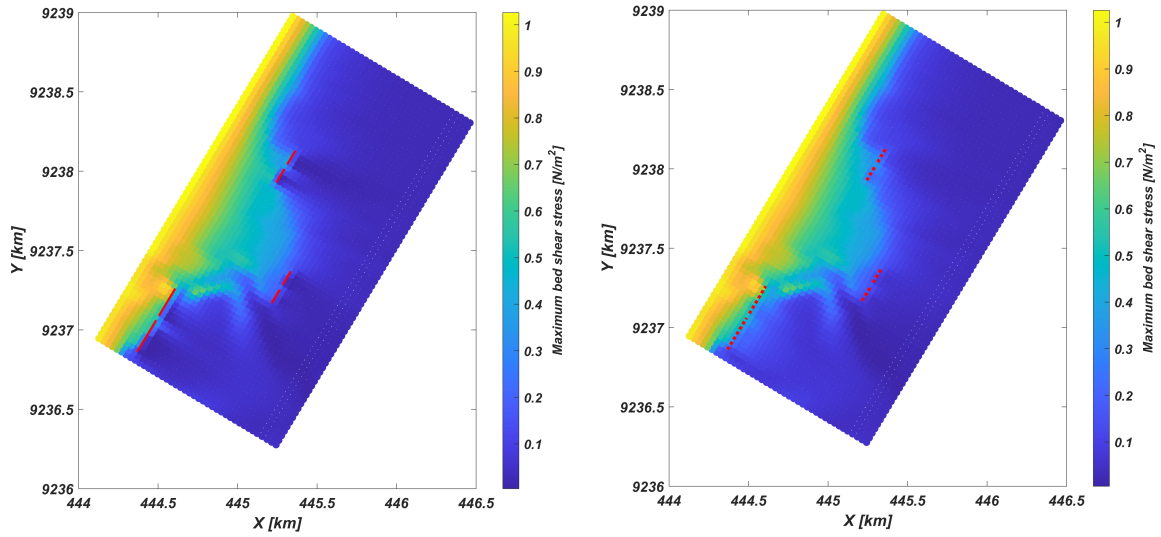

(a)

(b)

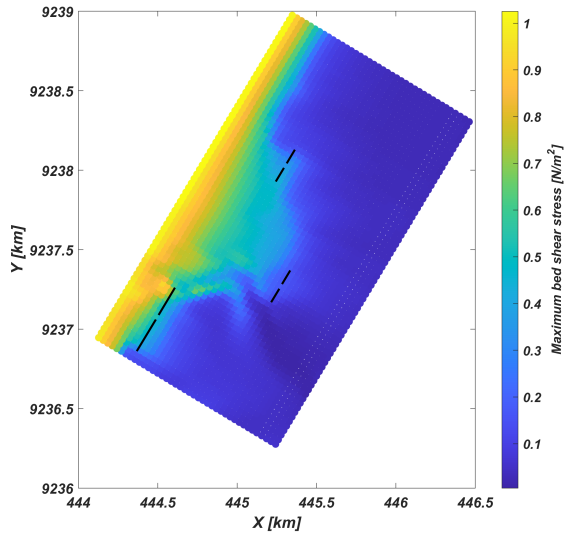

(c)

Figure C.1: Average maximum bed shear stress due to waves in the a) vicinity of hard structures (shown as solid red lines) b) presence of permeable dams (dotted red lines) and, c) absence of structures (location indicated using black lines)

D

Sediment Retention - Sensitivity Analysis

Comparison of the sediment retention capacities of structures with different characteristics are made in Chapter 5. However, to differentiate between the influence of regional differences and structure characteristics in the performance of the structures, a preliminary sensitivity analysis is performed.

Two sets of structures, one longer and another shorter are modelled at the same location as depicted in D.1. The sediment retention capacity of the two sets of thin dams is showcased in D.2. Sediments are better retained by the longer thin dams at the location, retaining up to 70% of the sediment behind the dams, compared to 25% by the shorter structures.

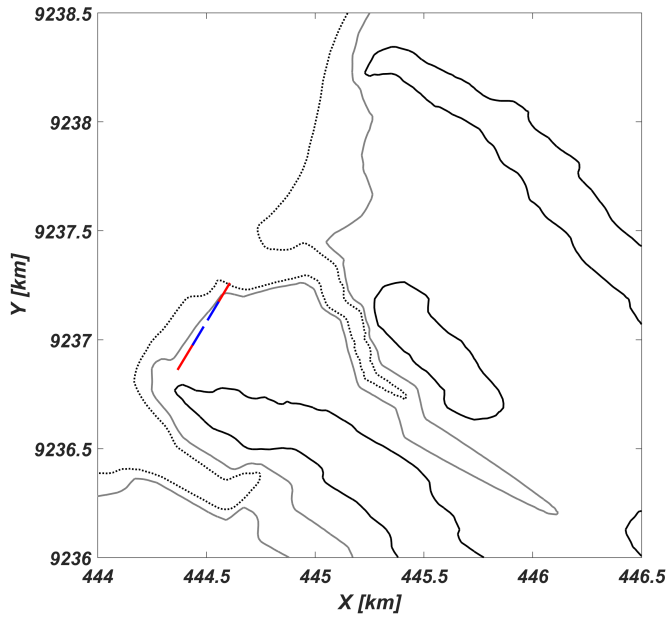

Figure D.1: Location of two set of structures, one longer (red) and one shorter (blue) in the intertidal basin

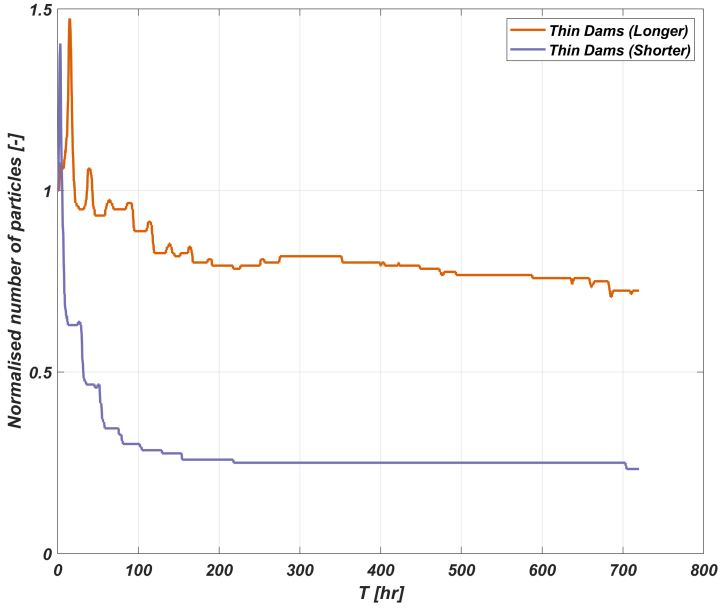

Figure D.2: Normalised number of sediment particles during the simulation period behind the thin dams at the southern end, depicted in Figure D.1. The number of sediment particles is normalised as the fraction of particles at each timestep to the initial number of particles behind the structures.

Another set of models were run with two sets of thin dams, one closer and another farther from the mangrove fringe at the same location as shown in D.3. The sediment retention capacity of the two sets of structures is showcased in D.4. The retention ability of the thin dams closer to the coastline is higher, retaining up to almost 80% of the sediment behind them, compared to 60% by the structures placed farther from the coastline.

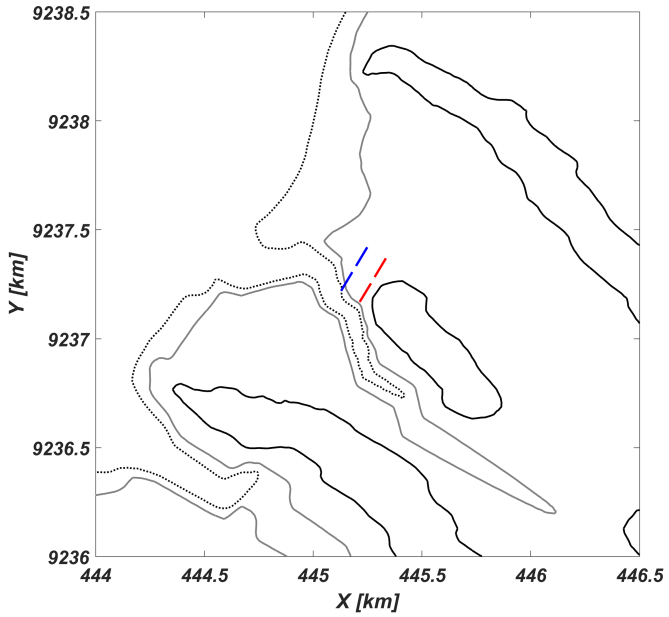

Figure D.3: Location of two set of structures, one closer (red) and one farther (blue) from the mangrove fringe within the intertidal basin

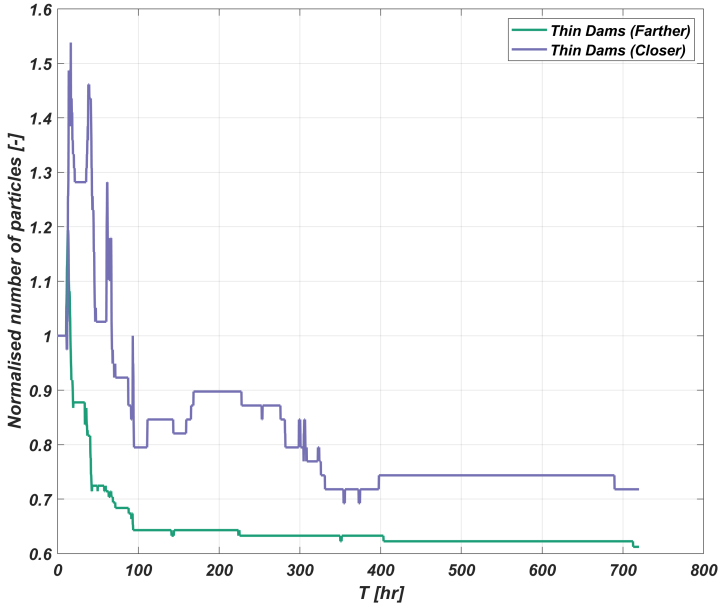

Figure D.4: Normalised number of sediment particles during the simulation period behind the thin dams farther into the basin, depicted in Figure D.3. The number of sediment particles is normalised as the fraction of particles at each timestep to the initial number of particles behind the structures.